Identification of vulnerabilities in an aggressive subtype of pancreatic cancer

Inaugural dissertation

for the attainment of the title of doctor
in the Faculty of Mathematics and Natural Sciences
at the Heinrich Heine University Düsseldorf

presented by

María Josefina Doffo
from Quilmes, Buenos Aires, Argentina

Düsseldorf, December 2020

from the institute for Hematology and Tumor Oncology
at the University Clinic Charité Berlin

Published by permission of the
Faculty of Mathematics and Natural Sciences at
Heinrich Heine University Düsseldorf

Supervisor: Prof. Dr. Ulrich Keller
Co-supervisor: Prof. Dr. Henrike Heise

Date of the oral examination:

To my family

Acknowledgements

First, I would like to thank Prof. Ulrich Keller and Prof. Irene Esposito for opening the doors of their labs and giving me opportunity to develop my research skills under their supervision.

I would like to thank Prof. Henrike Heise for her academic support to be part of my reviewer committee.

Of course, I would like to thank to Dr. Matthias Wirth for giving me the opportunity to be part of this project, for the insightful and fruitful conversations.

Thanks to Dr. Bamopoulos and Leo, for your constant help and patience with R scripts.

I cannot thank enough to my colleagues, the ones from Düsseldorf and the ones for Berlin, for the nice time in the lab. Special thanks to the usual suspects (including you Dorita and Paul). Thanks for all the scientific and not scientific discussions, for all the shared laughter and amazing mensa food.

A big thanks to them, Nikita and Stavri, for being just what I needed and more. No words are enough to express you how thankful I am. I love you forever.

To Tomás and Michay, thank you for supporting me and for the great scientific feedback.

To Flor and my long-life friends, thank you. Estefi, Juli, Vicky, Noe y Majo, thanks for being there for me even when 14000 km separate us.

The most special thanks to my parents, siblings and my sweet nephew. This thesis would not be complete without your unconditional support.

Contents

1. Summary

Evasion from drug-induced apoptosis is one crucial mechanism of treatment resistance in pancreatic ductal adenocarcinoma (PDAC). In an aggressive PDAC subtype, I identified high expression of the pro-apoptotic protein NOXA, suggesting that PDAC cells of this subtype are primed for apoptosis. To explore NOXA-associated vulnerabilities I generated CRISPR/Cas9 NOXA deficient human and murine cell lines and performed a large-scale drug screening experiment in human and murine cell lines. As a top hit, it was identified an inhibitor of the transcription factor heterodimer CBFβ and RUNX1, AI-10-49. By means of pharmacological inhibition of CBFβ/RUNX1 and genetic gain and loss of function experiments, I validated that AI-10-49 induced apoptotic cell death and growth inhibition in a RUNX1- and NOXA-dependent manner. It was confirmed that AI-10-49 treatment significantly blocked tumor growth *in vivo*. Furthermore, it was identified an association between *NOXA* mRNA expression and sensitivity towards pharmacological CBFβ/RUNX1 inhibition in primary patient derived PDAC organoids. Through genome wide analyses of RUNX1 binding together with histone acetylation, and global chromatin accessibility, I corroborated that RUNX1 depletion leads to modifications in the epigenetic landscape. The re-distribution of active and open chromatin towards apoptotic programs, together with higher genomic accessibility of the NOXA gene, gave indicators of the mechanism behind AI-10-49 induced cell death. Taken together this study demonstrates a novel way to trigger NOXA-dependent cell death and consecutively overcome treatment resistance in PDAC.

2. Introduction

2. 1. Hallmarks in cancer

The hallmarks of nearly all cancers are biological features that provide understanding of the cancer biology and enable tumor growth and spread. They consist of the evasion of apoptosis, indiscriminate proliferation, evasion of growth suppressors, replication of immortality, angiogenesis induction and activation of invasion and metastatic dissemination (Hamacher et al., 2008; Hanahan & Weinberg, 2011).

2. 2. Pancreatic cancer

Pancreatic cancer is the malignancy of the pancreas. The most common form is pancreatic ductal adenocarcinoma (PDAC), accounting for more than 90% of all pancreatic cancers.

2. 2. 1. PDAC

Pancreatic ductal adenocarcinoma is a lethal disease with a dismal prognosis, predicted to become the second leading cause of cancer death in Germany surpassing breast and colorectal cancer by the year 2030 (Quante et al., 2016). Even though it has a low incidence (it ranks number 10 of new cases), it is the 4th cause of cancer-related death nowadays (Siegel et al., 2020) and it is expected to become the 2nd by the year 2030 in the US (Rahib et al., 2014). It is often diagnosed at a late stage, contributing to a poor five-year survival rate, with a life expectancy of ~5% at 5 years after first diagnosis. Its dismal prognosis remains almost unchanged since the last 20 years, whereas incidence and mortality rates are remarkably similar. This late diagnosis is due to, among other reasons, lack of early indicators, risk factors and late onset of symptoms resulting in patients with metastatic PDAC at the time of diagnosis. It is characterized by having a great volume of stroma content (up to 80%), leading to difficulties in the treatment by impeding drug-delivery and absorption (Provenzano et al., 2012).

2. 2. 1. 1. PDAC progression

The pancreas contains cells of exocrine (acinar), epithelial (ductal), and endocrine (α, β, δ, ε) origin among which acinar cells are well known for their high degree of plasticity. Acinar cells trans-differentiate to a more epithelial state (ductal-like) in an event named “acinar-to-ductal metaplasia” (ADM) driven by several environmental stimuli such as, stress conditions, inflammation or tissue damage (Friedlander et al., 2009). During this phenomenon, the acinar cells acquire “progenitor” cell characteristics making them susceptible to pro-oncogenic hits, such as activating mutations in the proto-oncogene *KRAS* (*Kirsten rat sarcoma viral oncogene homolog*), which could in turn transform them into pancreatic intraepithelial neoplasias (PanINs) (Hruban et al., 2001). In addition to PanIN, there are other non-invasive neoplasms of the pancreas, mucinous cystic neoplasm (MCN) and intraductal papillary mucinous neoplasm (IPMN), which are also precursors of PDAC (Del Chiaro et al., 2013; Distler et al., 2013; Fasanella & McGrath, 2009; Matthaei et al., 2013; Ren et al., 2019; Sawai et al., 2011; Zamboni et al., 2013; Zhao et al., 2019).

Genome sequencing has revealed several genetic changes that occur during the development and progression of ductal adenocarcinoma of the pancreas. On average, there are up to 63 genetic aberrations in the PDAC, which lead to the activation of various core signal pathways (Jones et al., 2008). Most PDAC cases harbor alterations in mainly four genes: activating of oncogenic *KRAS* gene (Forrester et al., 1987; Mann et al., 2016), silencing of the *CDKN2A* (*cyclin-dependent kinase inhibitor 2A*) gene, mutation of *tumor suppressor TP53* (*tumor protein p53*) and gene inactivation of *SMAD4* (*mothers against decapentaplegic homolog 4*) (Cicenas et al., 2017; Iacobuzio-Donahue et al., 2000; Tanaka, 2018; Witkiewicz et al., 2015). The latter being the only mutation that shows a correlation with poorer prognosis (Blackford et al., 2009). In addition, some subsets of patients showed mutations in the TGF-β (*transforming growth factor-β*) and WNT signaling pathway (Jones et al., 2008) and germline mutations in DNA damage repair genes (e.g., breast cancer early onset genes 1-2(BRCA 1/2), partner and localizer of BRCA2 (PALB2), and ataxia telangiectasia mutated protein serine/threonine kinase (ATM) (Hu et al., 2018; Orth et al., 2019).

At the molecular level, PDAC development has two evolutionary routes posing its progression. On the one hand, the mutation in the *KRAS* gene (the most common one being the amino acid exchange G12D) leads to a gradual tumor progression with accumulation of additional mutations in the tumor suppressor genes *CDKN2A*, *TP53* and *SMAD4* (classic progression model) (Hruban et al., 2001). Accompanying these mutations, the normal duct epithelium will transform into infiltrating cancer through a series of histologically defined precursors, e.g., PanINs. On the other hand, the alternative progression model suggests that the mutations, chromosomal gains and losses are caused by a cataclysmic genetic event such as chromothripsis (Notta et al., 2016).

2. 2. 1. 2. Treatment

Pancreatic ductal adenocarcinoma is practically resistant to radio and chemotherapy, reason why the most viable option for a curative therapy is the resection of the pancreas (pancreaticoduodenectomy or Whipple procedure), a complex surgery where the head of the pancreas, the duodenum, the gallbladder and the bile duct are removed (Beger et al., 2003). Even though the surgery still remains as the only curative option for this disease, only 10-15% of patients are suitable for undergoing this procedure, due to the late stage of the disease at the time of diagnosis (Beger et al., 2003; Orth et al., 2019).

For those patients with locally advanced, non-resectable or borderline resectable tumors, the first-line treatment is systemic chemotherapy. This could include nucleoside analogues, such as gemcitabine and capecitabine, or the pyrimidine analogue 5-fluorouracil (5-FU) in monotherapy settings or in combination with radiotherapy to radio-sensitize the tumor and overcome radiotherapy resistance. FOLFIRINOX treatment, also known as “standard of care” treatment, is a poly-chemotherapeutic regimen consisting of a combination of 5-FU, the platinum derivative oxaliplatin and the topoisomerase I inhibitor irinotecan together with leucovorin (folinic acid) (McGuigan et al., 2018). This poly-therapy has been reported to nearly double median survival in the metastatic pancreatic cancer in comparison to gemcitabine alone. However, FOLFIRINOX treatment is associated with significant toxicity, thus limiting its

use to patients in general good shape (Vaccaro et al., 2011). Furthermore, it could be shown that the addition of nab-paclitaxel (nanoparticle albumin bound paclitaxel, cytoskeleton inhibitor) in addition to gemcitabine therapy can extend the median survival time from 6.7 to 8.5 months compared to gemcitabine monotherapy (Goldstein et al., 2015; Macarulla et al., 2018; Von Hoff et al., 2013).The success of current chemotherapy involving gemcitabine, FOLFIRINOX, and others, is limited by chemo-resistance, regardless of its intrinsic or acquired origin.

2. 2. 1. 3. Chemotherapy resistance

Resistance to chemotherapy is a significant obstacle to the effectiveness of treatments and leads to poor prognosis in patients. In general, chemoresistance is explained by a variety of factors, e.g., decreased cellular drug bio-availability, increased drug export, increased repair through drug-induced DNA damage signaling, evasion of apoptosis and deregulation of autophagy (Pan et al., 2016). In PDAC, this phenomenon could be caused by the heterogeneity and plasticity of the tumors, as well as by desmoplasia and apoptosis evasion (Cannon et al., 2018; Grasso et al., 2017; Hanahan & Weinberg, 2011; Schober et al., 2014). This underscores the need for the identification of novel biomarkers to advance towards the “precision medicine era”, where therapy can be adapted to each individual patient, avoiding toxic and unsuccessful treatments.

Since apoptosis is a key hallmark of pancreatic cancer, it arises as an attractive possibility to identify compounds to induce this physiological process, disrupt cancerous transcription programs and eventually lead to cell death of malignant cells as a novel therapeutic strategy (Delbridge & Strasser, 2015). In this context, the BH3 mimetics compounds were developed, to enhance intrinsic apoptosis (Delbridge & Strasser, 2015; Labi et al., 2008; Moujalled et al., 2019).

2. 2. 1. 4. Molecular subtyping in pancreatic cancer

Given that pancreatic cancer consists of a sum of complex contributions of many deregulated genetic, epigenetic and signaling pathways, as well as extracellular influences, its heterogeneity can be best captured at the mRNA level.

Throughout the years, different research groups made efforts to classify pancreatic cancer into subgroups by using patient samples and performing whole-exome sequencing, RNA-seq, microarray expression data, among others, to understand expression patterns/pathways (Bailey et al., 2016; Collisson et al., 2011; Moffitt et al., 2015; Waddell et al., 2015). Apart from classifying this entity by mutational status and altered molecular pathways, the subtypes were correlated with patient survival and histopathological stratification such as hepatocyte nuclear factor 1A (HNF1A) and cytokeratin-81 (KRT81) as bio-markers (Muckenhuber et al., 2018). Not surprisingly, these classifications differ in the number of subtypes identified and it was thoroughly reviewed in different occasions (Collisson et al., 2019; Orth et al., 2019; Torres & Grippo, 2018). However, there are overlapping subtypes between the proposed by Collison in 2011 and Bailey in 2016 (Torres & Grippo, 2018), among others that will not be discussed here. First, exocrine-like with aberrantly differentiated endocrine exocrine (ADEX), in which some of the altered pathways are transcriptional networks in later stages of pancreatic differentiation and genes associated with endocrine differentiation. The classic subtype overlaps with the pancreatic progenitor, where the pathways involved are regulation of fatty acid oxidation, steroid hormone biosynthesis, drug metabolism, among others. Lastly, the quasi-mesenchymal (QM) subtype overlaps with the he squamous, characterized by EGF signaling and hypermethylation of genes (epigenetic downregulation) that drive cell-fate in specific cells, causing a loss of endodermal identity, thus producing a more mesenchymal gene expression pattern. Interestingly, the QM subtype, described by Bailey and collaborators has the worst patient overall survival (Bailey et al., 2016), and, notably, it shows a high mRNA expression of the pro-apoptotic gene *NOXA* (Fig. 1).

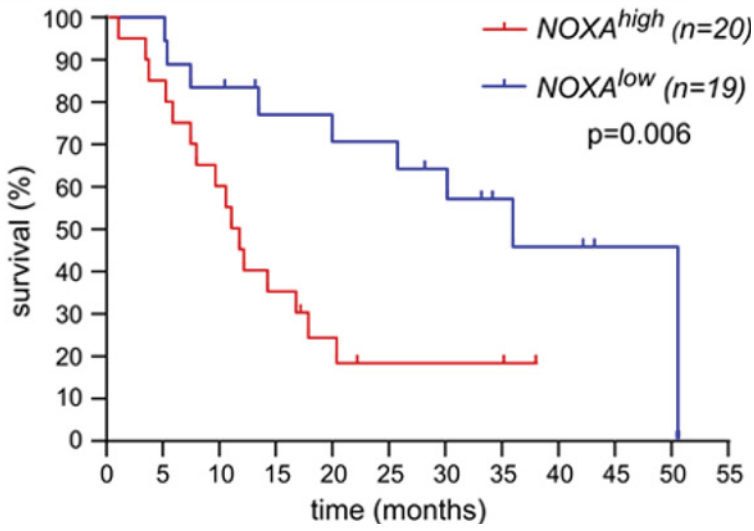

Figure 1: High *NOXA* expression correlates with poor patient survival. Survival of PDAC patients with a low (lower quartile) and a high (upper quartile) *NOXA* mRNA expression, derived from the transcriptomic analysis from Bailey and collaborators (Bailey et al., 2016). Log-rank test.

2. 3. Apoptosis

Programmed cell death or apoptosis (also known as “suicide program”) is a key regulator of homeostasis in normal tissues of vertebrates by balancing cell proliferation and cell death, phenomenon first described in 1972 (Kerr et al., 1972). It is the cellular program by which adult cells dispose of irreparably damaged cells or cells prone to become malignant, such as neoplastic cells (Kerr et al., 1972; Portt et al., 2011). Of note, cellular death plays a key role in embryogenesis as well, thus eliminating interdigital cells during limb formation or in neuron development by matching each neuron with its target cell (Kelly & Strasser, 2011). During this physiological process, several changes occur within the cells regarding molecular changes and morphological ones. Morphologically, the chromatin condenses, the DNA is fragmented, and the cell shrinks to later be engulfed by phagocytic cells. At the molecular level, a series of cysteine proteases, called caspases, are activated by cleavage next to their aspartate residues. The caspases are synthesized as inactive pro-forms and they cleave and activate each other, amplifying the signal in a cascade to precisely control the execution of programmed

cell death. At the same time, caspases cleave different substrates, like cytoskeletal proteins, nuclear laminas, leading to the morphological changes in the cell (Ouyang et al., 2012).

There are different external and internal signals that could trigger apoptosis thus activating the executioner caspases 3, 6 and 7 (e.g., cellular stress and cytotoxic agents). The death receptor (or extrinsic) pathway is triggered by engagement of cell surface receptors that belong to the tumor necrosis factor (TNF) family, containing intracellular “death domains”, such as Fas and TNF-R1 (Kelly & Strasser, 2011). These receptors trigger apoptosis by forming a “death-inducing signaling complex” (DISC) which consists of death ligands (i.e., FasL), death receptors (i.e., TRAIL-R) and the FADD adaptor protein, assisted in certain death receptors (i.e., TNF-R1) by the adapter TRADD. This complex recruit and activates pro-caspase 8 which in turn activates the effector caspases 3, 6 and 7. The mitochondrial (or intrinsic pathway) is mainly regulated by the BCL-2 protein family and consists of a balance of pro-survival and pro-apoptotic proteins to decide cell fate. Different stresses such as cytotoxic compounds, DNA damage, oncogene activation, lead to activation of the pro-apoptotic members of the BCL-2 protein family (Adams & Cory, 2007; Youle & Strasser, 2008). This imbalance finally leads to the activation of the pro-apoptotic BCL-2 family members BAX and/or BAK and the perturbation of the integrity of the mitochondrial outer membrane (MOM) (Strasser et al., 2011). Their action leads to the release from the mitochondrial intermembrane space not only of cytochrome c, which triggers APAF-1-mediated activation of caspase 9 and conformation of the apoptosome by these 3 players, but also of other apoptogenic proteins, such as SMAC/DIABLO (Second Mitochondria-Derived Activator of Caspase), which prevents XIAP (X-Linked Inhibitor of Apoptosis) from inhibiting its caspase targets (Green et al., 2014; Jost et al., 2010).

2. 3. 1. The BCL-2 family: key regulator of intrinsic apoptosis

The intrinsic or mitochondrial pathway is named as such because the mitochondria takes the key position by initiating apoptosis. The BCL-2 protein family regulates this process by controlling the integrity of the MOM, among other activities (Youle & Strasser, 2008).

The BCL-2 protein family consists of three functional subgroups: the pro-apoptotic initiator or sensors (BH3-only proteins), the pro-survival guardians and the pro-apoptotic effectors (Adams & Cory, 2007, 2018; Strasser et al., 2011). The pro-survival guardians are BCL-2 and its closest homologues BCL-XL, BCL-W, MCL-1 and A1, which contain four conserved sequence motifs (called BCL-2 homology (BH) domains) and promote cell survival. Within the pro-apoptotic effectors we find BAX, BAK and BOK which all have 4 BH regions, similar to the pro-survival proteins (Kvansakul & Hinds, 2014). Once BAX and BAK are activated, they form an oligomer that will produce the permeabilization of the MOM which provokes the release of cytochrome c into the cytosol, where it helps form the apoptosome that activates caspase 9. In turn, the apoptosome activates the effector caspases 3, 6 and 7 that cleave vital cellular proteins, ensuring cellular death.

Lastly, the pro-apoptotic initiators or sensors are the BH3-only proteins, which include BAD, BIK, HRK, BID, BIM, BMF, NOXA and PUMA. They carry that name because their only homology to BCL-2 (or each other) is the BH3 domain, through which they engage multi-BH domain interactions (Happo & Strasser, 2012). The BH3-only proteins are upregulated by distinct cytotoxic stimuli such as enhanced transcription and post-translational modifications (Puthalakath & Strasser, 2002). Upon stimuli they can bind with high affinity to their pro-survival counterpart, thus preventing their blockage of BAX and BAK or activate BAX/BAK oligomer formation by direct interaction (Kuwana et al., 2005). BH3-only proteins vary in affinity for different pro-survival relatives because of differences in the sequences within both the BH3 domain and groove (Chen et al., 2005; Kuwana et al., 2005). Whereas BIM, PUMA and cleaved BID (tBID) bind all five pro-survival proteins, BAD binds only to BCL-2, BCL-XL and BCL-W, and NOXA engages with MCL-1 and/or A1 (Happo & Strasser, 2012; Youle & Strasser, 2008). Even though BH3-only proteins that bind all pro-survival proteins (BIM, PUMA, tBID) are more efficient killers than those with limited binding partners, a combination of NOXA and BAD kills potently, suggesting that efficient killing requires neutralization of all pro-survival members in the specific cell type (Chen et al., 2005; Youle & Strasser, 2008). Interactions between these factions determine whether cells live or die (Chen et al., 2005; Delbridge & Strasser, 2015).

2. 3. 2. Apoptosis evasion and BCL-2 protein family implication in carcinogenesis

A disturbance in apoptosis or apoptosis evasion is usually a hallmark of multiple diseases, especially cancer. The reason is that programmed cell death is fundamentally an anti-neoplastic mechanism and the neoplastic changes that a cell undergoes from normal to cancerous are potent inducers of programmed cell death (Hamacher et al., 2008). Even though there is a great number of cancers portraying a strong pro-survival mechanism, there is a small proportion of malignancies carrying mutations in the BCL-2 protein family or death receptor family. Hence, the survival of cells undergoing neoplastic transformation seems to rely on changes happening in upstream pathways that in turn alter the expression of BCL-2 protein family members (Strasser et al., 2011).

In the context of pancreatic cancer, it was found that there is an absence of apoptotic cells in PanIN lesions, suggesting the contribution of an anti-apoptotic mechanism in the carcinogenesis of PDAC (Lüttges et al., 2003). For instance, as mentioned in the previous section (2. 2. 1. 4), different molecular subtypes of PDAC were proposed where the BH3-only gene *NOXA* was highlighted for being overexpressed in the most aggressive subtype correlating with poor overall survival (Birnbaum et al., 2016; Collisson et al., 2011).

2. 3. 3. NOXA as a prognostic marker of PDAC

The tumor cell death-inducing BH3-only protein NOXA, also known as *PMAIP1*, shows selective cell killing potency and it is the least potent of apoptosis inducers in comparison to the other pro-apoptotic proteins. However, NOXA becomes the dominant cell death inducer in response to this stimulus after oncogenic transformation (Naik et al., 2007) . It was shown that its overexpression via mRNA upregulation and/or protein stabilization after proteasome inhibition led to apoptotic cell death (Lankes et al., 2020; Nikiforov et al., 2007; Wirth et al., 2014) . NOXA expression can act as an efficient apoptotic sensitizer in HDAC2 depleted cells when treated with the topoisomerase II inhibitor, etoposide (Fritsche et al., 2009). On the other hand, loss of NOXA proved to be a key player in drug-resistance mechanisms in targeted

therapies such as the BH3 mimetic compound venetoclax in B-cell malignancies (Jullien et al., 2020). When downregulated, MCL-1 addiction of the cells increases thus binding more freely to BAX/BAK and now BIM, producing a potent antagonism to apoptosis (Montero et al., 2019). To date, it is known that *NOXA* expression can be activated via canonical *TP53* intrinsic apoptotic pathway (Oda et al., 2000; Villunger et al., 2003), *E2F Transcription Factor 1* (Hershko & Ginsberg, 2004), *MYC* and *EGR1* (Wirth et al., 2014) and *transcriptional factor hypoxia-inducible factor 1* (HIF-1α) (J. Y. Kim et al., 2004). Moreover, it interacts with several anti- and pro- apoptotic proteins (Fig. 2).

Even though NOXA seems to play a tumor suppressor role in the cells, this pro-apoptotic protein expression strongly correlates with poor prognosis in pancreatic cancer patients (Birnbaum et al., 2016) as well as in the retrospective analysis of the quasi-mesenchymal subtype (Fig. 1). It seems plausible that the cell-death-inducing NOXA could be a prognostic marker for this malignant PDAC subtype for which there are no specific therapies. As described in the previous sections, the complex interplay of pro- and anti- apoptotic proteins determines whether a tumor cell survives or dies, and the balance of these proteins is decisively influenced by therapeutics. In this context, the death-inducing BH3-only proteins must be activated by specific therapeutics in order to trigger apoptosis (Happo & Strasser, 2012). Therefore, pharmacological activation of NOXA and shift of the MCL-1/NOXA apoptotic balance may help to drive cell death and overcome apoptosis evasion.

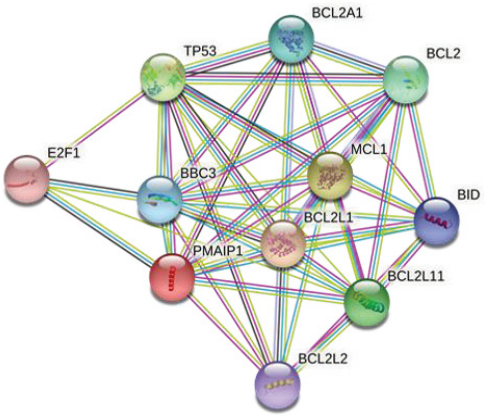

Figure 2: *NOXA* and its main interacting partners. A) String network analysis of NOXA (*PMAIP1*) main interacting proteins/genes. *BLC2L11* (BIM); *BCL2L*, BLC-W; *BBC3*, (PUMA). The freely available STRING database https://string-db.org (version 10.5) was used for the generation of this string network, which finds connections between genes using the following criteria: known interactions, predicted and others. Color code as follows: “known interactions”, light blue: from curated databases, pink: experimentally determined; “predicted interactions”, green: gene neighborhood, red: gene fusions; “others”, yellow: text-mining, black: co-expression.

2. 4. Cell cycle

The cell cycle is a complex biological process involved in growth and proliferation of the cells, DNA repair, tissue hyperplasia in response to injury and diseases such as cancer. The cell cycle is divided into “gap 1” (G1) phase, synthesis (S) phase, “gap 2” (G2) phase and mitosis (M) phase (Fig. 3) and gives as a result two daughter cells. In G1, the first “gap”, the cells are preparing for DNA synthesis. The replication of the DNA takes place in the S phase where the cells synthesize DNA, thus being temporarily aneuploid (between 2n and 4n). In G2, the second “gap”, the cells are preparing for mitosis or M phase (Schafer, 1998; Vermeulen et al., 2003). This process is tightly regulated by proteins called cyclins and cyclin-dependent kinases (CDKs), a family of serine/threonine protein kinases that are activated at specific points of the cell cycle and promote enter in the next phase by phosphorylation of their targets (Murray, 2004).

There are quality control points before each phase change in the cells to protect the integrity of the DNA. In response to DNA damage given by different reasons such as the administration of cytostatic compounds, checkpoint proteins arrest the cell cycle to provide time for DNA repair. DNA damage checkpoints are positioned before the cell enters S phase (G1-S checkpoint) or after DNA replication (G2-M checkpoint). Noteworthy, these kinds of controls are dysregulated and/or inactivated in tumor cells producing uncontrolled cell cycle progression and unlimited proliferation.

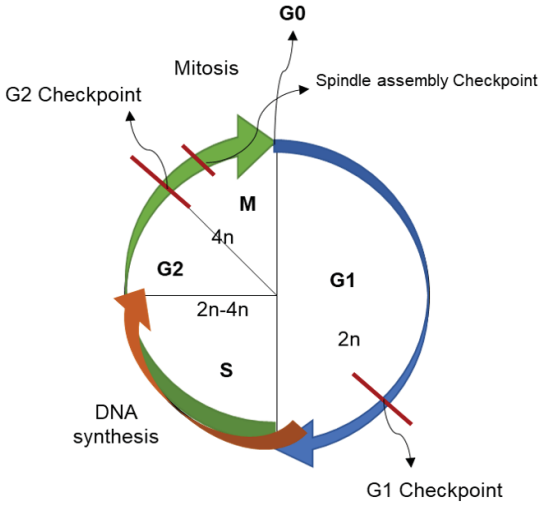

Figure 3: Cell cycle phases. Schematic drawing of normal cell cycle progression (self-made, inspired on (Schafer, 1998; Vermeulen et al., 2003). Once a cell divides (Mitosis), it can terminally differentiate, enter a quiescent state or G0, or start the cycle again. In the G1 quality control it is assessed the cell size, nutrients, growth factor and DNA damage. After the cell passes this checkpoint, it enters in the S phase, where the DNA is duplicated. Next, in G2 the cell undergoes a second quality control in which it is checked the cell size and DNA replication. Errors in this checkpoint can lead to cellular arrest and posterior resting state or arrest. Finally, before dividing into 2 daughter cells there is a minor checkpoint in which it is tested the correct attachment of the chromosomes to the mitotic spindle. 2n and 4n: DNA content.

2. 5. Epigenetics and transcriptional regulation

2. 5. 1. Chromatin modifications

The nucleosome is the unit of chromatin in which the DNA is packaged inside the nucleus of a cell and it is composed of an octamer of the four core histones (H3, H4, H2A, H2B) around which 147 base pairs of DNA are wrapped. The most remarkable feature of the histones, apart from the amino-acidic tail at the N-terminus, is the large number of residues they possess. Histone tails can be covalently modified with different residual groups, among which the most studied ones are acetylation, methylation, and phosphorylation. According to the kind and amount of these modifications on the histone tails, the chromatin will be condensed or relaxed, apart from being characteristic of different genomic features (e.g., enhancers, insulator regions, promoters). For example, the mono-methylation of lysine 4 at the histone 3, denoted as H3K4me1, marks an open enhancer, whereas the tri-methylation of the same lysine, H3K4me3, is an abundant mark of active promoters (Calo & Wysocka, 2013; Pekowska et al.,

2011). Active chromatin is generally associated with acetylation of the histones H2A, H3 and H4, from which the most studied is the acetylation of the lysine 27 of the H3, H3K27ac (Kouzarides, 2007). Listed in the table 1 are the chromatin signatures characteristic of regulatory elements and the current approaches used to map them (Spicuglia & Vanhille, 2012).

Table 1. Current techniques used to map genomic features

Approach	Activity	Specificity
FAIRE	Open	Non
P300 (ChIP-seq)	Open	Enh.=Prom.
H3K4me1 (ChIP-seq)	Open	Enh.>Prom.
H3K4me2 (ChIP-seq)	Open	Enh.=Prom.
H3K27ac (ChIP-seq)	Active	Enh.>Prom.
H3K4me3 (ChIP-seq)	Active	Prom.>Enh.

Table adapted from (Spicuglia & Vanhille, 2012). Activity refers to the characteristics in terms of discriminating between poised and active enhancers. The statement “open” refers to the approach which identifies both poised and active enhancers indiscriminately. For some cases, there might be observed a quantitative difference between poised and active enhancer in chromatin accessibility or in enrichment of a specified transcription factor, histone modification, etc. “Specifity” makes reference to whether the technique preferentially detects enhancers (Enh. > Prom.), promoters (Prom. < Enh.) or both regions (Enh. = Prom.).

2. 5. 2. The transcription factor MYC

MYC (myelocytomatosis oncogene) is a transcription factor which is often activated in tumorigenesis by chromosomal rearrangements as well as epigenetics events (Boxer & Dang, 2001; Daniell, 2012; Eilers & Eisenman, 2008) in more than half of human tumors (Escot et al., 1986; Gamberi et al., 1998; Kawate et al., 1999; Ladanyi et al., 1993). MYC is a basic helix-loop-helix leucine-zipper, which heterodimerizes with the MYC-associated factor X (MAX) and binds to E-boxes in the promoters and enhancer regions of genes, influencing a wide variety of cellular processes, such as, growth, proliferation or differentiation are influenced (Eilers & Eisenman, 2008).

The most recent studies In PDAC demonstrated that MYC can act as the sole driver, together with *KRAS* oncogenic mutation, of cancerogenesis (Sodir et al., 2020). Efforts have been made to utilize this transcription factor as a bio-marker for an aggressive subtype of pancreatic

cancer, where it was showed that its high expression correlates with poor patient prognosis and predicts sensitivity towards SUMO inhibition (Biederstädt et al., 2020) and proteasome inhibition (Lankes et al., 2020). The collaboration between oncogenic *KRAS* mutation and *MYC* overexpression continues to be studied, and recently it was shown how this contributes to evade immune response in adenocarcinomas (Kortlever et al., 2017).

It was previously described that MYC and EGR1 collaborate to trigger cell death by activating the pro-apoptotic proteins NOXA and BIM (Wirth et al., 2014). Moreover, *MYC* repression given by RUNX1 recruitment of Polycomb Repressive Complex 1 (PRC1) in the context of Acute Myeloid Leukemia (AML) proved to activate apoptosis within short hours of drug treatment (Pulikkan et al., 2018).

2. 5. 3. RUNX transcription factor family

Runt-related (RUNX) family proteins are master regulators involved in a broad range of biological processes including proliferation and apoptosis (Chuang et al., 2013). This family is composed of three members: RUNX1, RUNX2 and RUNX3, each one of them playing a distinct role in embryonic development (Mevel et al., 2019). They could act either as transcriptional activators or repressors, depending on many factors, such as cell type, target gene and collaborating co-factors. Given these attributes, in the context of cancer biology they can behave as tumor suppressors or oncogenes as reviewed previously (Otálora-Otálora et al., 2019). These transcription factors bind to the target DNA with higher affinity as well as with a higher stabilization by coupling with a non-DNA-binding protein called core binding factor beta (CBFβ).

RUNX1 is known to be involved in normal hematopoiesis development and function. Given that it plays a key role in this process, knockout mice for this gene are embryonic lethal due to a complete failure of hematopoiesis (Okuda et al., 1996). Probably due to its key role in hematopoiesis, RUNX1 is one of the most frequently mutated genes in a variety of hematological malignancies, such as AML (Gaidzik et al., 2016; Sood et al., 2017; Yokota et al., 2020).

RUNX2 is a key transcription factor for bone development (osteogenesis) and osteoblast differentiation (Carbonare et al., 2012; Vimalraj et al., 2015; Yoshida et al., 2004). This gene was found to be amplified in some osteosarcomas, in correspondence to its role in osteosarcoma-genesis (Lau et al., 2004; Lou et al., 2009). In a recent review, the authors claim that there is enough evidence to link this transcription factor to mammary lineage and a "context-dependent role in breast cancer" by using a mouse model where *Runx2* is driven by a specific mammary promoter in which they found that *Runx2* expression restricts the development of pubertal glands thus producing a failure in milk production (Ferrari et al., 2013; McDonald et al., 2014; Owens et al., 2014). Interestingly, it was found that *RUNX2* depletion in osteosarcoma cells carrying a loss-of-function mutation of the tumor suppressor *p53* overcame apoptosis resistance presumably due to *MYC* downregulation, underscoring the need to target such tumor survival signaling pathways (Shin et al., 2016).

RUNX3 plays an important role in development of gastrointestinal tract (Fukamachi & Ito, 2004) and development of dorsal root ganglion neurons (Inoue et al., 2002; Levanon et al., 2002). Its expression and loss-of-function point mutation are involved in progression of human gastric cancer (Q. L. Li et al., 2002) and, notably, its expression has been linked with pathogenesis in PDAC (J. Li et al., 2004). Moreover, it was demonstrated in a mouse model that depending on the dosage of *Smad4*, *Runx3* can behave either as a tumor suppressor or as an oncogene, inhibiting or promoting metastatic growth respectively (Whittle et al., 2015).

2. 5. 3. 1. RUNX1-CBFβ interaction

RUNX1 is strongly expressed in a broad spectrum of epithelial tumors such as skin, esophageal, lung, colon and also breast tumors (Scheitz et al., 2012; Scheitz & Tumbar, 2013) and its overexpression is associated with poor prognosis in PDAC (Birnbaum et al., 2016).

RUNX1 and its binding partner, CBFβ, are targets of many mutations in different kinds of cancers, as described in section 2. 5. 3. To target this specific interaction, a group of researchers performed a small molecule screening of the National Cancer Institute for compounds that interrupt the binding of the oncofusion CBFβ-SMMHC to the Runt domain of

RUNX1 (Illendula et al., 2015, 2016). They developed and perfected a monovalent compound that interrupts the RUNX1-CBFβ interaction, also referred as wild type, and a bivalent compound (AI-10-49) which targets more specifically the interaction between RUNX1 and the oncofusion CBFβ-SMMHC (present in one subtype of AML). It is known that in cells lacking the fusion protein, AI-10-49 may act like the monomeric lead molecule and inhibit wild type CBFβ-RUNX1. Later it was described its molecular mode of action, research in which it is shown that upon interruption of this interaction, RUNX1 is released from the CBFβ-SMMHC complex and changes its target genes, one of them being *MYC*, represses its expression and consequently apoptosis is activated (Pulikkan et al., 2018).

Little is known about the role of RUNX1 in the PDAC context, yet Cheng and collaborators showed that it can exert an oncogenic role in pancreatic cancer by negative regulation of the microRNA *miR-93* (Cheng et al., 2017) and patients presenting overexpression of *RUNX1* are grouped as high-risk with shorter survival (Birnbaum et al., 2016).

3. Aim

The career on the development of new therapeutic strategies accompanied by molecular understanding of the mechanism behind its action, has been a long subject of study in many cancers. Nevertheless, in pancreatic cancer starting from the patient stratification to their outcome, only small improvements have been made in the last years. It is believed that a thorough investigation of histological, molecular pathways and mutational landscape of the tumor samples as well as microenvironment could shed light on the high heterogeneity of PDAC. By means of this kind of study I might gain a deeper comprehension of different phenomena that are implicated in chemotherapeutics failure, such as apoptosis evasion and therapy resistance. Therefore, I aim to identify novel compounds that affect *NOXA* expression to exploit its pro-apoptotic function as a potential therapeutic option for an aggressive PDAC subtype (*NOXA*^{high}) and unravel the molecular mechanisms behind its mode of action.

4. Materials and methods

4. 1. Materials

4. 1. 1. Equipment

Table 2. Laboratory equipment

Instrument	Company
Agilent Bioanalyzer 2100	Agilent technologies, Santa Clara, USA
Camera	Carl Zeiss (Suzhou) Co., Ltd, China
Cell incubator (Heraeus Hera cell 240)	Heraeus, Hanau, Germany
ChemoStar PLUS Imager	Intas Science Imaging Instruments GmbH, Göttingen, Germany
Countess II FL Automated Cell Counter	Invitrogen by Life Technologies, Carlsbad, USA
Cytoflex S	Beckman Coulter, Brea, USA
Electrophoresis chamber	Bio-Rad Laboratories GmbH, Munich, Germany
Eppendorf Centrifuge 5417R	Eppendorf AG, Hamburg, Germany
Eppendorf Mastercycler PCR device	Eppendorf AG, Hamburg, Germany
Eppendorf Minispin Plus Centrifuge	Eppendorf AG, Hamburg, Germany
Epifluorescence microscope	Carl Zeiss Microscopy GmbH, Jena, Germany
Fridges and lab freezers	Liebherr-Hausgeräte GmbH, Ochsenhausen, Germany
GelDoc System Universal Hood II	Bio-Rad Laboratories GmbH, Munich, Germany
Glassware Duran®	Labware SCHOTT AG, Mainz, Germany
Incucyte® Live-Cell Analysis	Sartorius Lab Instruments GbmH & Co.KG, Göttingen, Germany
Liquid nitrogen tank Biosafe® MDβ	Cryotherm GmbH & Co. KG, Kirchen, Germany
Magnetic Stirrer MS 3000	neoLab Migge GmbH, Heidelberg, Germany
Magnetic stand DynaMag™-96 Side	Invitrogen by Life Technologies, Carlsbad, USA
Magnetic stand DynaMag™-2	Invitrogen by Life Technologies, Carlsbad, USA
Microplate reader - Luminometer	Berthold Technologies, Bad Wildbad, Germany
Microwave Oven	Commercial
Multi-Channel Pipettes Research Plus®	Eppendorf AG, Hamburg, Germany
Multi-Channel Pipette (electronic)	Brand GbmH & Co KG, Mannheim, Germany
Multi-step pipette	Eppendorf AG, Hamburg, Germany
NanoDrop 2000c	Thermo Fisher Scientific, Waltham, USA
Neubauer hemocytometer	Paul Marienfeld GmbH & Co. KG, Lauda-Königshofen, Germany
pH-meter HI2020 edge R	Hanna instruments, Woonsocket, USA
Pipetboy	Integra Biosciences Ag from INTEGRA Holding AG
Pipettes Research Plus®	Eppendorf AG, Hamburg, Germany
Power Pac 200	Bio-Rad Laboratories GmbH, Munich, Germany
Power Pac P25T	Biometra GmbH, Göttingen, Germany
Pump tube (Sample pump) kits	Beckman Coulter, Brea, USA
QuantiFluor® ONE dsDNA System	Promega Corporation, Madison, USA
Quintix® Analytical balance	Sartorius Lab Instruments GbmH & Co.KG, Göttingen, Germanyct

Safety cabinet HERAsafe® HSP18	Heraeus, Hanau, Germany
SDS-Gel electrophoresis chamber (Multigel Long)	Biometra GmbH, Göttingen, Germany
Spectophotometer CLARIOstar	BMG Labtech, Ortenberg, Germany
StepOne Plus tm Real-time PCR System	Applied Biosystem, Forster City, Usa
Vortex Genie 2	Bender&Hobein AG, Zürich, Switzerland
Vortex	neoLab Migge GmbH, Heidelberg, Germany
Water bath	Memmert GmbH + Co. KG, Schwabach, Germany
Wet-transfer device	Bio-Rad Laboratories GmbH, Munich, Germany

4. 1. 2. Chemicals and reagents

4. 1. 2. 1. Chemicals and reagents

Table 3. Chemicals

Reagent	Company
2-Mercaptoethanol, 50 mM	Sigma-Aldrich, St. Louis, USA
Acetic acid	Carl Roth GmbH + Co. KG, Karlsruhe, Germany
Acrylamide-Bisacrylamide mixture (37.5:1)	Carl Roth GmbH + Co. KG, Karlsruhe, Germany
Adenosine triphosphate (ATP)	Sigma-Aldrich, St. Louis, USA
Agarose	Byozim Scientific GmbH, Hessisch Oldendorf, Germany
AI-10-49	BIOZOL Diagnostica Vertrieb GmbH, Eching, Germany
Ammonium persulfate (APS)	Sigma-Aldrich, St. Louis, USA
Annexin V binding buffer (10X)	BD Pharmigen Inc, San Diego, USA
Bio-Rad Protein Assay Dye Reagent Concentrate (5X)	Bio-Rad Laboratories GmbH, Munich, Germany
Bovine Serum Albumin (BSA)	Carl Roth GmbH + Co. KG, Karlsruhe, Germany
Bromophenol blue	Sigma-Aldrich, St. Louis, USA
Calcium chloride ($CaCl_2$)	Sigma-Aldrich, St. Louis, USA
CellTiter-Glo Luminescent Cell Viability	Promega Corporation, Madison, USA
CytoFLEX Sheath Fluid	Beckman Coulter, Brea, USA
DAPI (4',6-Diamidino-2-Phenylindole, Dihydrochloride)	Invitrogen by Life Technologies, Carlsbad, USA
Dimethylsulfoxid (DMSO)	Carl Roth GmbH + Co. KG, Karlsruhe, Germany
Dithiothreitol (DTT)	Sigma-Aldrich, St. Louis, USA
Ethanol 70%	Carl Roth GmbH + Co. KG, Karlsruhe, Germany
Ethanol absolut	Nunc A/S, Roskilde, Denmark
Ethylenediaminetetraacetic acid (EDTA)	Carl Roth GmbH + Co. KG, Karlsruhe, Germany
Formaldehyde solution 37%	Carl Roth GmbH + Co. KG, Karlsruhe, Germany
Giemsa	Sigma-Aldrich, St. Louis, USA
Glycerol for molecular biology	Sigma-Aldrich, St. Louis, USA
Glycine	Carl Roth GmbH + Co. KG, Karlsruhe, Germany
Glycogen (from mussels)	Sigma-Aldrich, St. Louis, USA
Hydrogen chloride (HCl)	Merck KGaA, Darmstadt, Germany

IGEPAL CA-630	Sigma-Aldrich, St. Louis, USA
Isopropanol	Carl Roth GmbH + Co. KG, Karlsruhe, Germany
Kit ECL Prime detection reagent	GE Healthcare
LB-Agar (Luria/Miller)	Carl Roth GmbH + Co. KG, Karlsruhe, Germany
Magnesium chloride ($MgCl_2$)	Sigma-Aldrich, St. Louis, USA
Magnesium sulfate ($MgSO_4$)	Sigma-Aldrich, St. Louis, USA
Methanol	Carl Roth GmbH + Co. KG, Karlsruhe, Germany
N, N, N ', N'-Tetramethylethylenediamine (TEMED)	Sigma-Aldrich, St. Louis, USA
NP-40	Sigma-Aldrich, St. Louis, USA
Phenol – chloroform – isoamyl alcohol mixture	Sigma-Aldrich, St. Louis, USA
Polyethylene glycol 4000	Carl Roth GmbH + Co. KG, Karlsruhe, Germany
Ponceau Staining solution	VWR International, Radnor, USA
Potassium chloride (KCl)	Merck KGaA, Darmstadt, Germany
Propidium iodide (PI)	Sigma-Aldrich, St. Louis, USA
Restore™ PLUS Western Blot Stripping Buffer	Thermo Fisher Scientific, Waltham, USA
RNase*Zap*™-RNase Decontamination Wipes	Invitrogen by Thermo Fisher Scientific, Waltham, USA
Skim milk powder	Carl Roth GmbH + Co. KG, Karlsruhe, Germany
Sodium acetate anhydrous (NaOAc)	Merck KGaA, Darmstadt, Germany
Sodium chloride (NaCl)	Carl Roth GmbH + Co. KG, Karlsruhe, Germany
Sodium deoxycholate detergent	Sigma-Aldrich, St. Louis, USA
Sodium dodecyl sulfate (SDS pellets)	Carl Roth GmbH + Co. KG, Karlsruhe, Germany
Sodium hydroxide (NaOH)	Carl Roth GmbH + Co. KG, Karlsruhe, Germany
Thiazolyl Blue Tetrazolium Bromide (MTT solution)	Sigma-Aldrich, St. Louis, USA
Trichlormethan/Chloroform	Sigma-Aldrich, St. Louis, USA
Tris (hydroxymethyl) aminomethane HCl (Tris HCl)	Carl Roth GmbH + Co. KG, Karlsruhe, Germany
Triton X-100 (t-Octylphenoxypolyethoxyethanol)	Sigma-Aldrich, St. Louis, USA
Trypan Blue	Sigma-Aldrich, St. Louis, USA
Tryptone	Sigma-Aldrich, St. Louis, USA
Tween® 20 molecular biology grade	Serva Electrophoresis GmbH, Heidelberg, Germany
Yeast extract	BD Biosciences, Franklin Lakes, USA

4. 1. 2. 2. Buffers and solutions

Table 4. Buffers and solutions

Buffer/Solution	Composition
10X TBS (Tris-buffer saline) for WB in ddH_2O (pH 7.6)	0.2 M Tris-HCl 1.4 M NaCl
1X TBS-T	1X TBS + Tween20 0.1%

10X Running buffer (SDS-PAGE) in ddH_2O (pH 7.4)	35 mM SDS 0.25 M Tris HCl 2 M Glycine
10X Transfer buffer for wet blot in ddH_2O	0.25 M Tris HCl 2 M Glycine
1X Transfer buffer for wet blot	1 part transfer buffer 10 X 2 parts Methanol 100% 7 parts ddH_2O
Stacking gel buffer (SDS-PAGE) in ddH_2O	0.5 M Tris HCl pH 6.8
Resolving gel buffer (SDS-PAGE) in ddH_2O	1.5 M Tris HCl pH 8.8
Stacking gel (5%) (SDS-PAGE)	3 ml ddH_2O 1.3 ml stacking buffer 750 µl Acrylamide-bisacrylamide mixture 25 µl APS 10% 10 µl TEMED
Resolving gel (10%) (SDS-PAGE)	4.1 ml ddH_2O 2.6 ml resolving buffer 3.3 ml Acrylamide-bisacrylamide mixture 100 µl SDS 10% 50 µl APS 10% 15 µl TEMED
Gradient gel-heavy gel (20%) (SDS-PAGE)	2 ml resolving buffer 800 µl Glycerol 5.08 ml Acrylamide-bisacrylamide mixture 80 µl SDS 10% 40 µl APS 10% 4 µl TEMED
Gradient gel-light gel (10%) (SDS-PAGE)	2 ml resolving buffer 3.228 ddH_20 2.652 ml Acrylamide-bisacrylamide mixture 80 µl SDS 10% 40 µl APS 10% 4 µl TEMED
Blocking solution for WB	BSA 5% in TBS-T
Stripping buffer for WB	1 part Methanol 1 part Acetic acid 8 parts ddH_2O
5X Loading buffer for SDS-PAGE (Laemmli) pH 6.8	0.35 M SDS 25 ml Glycerol 0.23 M Tris HCl 0.75 mM Bromophenol blue 2.5 ml 2-Mercaptoethanol to 50 ml of H_2O
RIPA buffer for protein isolation in ddH_2O	150 mM NaCl 1% NP-40 0.5% Sodium deoxycholate 0.1% SDS

	50 mM Tris HCl (pH 8.0) 1 mM PMSF 2X Protease inhibitor 2X Phosphatase inhibitor
10X PBS (Phosphate buffer saline) in ddH_2O (pH 7.4)	1.4 M NaCl 27 mM KCl 0.1 M Na_2HPO_4
50X TAE (Tris-Acetate-EDTA buffer) in ddH_2O	2 M Tris-HCl 0.95 M Acetic acid 50 mM EDTA pH 8.0
TE (Tris-EDTA) buffer	10 mM Tris HCl pH 8.0 1 mM EDTA
Lysis buffer for 4C in ddH_2O	10 mM NaCl 250 mM Tris HCl (pH 8.0) 0.2% NP-40 1X Protease inhibitor
Ligation buffer for 4C in ddH_2O	50 mM Tris HCl (pH 7.6) 10 mM $MgCl_2$ 1 mM ATP 1 mM DTT
MTT solution in ddH_2O	5 mg/ml Thiazolyl Blue
DAPI solution for apoptosis assay in PBS	10 µg/ml DAPI
5X KCM buffer for bacteria chemical transformation in ddH_2O	2 M KCl 1 M $CaCl_2$ 1M $MgCl_2$
Propidium Iodide (PI) solution for cell cycle	0.2 µg/ml PI
ChIP buffers	Supplied in the kit

4. 1. 3. Cell culture

4. 1. 3. 1. Medium and reagents

Table 5. Cell culture medium, antibiotics and transfection reagents

Medium/antibiotic	Company
Ampicilin	Carl Roth GmbH + Co. KG, Karlsruhe, Germany
Ampuwa water (distilled and sterile) ddH_2O	Fresenius SE & Co. KGaA, Bad Homburg vor der Höhe, Germany
Antibiotic-Antimycotic (100X)	Thermo Fisher Scientific, Waltham, USA
Blasticidin S	Thermo Fisher Scientific, Waltham, USA
Dulbecco's Modified Eagle Medium (DMEM), high glucose	Thermo Fisher Scientific, Waltham, USA
Dulbecco's phosphate-buffered saline (DPBS)	Gibco by Thermo Fisher Scientific, Waltham, USA
Fetal Bovine Serum (FBS)	Gibco by Thermo Fisher Scientific, Waltham, USA
Hygromycin	Carl Roth GmbH + Co. KG, Karlsruhe, Germany

G418 (Geneticin) solution	Roche Diagnostics GmbH, Mannheim, Germany
Kanamycin	Sigma-Aldrich, St. Louis, USA
Lipofectamine 2000 Transfection Reagent-	Invitrogen by Life Technologies, Carlsbad, USA
Opti-MEM, Reduced Serum Media, no phenol red	Thermo Fisher Scientific, Waltham, USA
Polyethylenimine (PEI)	Sigma-Aldrich, St. Louis, USA
Polybrene Infection Reagent	Merck Milipore from Merck KGaA, Burlington, USA
Puromycin solution	Gibco by Thermo Fisher Scientific, Waltham, USA
Roswell Park Memorial Institute (RPMI) 1640 Medium	Thermo Fisher Scientific, Waltham, USA
Trypsin-EDTA (0.5%), no phenol red, 10X	Gibco by Thermo Fisher Scientific, Waltham, USA

4. 1. 3. 2. Cell lines

Table 6. Cell lines

Cell line	Organism	Tissue	Disease	Provider	Relevant aberrations
HEK293T	human	Embryonic kidney	NA	Dr. Matthias Wirth	*NA*
MIAPaCa-2	human	Pancreas	Carcinoma	ATCC, Manassas, USA	*CDKN2A-/-*; *KRASG12C*; *TP53R248W*
Panc1	human	Pancreas/duct	Epithelioid carcinoma	ATCC, Manassas, USA	*CDKN2A-/-*; *KRASG12D*; *TP53R282W*
PSN1	human	Pancreas	Adenocarcinoma	ATCC, Manassas, USA	*CDKN2A-/-*; *KRASG12R*; *TP53K132Q*
PaTu8988T	human	Pancreas	Adenocarcinoma	DSMZ, Braunschweig	*KRASG12V*; *TP53R282W*; *SMAD4-/-*
mPDAC-06	murine	Pancreas	Adenocarcinoma	Dr. Matthias Wirth	*Pdx1-Cre*; *LSL-KrasG12D*
mPDAC-95	murine	Pancreas	Adenocarcinoma	Dr. Matthias Wirth	*Pdx1-Cre; LSL-KrasG12D*

4. 1. 4. Consumables

Table 7. Laboratory plasticware and consumables

Consumable	Company
96-well cell culture plate, flat bottom	Sarstedt AG & Co., Nümbrecht, Germany
96-well cell culture plate, white	Nunc A/S, Roskilde, Denmark
96-well deep well, 2 ml	VWR International, Radnor, USA
48-well cell culture plate (Corning™ Falcon™)	Nunc A/S, Roskilde, Denmark

12-well cell culture plate (Corning™ Falcon™)	Nunc A/S, Roskilde, Denmark
24-well plate Falcon (Corning™ Falcon™)	Nunc A/S, Roskilde, Denmark
6-well plate Falcon (Corning™ Falcon™)	Nunc A/S, Roskilde, Denmark
Cell culture flasks 25 cm², 75 cm², 175 cm²	Nunc A/S, Roskilde, Denmark
Cell culture dish 10 cm, 15 cm	Sarstedt AG & Co., Nümbrecht, Germany
Cell scraper 25 cm, sterile	Sarstedt AG & Co., Nümbrecht, Germany
Conical tube 15 ml (Corning™ Falcon™)	Thermo Fisher Scientific, Waltham, USA
Conical tube 50 ml (Corning™ Falcon™)	Thermo Fisher Scientific, Waltham, USA
Multi-step tips, sterile, combitips advanced, 1.0 ml, 5 ml	Eppendorf AG, Hamburg, Germany
Countess Cell Counting Chamber Slides	Thermo Fisher Scientific, Waltham, USA
Cryovials 2 ml	Sarstedt AG & Co., Nümbrecht, Germany
FACS tubes	Sarstedt AG & Co., Nümbrecht, Germany
Filter tips sterile 200 µl, 100 µl, 20 µl Biosphere®	VWR International, Radnor, USA
Filter tips sterile 1250 µl	Greiner Bio-One GmbH, Frickenhausen, Germany
Filter 0.45 µm	neoLab Migge GmbH, Heidelberg, Germany
Glass Pasteur pipette 150 mm	Brand GbmH & Co KG, Mannheim, Germany
Parafilm	Brand GbmH & Co KG, Mannheim, Germany
Pipette tips 1250 µL, non-sterile	Greiner Bio-One GmbH, Frickenhausen, Germany
Pipette tips 2-200, 20 µL, non-sterile	Sarstedt AG & Co., Nümbrecht, Germany
PCR-strips Single Cap 8er-Soft-Strips 0.2 ml	Byozim Scientific GmbH, Hessisch Oldendorf, Germany
PCR plate 96-well	Eppendorf AG, Hamburg, Germany
Reaction tube 1.5 ml, 2 ml safe seal	Sarstedt AG & Co., Nümbrecht, Germany
Serological pipette 5 ml, 10 ml, 25 ml	Nunc A/S, Roskilde, Denmark

4. 1. 5. Molecular biology reagents

Table 8. Molecular biology reagents

Reagent	Company
1 kb Plus DNA Ladder	New England Biolabs GmbH, Frankfurt/Main, Germany
cOmplete Mini, EDTA-free (Protease inhibitor cocktail tablets)	Roche Diagnostics GmbH, Mannheim, Germany
Custom-made oligos	IDT Biologika GmbH, Dessau-Roßlau, Germany
DNA Ladder 100 bp	New England Biolabs GmbH, Frankfurt/Main, Germany
dNTP mix, 10 mM	Rapidozym GmbH, Berlin, Germany
Gel blotting paper (Whatman®)	Merck KGaA, Burlington, USA
Gel Loading Dye Purple (6X)	New England Biolabs GmbH, Frankfurt/Main, Germany
Immun-Blot® PVDF Membrane 0.2 µm	Bio-Rad Laboratories GmbH, Munich, Germany
Immun-Blot® PVDF Membrane 0.45 µm	Thermo Fisher Scientific, Waltham, USA
MicroAmp Fast Optical 96-Well Reaction P	Thermo Fisher Scientific, Waltham, USA
Midori Green Advance NonToxic DNA and RNA staining	Nippon Genetics Europe GmbH, Düren, Germany

Nuclease-Free Water (not DEPC-Treated)	Thermo Fisher Scientific, Waltham, USA
PageRuler™ Plus Prestained Protein Ladder, 10 to 250 kDa	Thermo Fisher Scientific, Waltham, USA
PHOSSTOP, 10 TABLETS	Roche Diagnostics GmbH, Mannheim, Germany
Random Hexamer Primer	Thermo Fisher Scientific, Waltham, USA

Table 9. Kits and enzymes

Kit/enzyme	Company
Agilent High Sensitivity DNA Kit	Agilent Technologies, Santa Clara, USA
Agilent RNA 6000 Pico Kit	Agilent Technologies, Santa Clara, USA
BbsI-HF	New England Biolabs GmbH, Frankfurt am Main, Germany
BsmBI	New England Biolabs GmbH, Frankfurt am Main, Germany
DNA 1000 Kit & Reagents	Agilent Technologies, Santa Clara, USA
DpnII	New England Biolabs GmbH, Frankfurt am Main, Germany
Expand™ Long Template PCR System	Roche Diagnostics GmbH, Mannheim, Germany
HiSpeed Plasmid Maxi Kit	Qiagen, Hilden, Germany
MMLV High Performance Reverse Transcript	Byozim Scientific GmbH, Hessisch Oldendorf, Germany
NEBNext Poly(A) mRNA Magnetic Isolation	New England Biolabs GmbH, Frankfurt am Main, Germany
NEBNext Ultra II Directional RNA Library	New England Biolabs GmbH, Frankfurt am Main, Germany
NEBNext Ultra II Q5 Master Mix	New England Biolabs GmbH, Frankfurt am Main, Germany
NlaIII	New England Biolabs GmbH, Frankfurt am Main, Germany
Power SybrGreen 2X	Thermo Fisher Scientific, Waltham, USA
Protector Rnase inhibitor	Sigma-Aldrich by Merck KGaA, Darmstadt, Germany
Proteinase K Solution (20 mg/mL)	Thermo Fisher Scientific, Waltham, USA
Pure Yield Plasmid Miniprep System	Promega Corporation, Madison, USA
Qiagen MiniElute PCR Purification Kit	Qiagen, Hilden, Germany
QIAshredder	Qiagen, Hilden, Germany
Quick Ligation Kit	New England Biolabs GmbH, Frankfurt am Main, Germany
RiboLock RNase inhibitor	Thermo Fisher Scientific, Waltham, USA
RNase A	Sigma-Aldrich, St. Louis, USA
RNase-Free DNase Set	Qiagen, Hilden, Germany
RNeasy Micro Kit	Qiagen, Hilden, Germany
RNeasy Mini Kit	Qiagen, Hilden, Germany
SimpleChIP Enzymatic Chromatin IP Kit	Cell Signaling Technology Europe, Frankfurt am Main, Germany
T4 DNA Ligase	Thermo Fisher Scientific, Waltham, USA
Taq 2X Master Mix	New England Biolabs GmbH, Frankfurt/Main, Germany
Terra PCR Direct Polymerase Mix	Takara Bio Inc. by Takara Holding, Kusatsu, Japan
Wizard SV Gel and PCR Clean-Up System	Promega Corporation, Madison, USA

4. 1. 6. Bacteria culture and cloning

4. 1. 6. 1. Competent bacteria

Table 10. Bacteria strains

Strain	Source
DH5α *E. coli*	Thermo Fisher Scientific, Waltham, USA
Stbl3 *E. coli*	Thermo Fisher Scientific, Waltham, USA
Top10 *E. coli*	Thermo Fisher Scientific, Waltham, USA

4. 1. 6. 2. Plasmids

Table 11. Plasmids

Plasmid	Source	Accession number
px330-U6-Chimerich_BB-CBh-hSpCas9	gift, Prof. Rada Iglesias	NA
lenti dCAS-VP64_Blast	Addgene	61425
lenti MS2-P65-HSF1_Hygro	Addgene	61426
lenti sgRNA(MS2)_puro backbone	Addgene	73795
dCAS9-VP64_GFP	Addgene	61422
MS2-P65-HSF1_GFP	Addgene	61423
sgRNA(MS2) cloning backbone	Addgene	61424
psPAX2	Addgene	12260
pMD2.G	Addgene	12259

4. 1. 7. Antibodies

4. 1. 7. 1. FACS antibodies

Table 12. Annexin V for apoptosis assay

Antigen	Reactivity	Conjugation	Company	Reference
Annexin V	All mammals	647	BioLegend, San Diego, USA	640912

4. 1. 7. 2. Western blot antibodies

Table 13. Primary antibodies

Antigen	Host	Company	Reference	Dilution
NOXA	Mouse	Bio-Techne GmbH, Wiesbaden, Germany	DL000329946	1:500
MCL-1	Mouse	Bio-Rad Laboratories GmbH, Munich, Germany	VMA00507	1:1000

BCL-2 (124)	Mouse	Cell Signaling Technology Europe, Frankfurt am Main, Germany	15071	1:1000
BCL-XL (54H6)	Rabbit	Cell Signaling Technology Europe, Frankfurt am Main, Germany	2764	1:1000
MYC	Rabbit	Cell Signaling Technology Europe, Frankfurt am Main, Germany	9402	1:1000
Housekeeping	**Host**	**Company**	**Reference**	**Dilution**
Vinculin (E1E9V)	Rabbit	Cell Signaling Technology Europe, Frankfurt am Main, Germany	13901	1:10000
Actin (AC-15)	Mouse	Sigma-Aldrich, St. Louis, USA	A1978	1:10000
α-Tubulin	Rabbit	Abcam, Cambridge, United Kingdom	ab4074	1:10000

Table 14. Secondary antibodies

Reactivity	Conjugated	Company	Reference	Dilution
Anti-mouse	DyLight™ 800 4X PEG Conjugate	Cell Signaling Technology Europe, Frankfurt am Main, Germany	5257	1:5000
Anti-mouse	DyLight™ 680 Conjugate	Cell Signaling Technology Europe, Frankfurt am Main, Germany	5470	1:5000
Anti-rabbit	DyLight™ 800 4X PEG Conjugate	Cell Signaling Technology Europe, Frankfurt am Main, Germany	5151	1:5000
Anti-rabbit	DyLight™ 680 Conjugate	Cell Signaling Technology Europe, Frankfurt am Main, Germany	5366	1:5000
Anti-rabbit	HRP-linked	Sigma-Aldrich, St. Louis, USA	NA934	1:5000
Anti-mouse	HRP-linked	Sigma-Aldrich, St. Louis, USA	NA931	1:5000

4. 1. 7. 3. ChIP antibodies

Table 15. ChIP antibodies

Antibody	Company	Reference	Pull down
Acetyl-Histone H3 (Lys27) (D5E4)	Cell Signaling Technology Europe, Frankfurt am Main, Germany	8173	5 µg
RUNX1	Abcam, Cambridge, United Kingdom	ab23980	10 µg
CTCF (CCCTC-binding factor, zinc finger protein)	Active Motif, Inc., Carlsbad, USA	61311	4 µg

4. 1. 8. Oligonucleotides

4. 1. 8. 1. Genotyping PCR primers

Table 16. Genotyping primers CRISPR/Cas9 knockouts

KO/WT Allele primer	Sequence	Target
FWD_KO	CACTAGTGTGGGCGTATTAGG	human *NOXA* (*PMAIP1*)
REV_KO	GATGTATTCCATCTTCCGTTTCC	human *NOXA* (*PMAIP1*)
Internal_REV	GTTCAGTTTGTCTCCAAATCTCC	human *NOXA* (*PMAIP1*)
FWD_KO	GGATTCCAGCGCTGGTGCTG	murine Noxa (*PMAIP1*)
REV_KO	TGCAGGCGCGTACATTCTAGCCC	murine *Noxa* (*PMAIP1*)
Internal_REV	TCAGAAACGCCGCGGCGATCT	murine *Noxa* (*PMAIP1*)
FWD_KO	CCGTAGATGCCAGCACGAGC	human *RUNX1*
REV_KO	TGGGTTTGTTGCCATGAAACG	human *RUNX1*
Internal_FWD	GTTATCATTGCTATTCCTCTGC	human *RUNX1*
FWD_KO	GGTGCTTCAGAACTGGGCCCT	human *RUNX2*
REV_KO	GTAGATAGCTAATCGATATAC	human *RUNX2*
Internal_REV	TGGCAGGTAGGTGTGGTAGTG	human *RUNX2*
FWD_KO	CAACAGCCAACCAAGTGAATCC	human *RUNX3*
REV_KO	CCTTGAAGGCGACGGGCAGC	human *RUNX3*
Internal_REV	CAGTGGAGGGACGTGGTCCG	human *RUNX3*

Table 17. sgRNAs for CRISPR/Cas9 knockout and CRISPRa

Name	sgRNA without PAM	Gene
sgRNA_1_KO	TCGAGTGTGCTACTCAACTC	human *NOXA* (*PMAIP1*)
sgRNA_2_KO	TGTAATTGAGAGGAATGTGA	human *NOXA* (*PMAIP1*)
sgRNA_1_KO	TTGCGCAGCCCGAGTCTTGG	murine *NOXA* (*PMAIP1*)
sgRNA_2_KO	ACGCGCCAGTGAACCCAACG	murine *NOXA* (*PMAIP1*)
sgRNA_CRISPRa	AAAGCGTGGTCTCTGGCG	human *NOXA* (*PMAIP1*)
sgRNA_1_KO	GAGCCCAGGCAAGATGAGCG	human *RUNX1*
sgRNA_2_KO	GCCATCTGGAACATCCCCTA	human *RUNX1*
sgRNA_1_KO	TGGCTGGATAGTGCATTCGT	human *RUNX2*
sgRNA_2_KO	ATATTGAAATTCCTCAGCAG	human *RUNX2*
sgRNA_1_KO	AATTCTCGCCTTCTTCAGAG	human *RUNX3*
sgRNA_2_KO	TGCGCACGAGCTCGCCTGCG	human *RUNX3*

Table 18. Genotyping PCR primers for stable transductions and cloning

Primer name	Sequence	Target
FWD_sgRNA	AAAGCGTGGTCTCTGGCG	*NOXA* sgRNA
REV_MS2_puro	CCACTCCTTTCAAGACCTAGAAG	lentisgRNA(MS2)_puro backbone
FWD_Cas9	CCAAAGAGGTGCTGGACG	lenti dCAS9-VP64_Blast
REV_Blast	GCTCTTTCAATGAGGGTGGA	lenti dCAS9-VP64_Blast

FWD_Hygro	GACGGCAATTTCGATGATG	lenti MS2-P65_HSF1_Hygro
REV_pBluescript	TCGAGGTCGACGGTATC	lenti MS2-P65_HSF1_Hygro
REV_px330	GGAAAGTCCCTATTGGCGTT	px330-U6-Chimerich_BB-CBh-hSpCas9

Table 19. Mycoplasma test primers

Name	Sequence
Myco_FWD	GGGAGCAAACAGGATTAGATACCCT
Myco_REV	TGCACCATCTGTCACTCTGTTAACCTC

4. 1. 8. 2. qRT-PCR primers

Table 20. qRT-PCR primers

Name	Sequence	Target gene
hNOXA_qPCR_FWD	CGGAGATGCCTGGGAAGAA	human *NOXA* (*PMAIP1*)
hNOXA_qPCR_REV	CCAAATCTCCTGAGTTGAGTAGCA	human *NOXA* (*PMAIP1*)
mNOXA_qPCR_FWD	GAGTGCACCGGACATAACTG	murine *Noxa* (*Pmaip1*)
mNOXA_qPCR_REV	CTCGTCCTTCAAGTCTGCTG	murine *Noxa* (*Pmaip1*)
hRUNX1_qPCR_FWD_E3	AACTTCCTCTGCTCCGTGCTG	human *RUNX1*
hRUNX1_qPCR_REV_E4	TCACAGTGACCAGAGTGCCATC	human *RUNX1*
hRUNX2_qPCR_FWD	ATTCTGCTGAGCTCCGGAATGC	human *RUNX2*
hRUNX2_qPCR_REV	TGGGGAGGATTTGTGAAGACGGT	human *RUNX2*
hRUNX3_qPCR_FWD	GTGGCCAGGTTCAACGACCTTC	human *RUNX3*
hRUNX3_qPCR_REV	GGTGGGGTTGGTGAACACAGTG	human *RUNX3*
hMYC_qPCR_FWD	TTCCTTTGGGCGTTGGAAAC	human *MYC*
hMYC_qPCR_REV	GCTGTACGGAGTCGTAGTCG	human *MYC*
hACTB_qPCR_FWD	CCTCGCCTTTGCCGATCC	human *Actin*
hACTB_qPCR_REV	CGCGGCGATATCATCATCC	human *Actin*
hGAPDH_qPCR_FWD	AGCTCAGGCCTC AAGACCTT	human *GAPDH*
hGAPDH_qPCR_REV	AAGAAGATGC GGCTGACTGT	human *GAPDH*

Table 21. ChIP-qPCR primers

Name	Sequence	Target
ChIP_hNXUTR_FWD	AGGCAGCTATTTTACCATCTGG	Human *NOXA* negative region
ChIP_hNXUTR_REV	GTTTACTGCCACAGTATCAACTTTT	Human *NOXA* negative region
ChIP_hNXBS5_FWD	GACGACGTCCAGCGTTTG	Human *NOXA* BS5 promoter
ChIP_hNXBS5_REV	GCCCCGAAATTACTTCCTTAC	Human *NOXA* BS5 promoter
hNXProm_RUNX1bindingFWD_I	AGCTCAGCCCTCCCACAAAAGA	Human *NOXA* promoter

hNXProm_RUNX1bindingREV_I	AGGGATTTGTGTGTGTCCTTCCA	Human *NOXA* promoter
hNXProm_RUNX1bindingFWD_II	CCCAAGTCTCTAATTGCCAAGGCC	Human *NOXA* promoter
hNXProm_RUNX1bindingREV_II	TGGCGGGAGGGGAAGGGTTTAA	Human *NOXA* promoter
ChIP_hNX_E1_FWDI	CGAAGGCTGACATGTCTCATGC	Human *NOXA* enhancer 1
ChIP_hNX_E1_FWDII	TGACATGTCTCATGCACCCAGA	Human NOXA enhancer 1
ChIP_hNX_E1_REV	TGGATTTGTCTCAGGCAGCTCT	Human *NOXA* enhancer 1
ChIP_hNX_E2_FWD	CAAGCCTCCTTTAGCCCAAAGC	Human *NOXA* enhancer 2
ChIP_hNX_E2_REVI	GGATCTCCAACTTTCGTCGGGA	Human *NOXA* enhancer 2
ChIP_hNX_E2_REVII	CTTTCTGGCAGGAGAGGAGCAT	Human *NOXA* enhancer 2
ChIP_hNX_E3_FWDI	GTCCAGAGATGGGAGCTTCTGG	Human *NOXA* enhancer 3
ChIP_hNX_E3_REVI	CAGGAGAATGTGAGTCGGCAGA	Human *NOXA* enhancer 3
ChIP_hNX_E3_FWDII	AGGGCAGGGAATTTTGAGGCTA	Human *NOXA* enhancer 3
ChIP_hNX_E3_REVII	ATCCACACTCACCAGCACTGAA	Human *NOXA* enhancer 3
Enhancer3_FWD_hChIPNX	TGGTAGGACACTCTGAGTTCCGG	Human *NOXA* enhancer 3
Enhancer3_REV_hChIPNX	AGTGTGGGGCTCTAGGTGGTTG	Human *NOXA* enhancer 3

4. 1. 8. 3. 4C primers

Table 22. Illumina adapters 4C

Primer	Illumina adapter
p5	AATGATACGGCGACCACCGAACACTCTTTCCCTACACGACGCTCTTCCGATCT
p7	CAAGCAGAAGACGGCATACGA

Table 23. 4C primers

Primer viewpoint	Sequence	Barcode	Sample
NOXApromotor_p5	ATCGTAAGTTTTCAGGCCAGC	ACAGTG	MIAPaCa2_WT_DMSO
NOXApromotor_p7	GCGAGCTGAACACGAACAGT	ACAGTG	MIAPaCa2_WT_DMSO
NOXApromotor_p5	ATCGTAAGTTTTCAGGCCAGC	GTGAA	MIAPaCa2_WT_AI
NOXApromotor_p7	GCGAGCTGAACACGAACAGT	GTGAA	MIAPaCa2_WT_AI
NOXApromotor_p5	ATCGTAAGTTTTCAGGCCAGC	CTTG	MIAPaCa2_*RUNX1*^{KO}_DMSO
NOXApromotor_p7	GCGAGCTGAACACGAACAGT	CTTG	MIAPaCa2_*RUNX1*^{KO}_DMSO

DMSO = vehicle

The final primer has the following scheme: Illumina adapter + Barcode + Primer viewpoint. Each 4C library (sample) was prepared with the specified final primer. More details in section 4. 2. 8. 1.

4. 1. 9. RNA-seq index primers

RNA-seq samples were prepared according to section X. Z: C. and the final libraries were amplified as described in the following table.

Table 24. Index combination for RNA-seq samples

Sample Name	Index combination
MIAPaCa-2_DMSO_1	i705+i501
MIAPaCa-2_DMSO_2	i707+i501
MIAPaCa-2_DMSO_3	i709+i501
MIAPaCa-2_DMSO_4	i711+i501
MIAPaCa-2_AI_1	i706+i501
MIAPaCa-2_AI_2	i708+i501
MIAPaCa-2_AI_3	i710+i501
MIAPaCa-2_AI_4	i712+i501
MIAPaCa-2_*RUNX1*^{ko}_DMSO_1	i703+i504
MIAPaCa-2_*RUNX1*^{ko}_DMSO_2	i705+i504
MIAPaCa-2_*RUNX1*^{ko}_DMSO_3	i707+i504
Panc1_DMSO_1	i701+i501
Panc1_DMSO_2	i701+i502
Panc1_DMSO_3	i711+i502
Panc1_AI_1	i702+i501
Panc1_AI_2	i702+i502
Panc1_AI_3	i712+i502
Panc1_*RUNX1*^{ko}_DMSO_1	i709+i504
Panc1_*RUNX1*^{ko}_DMSO_2	i711+i504
Panc1_*RUNX1*^{ko}_DMSO_3	i701+i505
PSN1_DMSO_1	i703+i501
PSN1_DMSO_2	i703+i502
PSN1_DMSO_3	i701+i503
PSN1_AI_1	i704+i501
PSN1_AI_2	i704+i502
PSN1_AI_3	i702+i503
PSN1_*RUNX1*^{ko}_DMSO_1	i707+i502
PSN1_*RUNX1*^{ko}_DMSO_2	i705+i503
PSN1_*RUNX1*^{ko}_DMSO_3	i709+i503

DMSO = vehicle. AI = AI-10-49 treatment. Index combination: Illumina index primers.

4. 1. 10. Drug libraries

The drug libraries (Table 25) were acquired as individual single-screw-cap compounds in 96-well format dissolved in DMSO at a final concentration of 10 mM. Upon arrival they were stored in a freezer at -80 °C. When needed, they were thawed at RT, shortly spined, unscrewed and diluted to 1 mM and 100 µM.

Table 25. Screening libraries, number of 96-well plates and drugs

Library	Plates	Drugs	Company
Anti-cancer library (L2000)	5	412	Selleckchem, Houston, USA
FDA-approved library (L1300)	17	1840	Selleckchem, Houston, USA

4. 1. 11. Software and databases

Table 26. Public repositories and software

Database/Software	Identifier
4C and Hi-C database	https://promoter.bx.psu.edu/hi-c/
Benchling	https://www.benchling.com
BioVenn	https://www.biovenn.nl/
CalcuSyn v2.1	(Chou, 2010)
Contra V3	https://bioit2.irc.ugent.be/contra/v3/#/step/1
Ensembl database	https://ensembl.org/
Fiji/Image J	Fijite (CITE)
FlowJo v10	Tree Star Inc
Galaxy	http://main.g2.bx.psu.edu/
Gene Expression Omnibus (GEO)	https://www.ncbi.nlm.nih.gov/geo/
GONetwork R package	https://github.com/saralinker/GONetwork
GraphPad Prism 8	GraphPad Software Inc, San Diego, USA
GSEA	https://www.gsea-msigdb.org/gsea/index.jsp
Image Studio v3.02	LI-COR Inc, Lincoln, USA
Incucyte S3 software	Sartorius Lab Instruments GbmH & Co.KG, Göttingen, Germany
Inkscape v0.92	Inkscape community
Mendeley	Elsevier, Amsterdam, The Netherlands
Microsoft Excel, Power Point and Word v18	Microsoft Corporation
R studio (v1.1.456)	https://rstudio.com/
R-3.4.1	https://www.r-project.org/
StepOne Software v2.3	Thermo Fisher Scientific, Waltham, USA
STRING database (v11.0)	https://string-db.org
TScratch	CSE-Lab, Zurich, Switzerland
UCSC Genome browser	https://genome.ucsc.edu/

4. 2. Methods

4. 2. 1. Cell culture and cell-based assays

4. 2. 1. 1. Culture of adherent cell lines

Pancreatic cancer cell lines (except for PSN1) and the virus packaging cell line HEK293T were cultured in DMEM supplemented with 10% FBS and 1% Antibiotic-Antimycotic (listed in Table 5). PSN1 was cultured in RPMI supplemented with 10% FBS and 1% Antibiotic-Antimycotic. The cells were incubated at 37°C in a humid atmosphere with 5% CO_2.

4. 2. 1. 1. 1. Splitting

The cells were kept in culture in T75 (unless otherwise specified) and left to grow until they reached 80% confluency. Passaging was carried out 3 times per week and up to 15 times in a 1:10 dilution. Briefly, old medium was discarded, adherent cells were washed with 10 ml of PBS then discarded and 1 ml of Trypsin-EDTA 1X was added. After 5 min incubation at 37 °C, 10 ml of corresponding medium were used to collect the cells in trypsin. Cells were collected in 15 ml conical tubes and spined down 5 min at 300 g. Supernatant was discarded and a 1:10 dilution of cells was used as a starter for a new culture.

4. 2. 1. 1. 2. Freezing and thawing

After thawing fresh cells, they were left to grow in one T175 flask. When they were 80-90% confluent, cells were split as described in the previous section and re-suspended in 5 ml of freezing medium (FBS supplemented with 10% DMSO). 1 ml of cells in freezing medium were quickly dispensed in cryotubes and transferred to a -80 °C freezer for at least 24 h. For long-term storage the cryovials were transferred to liquid nitrogen. For re-culturing, cells ere rapidly thawed at 37°C and DMSO was washed out with the corresponding culture medium. After each thawing cycle the cells lines were tested for Mycoplasma.

4. 2. 1. 1. 3. Mycoplasma test

All cultured cell lines were tested for presence/absence of contaminating *Mycoplasma spp*. Cells were left to grow until the medium turned yellow. 2 ml of this medium were centrifuged for 2 min at 250 g and the supernatant was transferred to a fresh 2 ml tube. The tubes were centrifuged for 10 min at 20.000 g, the supernatant was discarded, and the pellet was resuspended in 50 ul of PBS. Next, they were boiled at 95°C for 3 min and this mixture was used as PCR template. The PCR was done as described in table 27 and 28 with the primers listed in table 19. The template was mixed with 6X loading buffer, run in a 1.5% agarose gel and if the PCR is positive (270 bp), the cells have a *Mycoplasma spp*. contamination.

Table 27. Mycoplasma PCR mix

Component	20 µl reaction
2X Taq Ready Mix	10 µl
Primer FWD 10 µM	1 µl
Primer REV 10 µM	1 µl
Template	1 µl
Water	7 µl

Table 28. PCR program for Mycoplasma test

Step	Temperature	Time
Initial denaturation	98 °C	5 min
x 35 cycles	94 °C	1 sec
	60 °C	1 sec
	72 °C	1 sec
Final extension	72 °C	10 min
Hold	12 °C	-

4. 2. 1. 2. Transfection of pancreatic cancer cells for CRISPR/Cas9 mediated knockout and cell line generation

Pancreatic cancer cells were grown on 6 well plates with standard cell culture medium. Cells were transfected using Lipofectamine 2000 plus Opti-MEM without antibiotics according to the manufacturer's instructions. A total of 1 µg of DNA was co-transfected (500 ng of each px330

plasmid with carrying one sgRNA targeting the region to be excised). Transfection efficiency was checked by microscopic GFP signal 16 hours later. When transfection efficiency was between 40-70%, puromycin selection was performed for 72 hours at 1 µg/ml concentration (until negative control died). Afterwards, cells were left to recover for 3-5 days and surviving cells were used to assess knockout presence with knockout primers (Table 4). Positive cells were serially diluted and seeded at a density of 0.75 cells/well. Single cells were left to grow for approximately 2 weeks until a visible colony was formed and screened via PCR for knockout/wild type with flanking primers (Table 16 and 31) and posterior Sanger sequencing. All screened clones were expanded and stored in nitrogen for future use. Knockout efficiency was confirmed via western blot. Absence of wild type allele was assessed by internal controls within the knockout region.

4. 2. 1. 3. Lentivirus production

Lentivirus production was performed as described by Joung and collaborators (Joung et al., 2017) . Briefly, $3x10^6$ HEK293T cells were seeded in 10 cm dishes. After 24 h the cells were co-transfected with a mixture of 4.9 µg of expression plasmid (listed in Table 11), 3.6 µg of psPAX2 and 1.5 µg of PMD2.G in Opti-MEM plus 30 µl of PEI as transfection reagent. Virus was collected 36 h after transfection and filtered through a 0.45 µm membrane every 12 h after for 3 days. Spinfection was performed at 32 °C, 1000 g for 2 h with a final concentration of $5x10^5$ cells and 8 µg/ml polybrene.

4. 2. 1. 4. Establishment of *NOXA-CRISPRa* overexpressing cell line

To establish a stable *NOXA* overexpressing cell line the cloning and design of the sgRNAs was performed according to section 4. 2. 2. 3. Briefly, 3 sgRNAs were designed with the genome engineering toolbox from Zhang lab with the online platform Benchling (https://benchling.com). As target region I used 150 bp upstream and downstream the

transcriptional start site (TSS) of *NOXA* extracted from the UCSC genome browser (https://www.genome.ucsc.edu). The sgRNAs were first cloned into the sgRNA(MS2) cloning backbone (Table 11) and transiently co-transfected together with dCas9-VP64 and MS2_HSF1 in HEK293T cells via PEI transfection (see 4. 2. 1. 3) (Konermann et al., 2014). To assess CRISPRa efficiency, 72 h after transfection RNA was isolated to perform cDNA and qRT-PCR assays. *NOXA* mRNA level was compared to a negative control consisting of the same transfection but without the NOXA sgRNA. The sgRNA with the best upregulation score was used to produce the stable cell line.

Establishment of the overexpressing cell line was done by lentivirus infection. First, $1x10^6$ MIAPaCa-2 cells were infected with lenti-dCas9-VP64_Blast as described previously (see 4. 2. 1. 3). 24 h after transduction, cells were selected with 30 µg /ml of blasticidin until the negative control died. Presence of the transgene was assessed by PCR with the corresponding primers (Table 16). The cells were left to recover for 3-5 days and after, they were co-infected with the last 2 lentiviruses: one carrying *NOXA*-sgRNA and the dCas9-co-activators (lenti sgRNA(MS2)_puro backbone + lenti MS2-P65-HSF1_Hygro). 24 h after transduction the selection was performed for 72 hours with puromycin 1 µg/ml and hygromycin 100 µg/ml. Single cell culture and genotyping PCR was done as described in the previous section (4. 2. 1. 2). Clones positive for the 3 transgenes were grown and preserved in nitrogen for future use. The transcriptional activation efficiency was corroborated by qRT-PCR and Western blot.

4. 2. 1. 5. Apoptosis assay by flow cytometry

For detection of apoptotic cell death, $1x10^6$ cells were seeded on 10 cm dishes and 24 h later treated accordingly. After treatment, cells and supernatant were collected and washed with PBS. Afterwards, $1x10^6$ cells were counted and centrifuged at 300 g for 5 min, resuspended in 300 µl 1X Annexin V binding buffer, 4 µl Annexin V antibody and 10 µg/ml DAPI. The cells were transferred to FACS tubes and incubated for 15 min at 4°C in the dark to then be analyzed by flow cytometry. Those cells that appear in the lower left quadrant of the analysis (Annexin

$V^{low/-}$ and $DAPI^-$ are living cells. Apoptotic fractions were classified as early apoptotic (Annexin V^+, $DAPI^-$), apoptotic/late apoptotic (double positive, upper right quadrant) and total dead cells (single and double positive) as previously described (Hammill et al., 1999). Analysis was performed using FlowJo v10.6.0.

4. 2. 1. 6. Cell cycle assay by flow cytometry

For quantification of the cell cycle phases, $1x10^6$ cells were grown in 10 cm dishes and 24 h later treated accordingly. 48 h after treatment the cells were collected, washed and counted for $1x10^6$. Cells were fixed with ethanol 70% at 4 °C for 1 h and washed with cold PBS. RNase A was added at a final concentration of 50 µg/ml and incubated at 37°C in the dark for 30 min. Cells were washed and resuspended in PBS plus PI dye at a concentration of 0.2 µg/ml, incubated for 5 min in the dark and analyzed by flow cytometry. The percentage (%) of cells in each phase of the cell cycle was determined as previously described (K. H. Kim & Sederstrom, 2015; Ormerod, 2002) with the software FlowJo v10.6.0.

4. 2. 1. 7. Viability assay by MTT

Cells were seeded onto 96-well plates at a density of $4x10^3$ cells/well, grown for 24 h and drug-treated. After 72 h of treatment, 10 μl of MTT reagent (preparation described in Table 4) was added and the plates were incubated 4 h at 37 °C in the dark. Medium was discarded and MTT crystals were dissolved in a horizontal shaker with 100 µl of a 1:1 DMSO:ethanol solution. Absorbance was measured at 595 nm on a microplate reader. Percentage of living cells was calculated in comparison to vehicle (DMSO) control, which was arbitrarily set to 100%.

4. 2. 1. 8. High-throughput drug screening

Two libraries were used for manual high throughput drug screening (Table 26) in pancreatic cancer cell lines (Table 6). On the one hand, the anti-cancer library was used to treat PSN1 parental, PSN1 *NOXA^{ko}*, MIAPaCa-2 parental, MIAPaCa-2 *NOXA^{ko}*, mPDAC-06 parental, mPDAC-06 *NOXA^{ko}*, mDAC-95 parental and mPDAC-95 *NOXA^{ko}* pancreatic cancer cell lines

covering a total of 412 drugs. On the other hand, the FDA-approved library was used to treat PSN1 (characterized by a high *NOXA* expression), MIAPaCa-2 (characterized by a mild-to-low *NOXA* expression) and the 4 murine cell lines, mPDAC-06 parental, mPDAC-06 $NOXA^{ko}$, mDAC-95 parental and mPDAC-95 $NOXA^{ko}$.

For the drug screening a final concentration of 600 nM was used as previously described (Christensen et al., 2014). Cell viability was measured according to previous section (see 4. 2. 1. 7) in technical and biological triplicates. The absorbance measured of vehicle treated (DMSO) cells was arbitrarily set to 100% and the response was calculated as relative viability. After viability (%) was calculated, I selected those inhibitors that differentially reduced growth in parental/$NOXA^{high}$ cell lines up to 10% more when comparison to $NOXA^{ko}$ cells. Each cell line was compared against its parental counterpart. All the drugs that differentially affected cell viability in $NOXA^{high}$ cells were compared to find the overlaps with BioVenn software (Hulsen et al., 2008) (Table 26) and those present exclusively in all parental cell lines ($NOXA^{high}$ subtype) were further investigated.

For mere visualization purposes, the compounds were grouped in 20 clusters with the k-means algorithm (Kaniwa et al., 2017) according to similarity in cell inhibition efficacy. To visualize the drug clusters relative to cell viability, a hierarchical clustering with bootstrap was performed with 1000 iterations in R studio depicted in a heatmap.

4. 2. 1. 9. Dose-response assay (GI_{50})

Cells were seeded onto 96-well plates at a density of $4x10^3$ cells/well, grown for 24 h and treated accordingly with seven 1:2 dilution doses starting from 1200 nM (1200, 600, 300, 150, 75, 37.5, 18.75 nM, and DMSO control). Cell viability was measured and calculated as described in the previous section (4. 2. 1. 7). GraphPad Prism 8 was used to estimate the half-maximal growth inhibitory concentration (GI_{50}) modelled as a non-linear regression and tested for statistical significance by comparing best-fit values of each curve.

4. 2. 1. 10. Synergism

Cells were seeded in 96-well plates at $4x10^3$ cells /well. The following day, cells were treated in triplicate with single agents and their fixed-ratio combination for 72 h over a 7-point, 2-fold concentration range, which was centered on the single-agent AI-10-49. Cell viability and the fraction of living cells was measured and calculated by MTT assay as previously described (section 4. 2. 1. 7). These results were used to estimate the combination index (CI) scores with the Chou-Talalay method as described before (Chou, 2006) using CalcuSyn software (Chou, 2010). Brifely, the viability from the single drug treatments and the combinations obtained from MTT was entered into CalcuSyn to determine the CI for each combination point. Each CI quantitatively defines additivity (CI = 1), synergy (CI < 1), and antagonism (CI > 1.5). The resulting values were plotted in GraphPad Prism v8.

The synergy treatment was performed in MIAPaCa-2 and PSN1 cells using 5 inhibitors: JQ1, obatoclax, quisinostat, gemcitabine and oxaliplatin. For each inhibitor 3 doses were used (GI_{10}, GI_{50} and $GI_{75,}$ calculated from results in section 4. 2. 1. 9. AI-10-49 was used in the same doses as for the dose-response experiment (section 4. 2. 1. 9).

4. 2. 1. 11. Colony formation assay (CFU assay)

Cells were seeded in 6-well dishes at a density of $2x10^3$ cells/well. After 24 h, medium was exchanged for medium with vehicle (DMSO) or AI-10-49 400 nM. Medium with drug was refreshed every 3 days. After 2-3 weeks of treatment, the wells were washed with PBS, fixed with methanol for 1 h. Methanol was washed out and the plates were stained with a 1:20 dilution of Giemsa in a horizontal shaker at 4 °C overnight. The Giemsa solution was discarded, the plates were washed and left to dry in a vertical flow for 30 min. Afterwards, the plates were scanned in a computer scanner and all the colonies were manually counted with ImageJ. Vehicle treated cells (DMSO) were set to 100% of colonies and the treatments were calculated as relative clonogenic growth.

4. 2. 1. 12. Growth curves by Cell-live imaging

Cells were seeded in 96-well plates at a density of $4x10^3$ cells/well. After 2 h they were placed inside the Cell-live imaging system Incucyte at 37 °C and a program was set to make pictures every 8 h. Confluency was determined by monitoring cells and confluency image mask performed with the Incucyte S3 software. Relative growth was calculated in comparison to d0.

4. 2. 1. 13. Patient derived organoids culture and viability assay

PDAC biopsies and tissues were received from endoscopy punctures or surgical resection in collaboration with Maximillian Reicher, Technical University of Munich. 3D organoids were collected, propagated, and analyzed in agreement with the declaration of Helsinki and were approved by the ethical committee of TUM (Project 207/15). Written informed consent from the patients for research use of tumor material was obtained prior to the use.

Cellular viability of human patient derived organoids (PDOs) was determined using the CellTiter-Glo 3D ATP viability assay according to manufacturer's protocol. Briefly, $1x10^3$ cells/well were plated in 80 µl of PDO medium in 96-well plate. 24h after plating of PDOs, a 7-point dilution (dose-response) of AI-10-49 was added and viability was determined by measuring luminescence microplate reader after 3 days of treatment. PDOs viability assays and RNA-seq were performed in a collaboration by Felix Orben, Technical University of Munich.

4. 2. 2. Molecular biology

4. 2. 2. 1. Polymerase Chain Reaction (PCR)

The screening PCR for knockout, wild type and transgenic cell lines were performed as described in Table 29 with cell pellet as DNA template. The primers are listed in Table 16 and Table 18.

Table 29. Terra PCR master mix

Component	50 µl reaction
2X Terra PCR	25 µl
Primer FWD 10 µM	1.5 µl
Primer REV 10 µM	1.5 µl
Template	5 µl
Water	10 µl

Table 30. Genotyping PCR program with Terra PCR master mix

Step	Temperature	Time
Initial denaturation	98 °C	2 min
x 40 cycles	98 °C	30 sec
	59 °C	30 sec
	72 °C	20 sec
Final extension	72 °C	2 min
Hold	12 °C	-

The PCR products were separated in a 1.5% agarose gel, run for 90 min at 100 V and developed with a UV lamp. Expected product sizes for CRISPR/Cas9 deletion (primers listed in Table 16) and presence of CRISPRa transgenes (primers listed in Table 18) are listed in the Table 31 and 32.

Table 31. Knockout and wild type allele PCR

Target	Primers (Table 16)	Product WT size (bp)	Product KO size (bp)	Outcome size (bp) if Homozygous deletion
NOXA (human)	FWD_KO (1) + REV_KO (2)	342	160	-
	Internal_REV (3)	(1+3) 137	-	(1+3) No band
Noxa (murine)	FWD_KO (1) + REV_KO (2)	313	198	-
	Internal_REV (3)	(1+3) 156	-	(1+3) No band
RUNX1	FWD_KO (1) + REV_KO (2)	No band expected*	260	
	Internal_FWD (3)	(2+3) 352	-	(2+3) No band
RUNX2	FWD_KO (1) + REV_KO (2)	589	184	-
	Internal_REV (3)	(1+3) 183	-	(1+3) No band
RUNX3	FWD_KO (1) + REV_KO (2)	No band expected*	159	-
	Internal_REV (3)	(1+3) 200	-	(1+3) No band

*No band expected = the deletion region is too large (more than 10 kb) to be amplified in a normal PCR program. If possible, all sgRNAs were designed to excise large genomic regions and facilitate the PCR screening process. Schematic positions of the sgRNAs and genotyping primers are depicted in Fig. 4, 5 and 24. No band = if the deletion is homozygous, the primer has no binding capacity, hence, there is no PCR simplification. When the PCR gives a band with the internal primer it means that there is left at least 1 allele of the target gene. "-" means that no result is expected under that category for that combination.

Table 32. Genotyping PCR for stable transduction plasmids

Target	Primer combination (Table 18)	Product size (bp)
NOXACRISPRa *	FWD_sgRNA + REV_MS2_puro	248
lenti dCAS9-VP64_Blast	FWD_Cas9 + REV_Blast	460
lenti MS2-P65_HSF1_Hygro	FWD_Hygro + REV_pBluescript	831

* = this PCR exclusively detects the lenti sgRNA(MS2)_puro backbone (Table 11) after cloning of *NOXA* sgRNA.

4. 2. 2. 2. RNA analysis

4. 2. 2. 2. 1. RNA isolation

Cells were seeded at day 0 in 6-well dishes at a density of $5x10^5$ cells/well. After 24 h the cells were washed with PBS and treated accordingly. Cells were lysed and RNA isolated with Qiagen RNeasy Isolation kit as per manufacturer's instructions including in-column DNase treatment. Total RNA concentration was measured by spectrophotometry and the 260/280 ratio was obtained. For RNA-seq samples the RNA Integrity Number (RIN) was calculated to describe the quality of the obtained RNA as described in section 4. 5. 6. 7. In order to determine the transcript levels of specific genes, the RNA was retro-transcribed as described in the next section (4. 2. 2. 2. 2).

4. 2 .2. 2. 2. Reverse transcription (RT)

A total of 1 µg of RNA was retro-transcribed with MMLV kit according to manufacturer's recommendations and 10 ng of random primers (random hexamer). Briefly, the RNA was annealed with the primers in 0.2 ml tubes as described in following table (Table 33).

Table 33. RNA-primers annealing

Component	10 µl reaction
RNA 1 µg	X µl
Random primers	0.9 µl
Water	to 10 µl

The mix from table 33 was incubated at 65 °C for 2 min, chilled on ice for 1 min and kept on ice until next use. Next, a master mix was prepared to perform the reverse transcription, described in table 34.

Table 34. Master mix for RT

Component	20 µl reaction
Annealed primers (table 33)	10 µl
10 X MMLV Reaction buffer	2 µl
DTT 100 mM	2 µl
dNTPs 10 mM	4 µl
MMLV High performance Reverse Transcriptase (200 U/µl)	0.5 µl
RNase inhibitor (RiboLock 40 U/µl)	0.5 µl

The mix was retro-transcribed in a thermocycler as follows: 10 min at RT, 60 min at 37 °C and a final step of heat inactivation at 85 °C for 5 min. The final product was used for qRT-PCR or stored at -20 °C for further use.

4. 2. 2. 2. 3. Quantitative RT-PCR (qRT-PCR)

The cDNA obtained in section 4. 2 .2. 2. 2 was diluted with nuclease free water in 1:10 and used for the qRT-PCR as shown in Table 35.

Table 35. qRT-PCR master mix

Component	20 µl reaction
2X Power SybrGreen	10 µl
Primer FWD 10 µM	0.5 µl
Primer REV 10 µM	0.5 µl
cDNA (1:10)	4 µl
Water	5 µl

Quantitative RT-PCRs were done as follows: 95°C for 10 min, 40 cycles of 95°C for 15 s and 60°C for 1 min and a final melting curve stage in StepOne Plus System. Expression levels of target genes were determined with the $2^{-\Delta\Delta CT}$ method (Livak & Schmittgen, 2001) from technical triplicates and normalized to *ACTB* and *GADPH* mRNA. Relative expression (fold change) was calculated with control samples (DMSO) arbitrarily set as 1. Primer sequences are listed in Table 20.

4. 2. 2. 3. Cloning of sgRNAs for genomic deletion and CRISPRa

4. 2. 2. 3. 1. Digestion of plasmid DNA and gel purification

For cloning purposes, plasmid DNA was restricted overnight at 37 °C with the appropriate enzyme and buffer. Generally, 3 µg of DNA was cut, with 3 U of enzyme in a total volume of 30 µl. After overnight incubation, the mix was heat inactivated at 80 °C for 20 min. For sgRNA cloning in the lenti sgRNA(MS2)_puro backbone I used BsmBI restriction, whereas for sgRNA(MS2) cloning backbone and px330-U6-Chimerich_BB-CBh-hSpCas9 the enzyme used was BbsI. Restricted plasmid was run in a 1% agarose gel at 90 V for 90 min and purified with Wizard SV Gel and PCR Clean-Up System according to manufacturer's recommendations. Final concentration was determined by absorbance in a nanodrop spectrophotometer.

4. 2. 2. 3. 2. Oligo annealing and ligation

The design of the sgRNAs was done following the guidelines from the publicly available database from the Zhang lab (https://www.addgene.org/crispr/zhang). To minimize potential off-targets, all the sgRNAs chosen had on-target score >80 (Doench et al., 2016). Furthermore, a G was added at the 5' end of the sgRNA since it was reported to help the transcription of the sgRNAs (Fu et al., 2014). For each sgRNA (listed in Table 17), a complementary oligo was designed and for each one the appropriate overhangs were added. For BbsI and BsmBI restrictions the overhangs were 5'-CACC-3' for the main sgRNA and 5'-AAAC-3' for the reverse complement. Complementary oligos were annealed by incubation at 95 °C for 5 min and

subsequent ramp down of temperature at a rate of 5 °C/min until 25 °C were reached. Annealing mix was performed as depicted in table 36.

Table 36. Oligo annealing

Component	10 µl reaction
sgRNA A 100 µM	1 µl
sgRNA B 100 µM	1 µl
10X T4 ligation buffer (NEB)	1 µl
Water	7 µl

A dilution 1:120 of the annealed oligos (Table 36) and 60 ng of digested vector (section 4. 2. 2. 3. 1) were ligated at RT for 30 min with 1 U of T4 Quick Ligase (NEB) in a final volume of 20 µl. Ligation product was used for bacteria transformation.

4. 2. 2. 3. 3. Bacteria transformation

Bacteria was either heat shocked or chemically transformed, depending on the plasmid and the strain used (Stbl3 for lentiviral plasmid, Top10 and DH5α for the remaining cloning) (Table 10). For heat shock transformation, 50 µl of competent bacteria were thawed on ice and mixed with 5 µl of ligation product in a 2 ml tube. After carefully tapping the tube, they were incubated 20 min on ice, heat shocked at 42 °C for 45 sec and recovered on ice for 2 min. Next, 1 ml of SOC medium was added and bacteria was left to grow (to synthesize the antibiotic resistance) shaking at 37 °C for 1 h. 200 µl of this liquid culture were plated in LB agar plates with appropriate antibiotic. The next day the bacteria plates were analyzed by colony PCR to determine success of the cloning procedure.

4. 2. 2. 3. 4. Colony PCR and plasmid purification

To determine whether the bacterial colonies have the vector of interest, PCRs were performed using Taq Ready Mix as described previously (table 26). Colonies were resuspended in 30 µl of ddH_2O in 0.2 ml tubes. 20 µl were transferred to a clean tube and heat inactivated at 95 °C for 5 min and the remaining 10 µl were left at 4 °C for future use. 3 µl of the boiled bacteria were used as template for the colony PCR. The main sgRNA was used as forward primer and

the REV_px330 (Table 18), which binds in the plasmid, as reverse. A band of 300 bp is expected if the cloning was successful.

The remaining 10 µl of the colony suspension were used to inoculate 5 ml of liquid LB supplemented with ampicillin 100 µg/µl. The bacteria were incubated overnight at 37 °C with vigorous shaking. The plasmids were purified the next day with Pure Yield Plasmid Miniprep System following the manufacturer's instructions. DNA concentration was measured by nanodrop and the plasmids were sequenced with Sanger sequencing to corroborate correct cloning of the sgRNAs.

4. 2. 3. Protein analysis

4. 2. 3. 1. Protein isolation

Cells were seeded at $2x10^6$ density in 10 cm dishes. The following day, dishes were washed with PBS and medium replaced with medium plus corresponding treatment. At the indicated time points cells were harvested in 1.5 ml tubes with a cell scraper in 100 µl of RIPA buffer (Table 4). The tubes were incubated in ice for 30 min, centrifuged 10 min at 4 °C and the supernatant was transferred to a clean 1.5 ml tube. Protein concentration was determined by Protein Assay following the provider's guidelines.

4. 2. 3. 2. SDS polyacrylamide gel electrophoresis (SDS-PAGE)

Gels were prepared as described in Table 4. For NOXA detection a 10-20% gradient gel was used. To prepare it, a 1:1 mixture of heavy and light gel was poured in 1.5 mm glasses and the polymerization process was done overnight. Per run it was used a total of 100 µg of total resuspended in 6X Laemmli buffer in a final volume of 30 µl. Once mixed, the samples were boiled at 95 °C for 10 min and stored at -20 °C for future use. The polyacrylamide gels were loaded with the samples, 30 µl of the pre-stained molecular weight marker and any empty well was filled with 30 µl to avoid differences in the run. The electrophoresis chamber was loaded with 1X running buffer and the cassette containing the loaded gels. The protein samples were separated at 80 v for 4 h.

4. 2. 3. 3. Wet blot transfer and protein detection

The gel was then transferred onto a 0.45 µm PVDF membrane or in the case of NOXA a 0.2 µm membrane. The membranes were previously activated with methanol for 5 min. The wet blot “sandwich” was placed in a transfer chamber completely submerged in 1X transfer buffer and a block of ice. The gel-to-membrane sandwich was left for blotting for 2 h at 100 V. After transferring, the membrane was blocked with 5% BSA in TBS-T or 5% skim milk in TBS-T for 1 h at RT. In case of NOXA detection, the lower part of the membrane was cut out and directly incubated with anti-NOXA overnight at 4 °C on a shaker. The rest of the membrane was blocked. After blocking, membranes were washed 3 times for 10 min in TBS-T and left for overnight incubation with the corresponding antibodies at 4 °C on a shaker. Next, membranes were washed 3 times for 10 min with TBS-T and incubated with the corresponding HRP- or fluorescent- conjugated secondary antibody.

As HRP substrate I used Kit ECL Prime detection reagent on the membranes for 30 sec. For ECL visualization ChemoStar PLUS Imager was used. Protein quantification was done with Image J software.

4. 2. 3. 4. Membrane stripping

To re-probe the PVDF membranes with more antibodies, the membranes were incubated with stripping buffer for 10 min. Next, the membranes were washed 3 times for 10 min in TBS-T on a shaker. Last, the membranes were blocked again (as described in the previous section) and incubated overnight with the corresponding primary antibody at 4 °C on a shaker.

4. 2. 4. Xenograft assay

Xenograft assays were performed by EPO (Experimental Pharmacology and Oncology, Berlin-Buch). All animal experiments were approved by the local responsible authorities and performed in accordance with the German Animal Protection law. Subcutaneous MIAPaCa-2 xenograft experiments were performed in NSG (*NOD.Cg-Prkdcscid Il2rgtm1Wjl/SzJ, NOD scid*

gamma) mice. Tumor growth was monitored daily by measurement with a caliper. Once the tumor volume reached 0.2 cm^3 mice were treated with vehicle (2% DMSO + 30% PEG300 + 5% Tween80 + ddH_2O) or AI-10-49 (200 mg/kg daily) for 9 days. Xenograft tumors were harvested, formalin fixed, and paraffin embedded after a total of 12 days. Immunohistochemistry (IHC) was done in a collaboration with Prof. Esposito, by Martin Schlensog and Yakup Yasar, University Clinic Düsseldorf. Briefly, IHC of tumor sections was performed on 2 µm-thick paraffin sections and analysis was performed using a Ki67 (DakoCytomation, Glostrup, Denmark; 1:50) antibody. Slides were scanned using the Aperio digital whole slide imaging (Leica Biosystems, Germany). Analysis of positive stained cells has been performed using the Positive Pixel Count algorithm (standard settings) to quantify the amount of a specific stain present in the respective scanned slide images.

4. 2. 5. RNA sequencing

4. 2. 5. 1. Sample preparation

Cells and RNA isolation were prepared as described for qRT-PCR (section 4. 2 .2. 2. 3). RNA quality was assessed with Agilent RNA 6000 Pico Kit according to manufacturer's instructions in the Agilent Bioanalyzer 2100. Only RNA with a RIN higher than 8 was considered of good quality to be used for further analyses. After determining the RIN and RNA concentration, 1 µg of total RNA was enriched in mRNA with NEBNext Poly(A) mRNA Magnetic Isolation following manufacturer' protocol. The libraries were prepared with the commercial kit NEBNext Ultra II Directional RNA Library according to manufacturer's instructions. Afterwards, the sample indexes were added by PCR according to Table 24 with NEBNext Multiplex Oligos for Illumina following the provided guidelines. Afterwards, the libraries were quantified and checked for fragment size with the commercial kit Agilent High Sensitivity DNA in the Agilent Bioanalyzer 2100 following the given protocol. The samples were pooled in a 1.5 ml tube in equimolar ratios and sent out for sequencing.

4. 2. 5. 2. Illumina sequencing

The samples were sequenced on an Illumina NextSeq500 for 75 bp in single-end way in a collaboration with Apoorva Baluapuri and Elmar Wolf, University of Würzburg. The raw FASTQ files and downstream analyses were done in-house with the help of Stefanos Bamopoulos, Charité University Clinic Berlin.

4. 2. 5. 3. Read alignment and processing

Raw reads were quality checked with Galaxy software (Jalili et al., 2020) and the Illumina adapters trimmed using Trimmomatic (Bolger et al., 2014). Reads were aligned to the human reference genome GRCh38 using HISAT2 with default parameters (D. Kim et al., 2015) in Galaxy. Downstream analyses were carried out using R-3.4.1. Differential gene expression analysis was carried out with the limma package (Ritchie et al., 2015) and the table of gene counts was used for further processing.

4. 2. 5. 4. Gene Set Enrichment Analysis (GSEA)

Pathway enrichment was done with the GSEA software (Mootha et al., 2003) (www.broadinstitute.org/gsea). The gene set used were Hallmark (hallmark gene sets), C2 (curated gene sets) and C5 (Ontology gene sets) from the Molecular Signature Database (https://www.gsea-msigdb.org/gsea/msigdb/). Gene sets with false discovery rate less than 0.25 were taken as statistically significant.

4. 2. 6. Chromatin Immunoprecipitation (ChIP) qPCR

MIAPaCa-2 cells were seeded in 15 cm dishes at a density of $4x10^6$. After 24 h, they were treated with vehicle (DMSO) or AI-10-49 3 µM for 6 h. Cells were crosslinked in 1% formaldehyde for 10 min and quenched in 0.125 M Glycine for 20 min. Posterior lysis and harvesting was performed using SimpleChIP Enzymatic Chromatin IP Kit according to manufacturer's recommendations. 4-10 µg of antibodies of interest were used to pull down the

chromatin (Table 15). Immunoprecipitated DNA was analyzed by qPCR on a StepOne Plus as described previously (see section 4. 2 .2. 2. 3) except that 1 µl of pull-down sample was used as template. As negative controls for the immunoprecipitation an IgG pull down was performed. For qPCR binding control I used “negative” regions of the genome, regions with no-binding sequences for the used antibodies. The Ct value of each sample was normalized with the input used and chromatin occupancy of each antibody was calculated as % of input. The primers used in this study are listed in Table 21.

4. 2. 7. Chromatin Immunoprecipitation followed by high-throughput sequencing

4. 2. 7. 1. Sample preparation

The samples were prepared as described for ChIP-qPCR (4. 2. 5). After purification of pulled down DNA the concentration was measured by QuantiFluor® ONE dsDNA System following standard procedure. 10 ng of immunoprecipitated DNA was sent for sequencing to Erasmus University Medical Centre in a collaboration with Wilfred F. J. van Ijcken and his team. The DNA libraries were prepared using the ThruPLEX DNA sample preparation protocol from Takara Bio.

4. 2. 7. 2. Sequencing and reads processing

Libraries were sequenced on an Illumina HiSeq 2500 sequencer and single end reads were generated of 50 base-pairs in length. The reads were aligned to the reference genome GRCh38 using the HISAT2 aligner (D. Kim et al., 2015). From the alignments, secondary alignments, supplementary alignments, low quality alignments (Q<10) and fragmented alignments (fragment > 150 base pairs) were filtered. Subsequently analyses were done in-house.

4. 2. 7. 3. Analysis of high-throughput data and Gene Ontology (GO)

To determine genomic region bound by the antibodies, the reads had to be further processed. The binding peaks were called with the MACS2 algorithm normalizing by the input (Zhang et

al., 2008) in the software Galaxy (Jalili et al., 2020). Next, the MACSbdgdiff tool from Galaxy (Feng et al., 2012) was used to quantify and identify the genomic regions with differential binding between control AI-10-49 treated samples. The peak genomic distribution and annotation was performed with the Bioconductor package ChIPpeakAnno (Zhu et al., 2010) with R-3.4.1. For the visualization of the genomic data, narrowPeak or bigwig files were used as input for the pyGenomeTracks tool from Galaxy v2.1.1 with GRCh38 as reference genome. The annotated peaks (narrow peak files) and the p-values from MACSbdgdiff were used as input to perform pathway enrichment analysis with the function *getEnrichedGO* for R studio. The database used for this analysis was Gene Ontology (GO) and the output contained a list of enriched GO biological process, GO molecular functions, and GO cellular components. The GO-terms depicted in this study belong to GO biological process.

4. 2. 8. Omni-Assay for Transposase-Accessible Chromatin with sequencing (Omni-ATAC-seq)

MIAPaCa-2 cells were seeded in 6-well plates and 24 h later treated with vehicle (DMSO) or AI-10-49 3 μM for 6 h in 2 biological replicates. $5x10^4$ cells were collected, washed with PBS and snap frozen. Further sample processing was done in the Erasmus University Medical Centre in a collaboration with Wilfred F. J. van Ijcken and his team. Briefly, the Ilibraries were prepared and sequenced on an Illumina HiSeq 2500 sequencer. Paired-end reads were generated of 50 base-pairs in length. Reads were aligned to reference genome GRCh38 using HISAT2 (D. Kim et al., 2015).

4. 2. 8. 1. Analysis of Omni-ATAC-seq data

The aligned reads from the same samples were merged and used for peak calling with MACS2 (Zhang et al., 2008) and Genrich following Galaxy available protocols (Batut et al., 2018; Lucille et al., 2020). After comparing both algorithms, the downstream analyses were carried out with the MACS2 peaks. The heatmaps were generated with deepTools plot Heatmaps from Galaxy v2.1.1 with default parameters. For the visualization of the genomic data, bigwig files were

used as input for the pyGenomeTracks tool from Galaxy v2.1.1 with GRCh38 as reference genome.

4. 2. 9. Circular Chromatin Conformation Capture sequencing (4C-seq)

4. 2. 9. 1. Sample preparation

Cells were seeded in 10 cm dishes and after 24 h they were treated with DMSO or AI-10-49 3 μM for 6 h. The crosslinking was performed with 1% of formaldehyde for 20 min and quenched with 0.125 M Glycine for 10 min. The downstream processing of the samples, including the 4C-seq libraries, were generated from cross-linked cells as described previously (Stadhouders et al., 2013) with some modifications. NlaIII (four-cutter) was used as primary restriction enzyme. DpnII was used as secondary restriction enzyme (four-cutter).

The cross-linked cells were washed with PBS and resuspended in lysis buffer (Table 4) during for 10 min on ice. Afterwards, cells were centrifuged at 650 g for 5 min at 4°C, the nuclei were re-suspended in 0.5 ml of 1.2X NlaIII buffer and incubated at 37°C and 900 rpm for 1 h. Next, Triton X-100 was added to a final concentration of 2% followed by 1 h incubation at 37°C on a shaker at 900 rpm. The chromatin was then digested with 400 U of NlaIII overnight at 37°C and 900 rpm. NlaIII was inactivated by SDS addition in a final concentration of 1.6% and the mix at 65 °C for 20 min on a shaker at 900 rpm. The digested chromatin was transferred to 50 ml conical tubes and 6.125 ml of 1.15X ligation buffer (Table 4) was added together with Triton X-100 1%. The tubes were incubated on a shaker for 1 h at 37 °C. Subsequently, the digested chromatin was ligated with 100 U of T4 DNA ligase for 8 h at 16 °C followed by RNase A treatment for 45 min at 37 °C. Moreover, the chromatin was treated with 300 mg of Proteinase K (to de-crosslink it) and incubated at 65 °C overnight. The resulting DNA was then purified by standard phenol/chloroform extraction, precipitated with ethanol, and re-suspended in 100 ml of ddH_2O. At this point the digestion and ligation efficiencies were corroborated by analyzing a small fraction of the purified DNAs by gel electrophoresis as previously indicated (Stadhouders et al., 2013).The remaining DNA was digested with 50 U of DpnII at 37°C overnight. The resulting DNA was then purified by standard phenol/chloroform extraction, precipitated with

ethanol and re-suspended in 500 ml of ddH_2O. Afterwards, a second ligation was performed overnight at 16°C by adding 200 U of T4 DNA ligase into a final volume of 14 m 1X ligation buffer (Table 4). DNA samples were again purified by phenol/chloroform extraction, ethanol precipitation and re-suspended in 100 µl of Nuclease Free Water. This product was then purified with the commercial kit QIAgen PCR purification following manufacturer's instructions. For each sample a total of 1 µg of each library was amplified by inverse PCR with the Expand™ Long Template PCR System with 30 amplification cycles (94°C 2 min, 30x [94°C 10s,60°C 1 min, 68°C 3 min], 68°C 5 min). The primers were designed samples specific (Table 23) following the public guidelines (Stadhouders et al., 2013) targeting the selected viewpoint (*NOXA* promoter). The purified libraries were measured by QuantiFluor® ONE dsDNA System and sent for sequencing to the Erasmus University Medical Centre in a collaboration with Wilfred F. J. van Ijcken and his team.

4. 2. 9. 2. 4C downstream analysis

The 4C-seq libraries were sequenced on an Illumina HiSeq 2500 sequencer, with single reads of 74 bp. From these reads, the sequence next to the viewpoint was removed starting before the NlaIII restriction site (CATG). The sequences were trimmed with Trimmomatic (Bolger et al., 2014) and aligned to the human reference genome GRCh38 using HISAT2 with default parameters (D. Kim et al., 2015). The aligned reads were normalized to reads per million (RPM) and bedgraph files were generated for downstream analysis and visualization. The genomic visualizations were performed with pyGenomeTracks tool in Galaxy (Jalili et al., 2020) with GRCh38 as reference genome.

4. 2. 10. Statistical analysis

For each dataset, normality was assessed by Shapiro-Wilk test and homoscedasticity of the residuals was tested by Levene's test. Analyses were done with Infostat statistical software (www.infostat.com.ar), GraphPad Prism v8 (GraphPad Software Inc., USA) or R-3.4.1. For analysis of significant differences, Student's t-test, analysis of variance (ANOVA) test or

Fisher's exact test was used as indicated in the figure legends. For dose-response assay (non-linear regression) GraphPad Prism 8 was used to estimate the half-maximal growth inhibitory concentration (GI_{50}) and tested for statistical significance by comparing best-fit values of each curve, thus obtaining a p value for each treatment. Generally, the results are shown as the mand and the standard deviation (SD). p-value < 0.05 was taken as significant. *p<0.05, **p<0.01, ***p<0.001.

4. 2. 11. Data availability

The RNA-seq results from section 4. 2. 4. are placed in Gene Expression Omnibus (GEO) under the accession No: GSE148188. ChIP-seq and ATAC-seq genomic results are available under accession No.: PRJEB39828.

5. Results

5. 1. High-throughput drug screening identifies a CBFβ/RUNX1 inhibitor in *NOXA*^{high} cell lines

5. 1. 1. Establishment of NOXA-CRISPR/Cas9 knockout

To investigate NOXA-associated vulnerabilities, first I generated PDAC cell line models. I performed CRISPR/Cas9-mediated knockouts of the endogenous *NOXA* gene in two human (PSN1 and MIAPaCa-2) and two murine *Kras*^{G12D}-driven PDAC cell lines (mPDAC-06 and mPDAC-95) as described in section 4. 2. 1. 2.. The presence of the genomic deletion was corroborated via PCR with flanking primers (Fig. 4. A and B and Fig. 5; see section 4. 2. 2. 1 Table 31). Given that immunoblot for *Noxa* (mouse) is not possible, I did the knockout validation via Western blot only of the human cell lines (Fig. 4. C). I proceeded to work with those clones that were positive for the knockout PCR and showed no amplification of the wild type allele, to ensure complete removal of *NOXA* gene, regardless of the copy number.

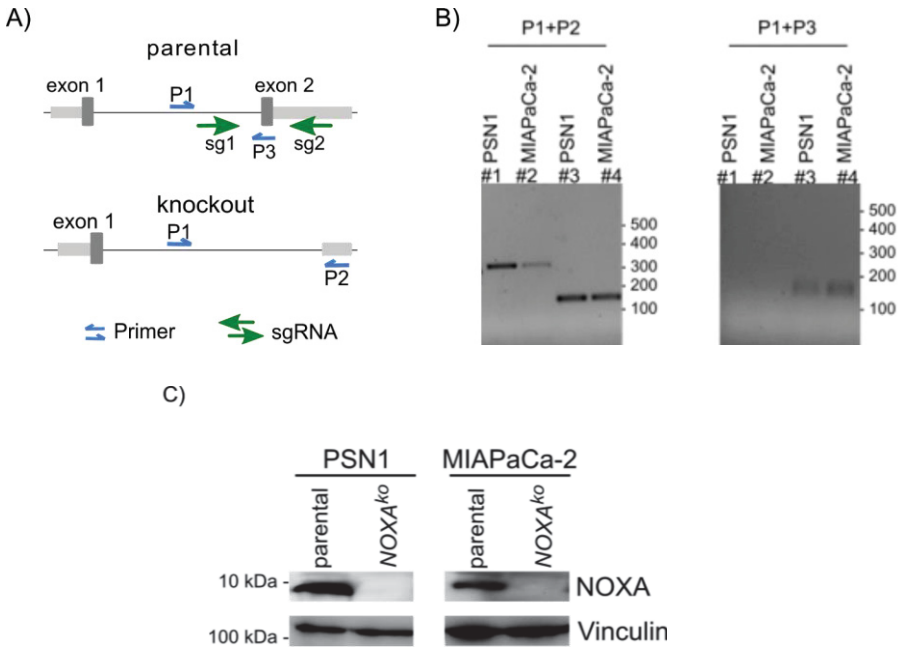

Figure 4: Human cell line generation. **A)** Schematic representation of the genomic positions of the sgRNAs and the genotyping primers for human *NOXA*. The primers are shown with their orientation (forward or reverse) and genomic position (inside or outside the knockout region). **B)** Selected clones shown in a 1.5 % agarose gel of the knockout and the parental counterpart cells with the indicated primers. P1+P2=knockout PCR. P1+P3=WT allele PCR. Clones #1 and #2 are positive for the knockout band and negative for the wild type PCR meaning the excision

of this genomic region, regardless of the number of copies, was complete. Shown is the ladder used as a molecular weight reference in base pairs (bp). Expected PCR products are depicted in Table 31. **C)** Representative western blot analysis of NOXA protein in PSN1 and MIAPaCa-2 parental and knockout lines. Vinculin served as loading control.

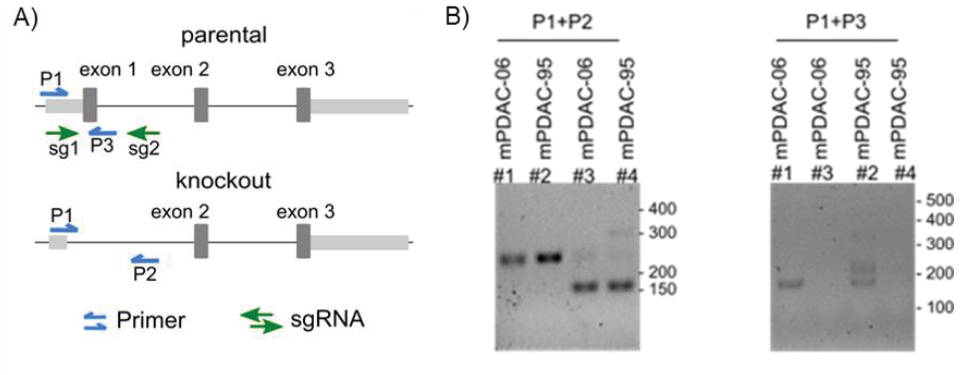

Figure 5: Murine cell line generation. A) Schematic representation of the genomic positions of the sgRNAs and the genotyping primers for murine *Noxa*. The primers are shown with their orientation (forward or reverse) and genomic position (inside or outside the knockout region). **B)** Selected clones shown in a 1.5 % agarose gel of the knockout and the parental counterpart cells with the indicated primers. P1+P2=knockout PCR. P1+P3=WT allele PCR. Clones #3 and #4 are positive for the knockout band and negative for the wild type PCR meaning the excision of this genomic region, regardless of the number of copies, was complete. Shown is the ladder used as a molecular weight reference in base pairs (bp). Expected PCR products are depicted in Table 31.

5. 1. 1. 1. Growth rate validation

I performed a growth curve in a Live-Cell Analysis System (Incucyte) to test whether there are duplication differences among the clones when compared to their parental cell lines. It was not observed any variation between each clone and its parental counterpart for the human cell lines (Fig. 6).

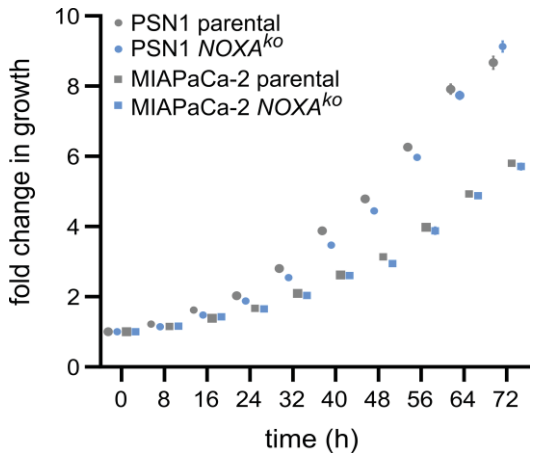

Figure 6: Duplication rate of pancreatic cancer cell lines. Duplication curves of PSN1 and MIAPaCa-2 parental and isogenic *NOXA*^{ko} cell lines performed with live-cell imaging. 5 pictures per well were taken every 8 h and growth was calculated as confluence (%) normalized to 0 h control. Shown is the mean and SD (n=24 technical replicates).

5. 1. 2. Drug screening results

To detect pharmacological activators of *NOXA*, I performed an unbiased drug screening with a total of 1842 compounds divided in 2 libraries: the anti-cancer compound library with 412 compounds and the FDA approved library composed of 1430 drugs.

The anti-cancer compound library was used to treat the murine and human *NOXA* knockout (*NOXA*^{ko}) and parental cell lines. Figure 7 shows the results of the viability assay for these 8 cell lines after treatment with the first 412 compounds depicted as % of living cells in a heatmap. Around 20% of the compounds show a reduction in cellular viability (orange). For visualizations purposes the drugs are randomly assigned by similarity in the response (%) in 20 clusters varying in size.

For technical reasons, the FDA library was used to test vulnerabilities in the two human cell lines that show contrasting *NOXA* mRNA and protein level (PSN1 and MIAPaCa-2) and the parental murine cell lines with the corresponding knockout clone. The result of this screening is shown in Figure 8 as a clustered heatmap of the viability of each cell line in response to each compound. For visualization purposes, the 1430 drugs were grouped into 50 clusters by

similarity in the response (%) thus producing clusters with different sizes. Surprisingly, around 8% of these compounds reduced cell viability to 20% or less in all the tested cell lines.

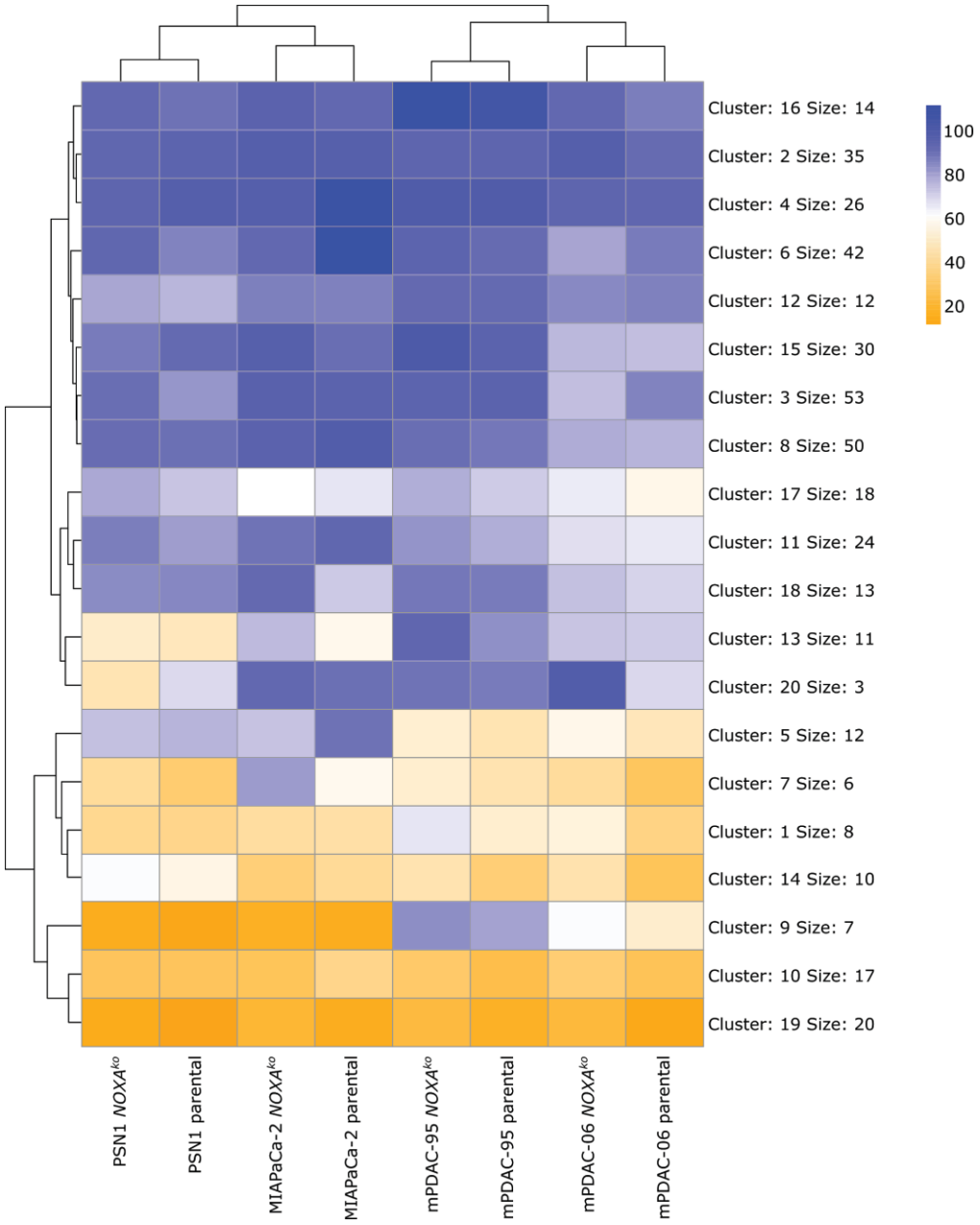

Figure 7: Drug screening: anti-cancer compound library. Clustering of viability results depicted as % of living cells, varying from 20-120% (normalized to DMSO control). Shown is the mean of biological triplicates as well as technical triplicates contained in 20 “drug clusters”. Each drug was grouped according to similarity in viability via hierarchical clustering, thus producing the difference in cluster size.

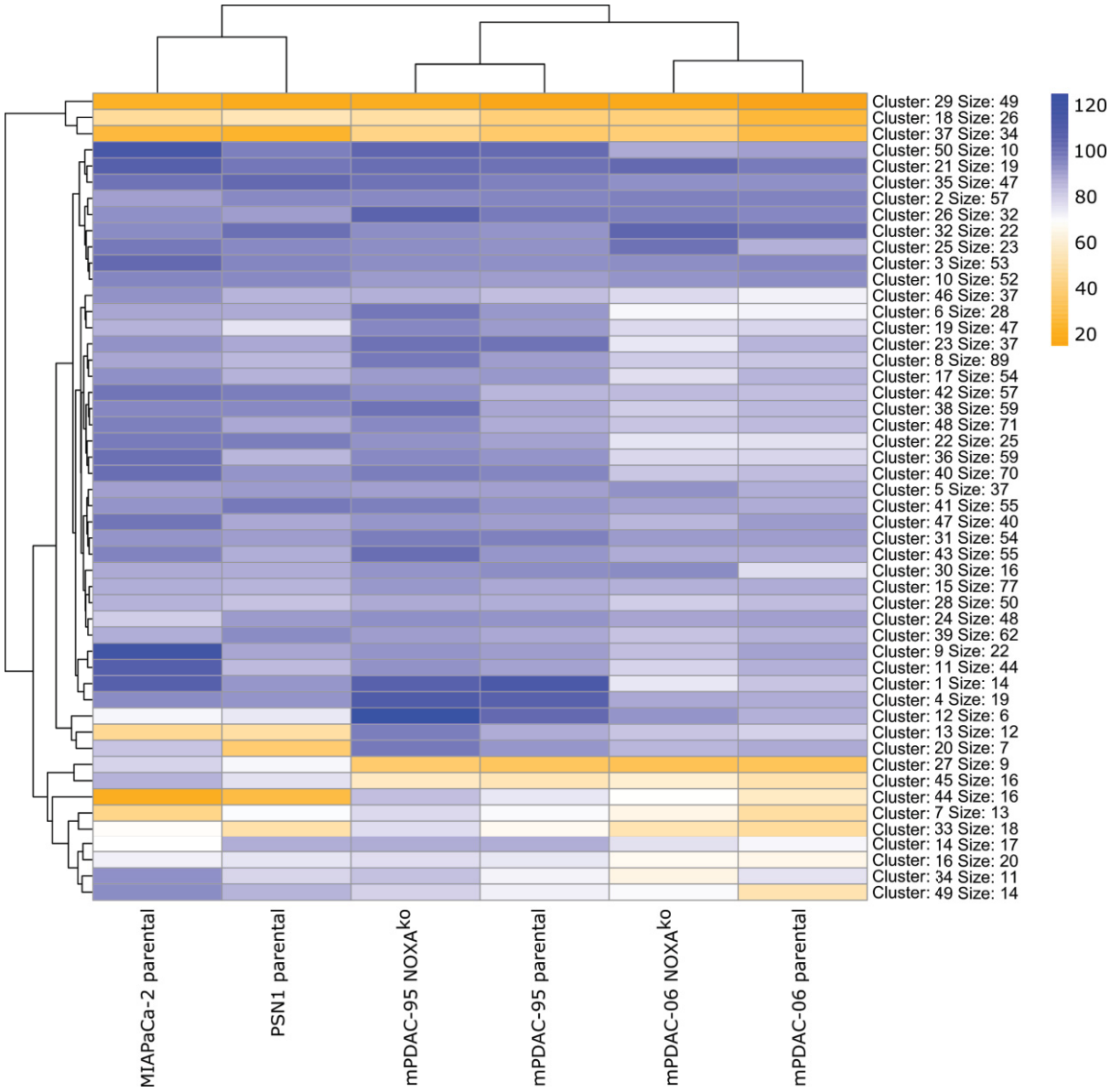

Figure 8: Drug screening: FDA-approved compound library. Clustering of viability results depicted as % of living cells, varying from 20-100% (normalized to DMSO control). Shown is the mean of biological triplicates as well as technical triplicates contained in 50 “drug clusters”. Each drug was grouped according to similarity in viability via hierarchical clustering, thus producing the difference in cluster size.

5. 1. 3. Drug filtering and selection

Since the aim was to find NOXA-associated vulnerabilities, the first criteria I took to narrow down the selection was to choose those compounds that were more effective in the parental/*NOXA*^{high} cell lines. I used a cut-off of at least 10% difference in cell viability when comparing each parental to its *NOXA*^{ko} counterpart and analyzed its statistical significance. Out of the 1842 compounds, I identified 50 drugs that showed higher efficiency in parental cell

lines compared to isogenic *NOXA*^{ko} cell lines. Among these compounds I found, for example, DNA synthesis inhibitors/nucleoside analogues (20%), cytoskeleton and topoisomerase inhibitors (17.5%), epigenetic-related compounds (7.5%), Polo Like Kinase 1 inhibitors (10%), proteasome inhibitors (5%), MEK inhibitors (7.5%), mTOR/PI3K (2.5%). Given that many compounds are promising when used *in vitro* but fail in clinical trials, the chosen compounds followed these criteria: efficient cell killing, differential cell inhibition between parental and knockout lines and drug novelty or unknown in the field of pancreatic cancer. With these criteria I selected 12 compounds to do a dose-response drug treatment (7 concentrations in the aforementioned 8 cell lines and modeled the GI_{50} (concentration of a drug that inhibits 50% of cell proliferation). I aimed to find a compound capable of inhibiting cell growth in all *NOXA*^{wt} (proficient) cell lines robust enough to act in a human and murine background. Out of those 12, the only drug that significantly inhibited more efficiently all 4 parental cell lines was AI-10-49 (Fig. 9. A and B). Moreover, all the knockouts lines were more resistant to this drug treatment than the parental lines (Fig. 9. B). In the following table (Table 37) are listed the 12 compounds and their most studied mode of action.

Table 37. **List of compounds to be tested after filtering and selection**

Compound	Mode of action
AI-10-49	RUNX1/CBFβ-SMMHC interaction blocker
AZD7762	CHK1/CHK2 inhibitor
bAp15	Deubiquitinase inhibitor
CB-5083	p97 AAA ATPase inhibitor
CX-6258	pan-PIM kinase inhibitor
GMX1778	Nicotinamide phosphoribosyltransferase (NAMPT) inhibitor
JIB-04	pan-Jumonji histone demethylase inhibitor
MK1775	WEE1 inhibitor
Obatoclax	Antagonist of BCL-2 (BH3 mimetics)
RSL3	GPX4 inhibitor (ferroptosis activator)
SC144	gp130 inhibitor
SGI-1027	DNA methyltransferase (DNMT) inhibitor

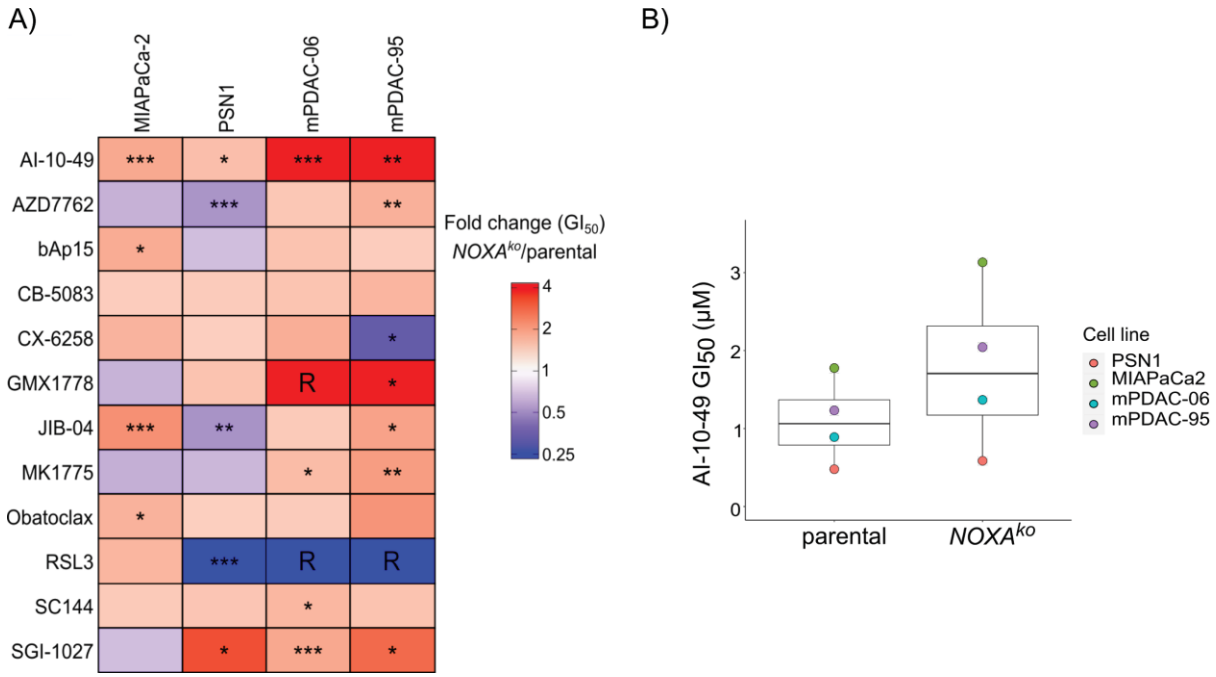

Figure 9: Dose-response treatment in human and murine cell lines identifies AI-10-49 as the most efficient compound in *NOXA* expressing cells. A) Seven concentrations were used to treat the parental and *NOXA*^{ko} human cell lines MIAPaCa-2, PSN1 and the parental and *NOXA*^{ko} murine cell lines mPDAC-06 and mPDAC-95. Viability was measured with MTT after 72 h of treatment. Here is depicted the fold change of the GI_{50} of the *NOXA*^{ko} line over its respective parental. n=4; all biological replicates were performed as technical triplicates. From the *NOXA*^{ko}GI_{50}/*NOXA*^{wt}GI_{50} calculation I obtained the difference in the response: red represents sensitivity in the parental cell line (smaller GI_{50}) in respect to the knockout (higher GI_{50}). Blue stands for higher sensitivity in the knockout cell line and R means that the cell lines showed resistance against the drug and the GI_{50} could not be calculated within the tested concentrations. Dose-response inhibition was calculated with logarithmic regression and tested for significance with logit model (*p<0.05, **p<0.01, ***p<0.001). **B)** Seven concentrations were tested on the parental and *NOXA*^{ko} human cell lines MIAPaCa-2, PSN1 and the parental and *NOXA*^{ko} murine cell lines mPDAC-06 and mPDAC-95. Viability was measured with MTT after 72 h of treatment. Here is shown the GI50 of each cell line calculated with a logarithmic regression of dose-response inhibition. n=3; all biological replicates were performed as technical triplicates.

5. 1. 4. Validation of drug screening results with Cancer Cell Line Encyclopedia (CCLE)

To validate the robustness of the high-throughput screening results I analyzed the public database CCLE from the Broad institute (https://portals.broadinstitute.org/ccle). Here is deposited the results of a dose-response drug viability assay represented as area under curve (AUC) with the 49 available pancreatic cancer cell lines and 444 drugs. Given that not all the compounds were tested in all the cell lines, I did several steps of filtering and clustering after

which only 18 remained in which 444 compounds were tested. I could corroborate that among the most effective compounds one can find topoisomerase inhibitors (e.g., topotecan), cytoskeleton inhibitors (e.g., docetaxel, paclitaxel), MEK inhibitors (e.g., selumetinib) and more importantly, the same compounds I found in the screening, such as obatoclax, AZD7762 and MK1775 among others (Fig. 10).

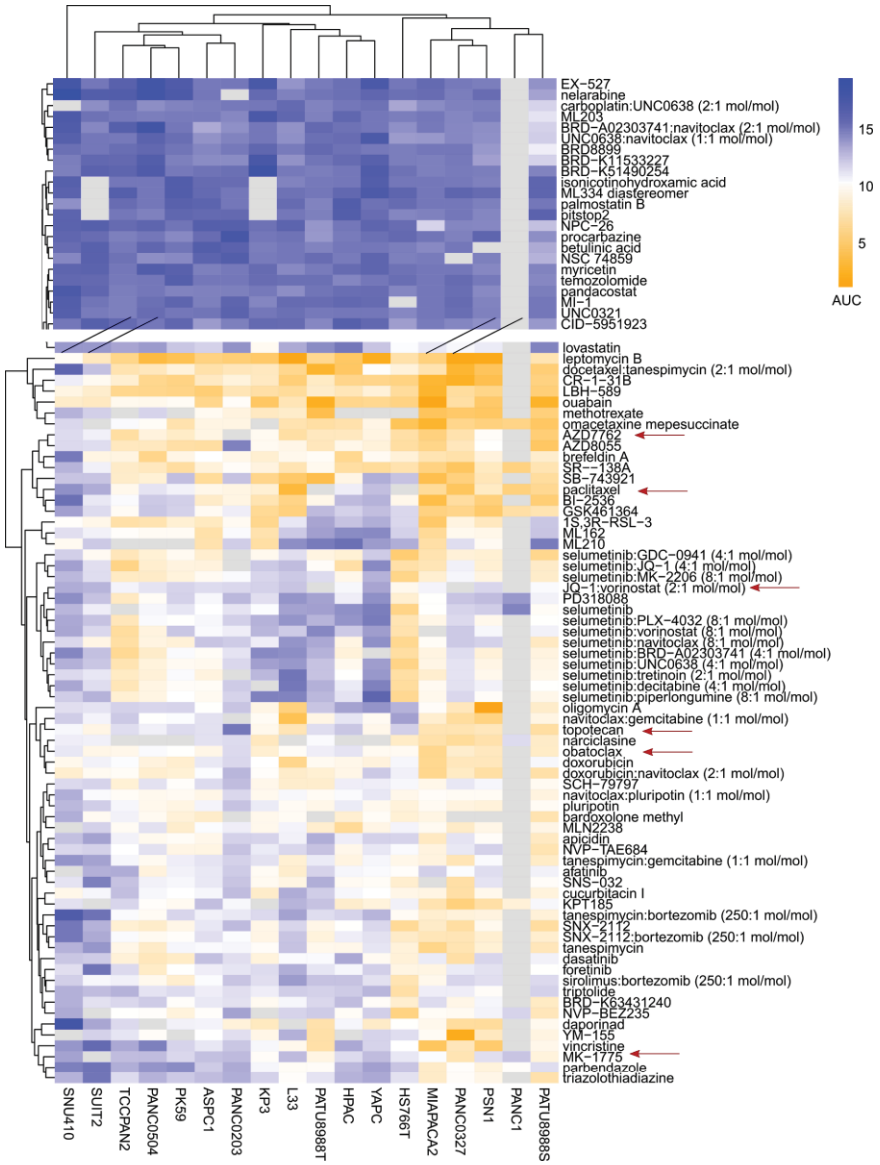

Figure 10: CCLE drug treatment (AUC) in 18 PDAC cell lines. Seven concentrations were used to treat the CCLE collection database, and they are depicted as a heatmap of the area under curve (AUC). The smaller the AUC the more sensitive the cell lines are towards the treatment. Shown is the number of cell lines in which at least 3 drugs were tested. In red arrows are marked some of the parallelisms between my high throughput drug screening and the one from CCLE. For visualization reasons, this heatmap is shown incomplete (denoted transversal black with lines). Only the most effective and the least effective compounds are shown.

5. 1. 5. AI-10-49 synergizes with different compounds

Combination therapies are one of the most common strategies to deal with cancer patients in the clinic (Mizrahi et al., 2020). Since the aim is finding new therapeutic options, it was decided to test the new selected compound, AI-10-49, with different compounds that belong either to standard of care treatment (e.g., oxaliplatin and gemcitabine) or are being tested in clinical trials. In addition, I chose compounds that were tested in the high-throughput drug screening: the BRD4 inhibitor JQ1, the novel HDAC inhibitor quisinostat, the nucleoside analogue gemcitabine (PDAC standard of care) the DNA-synthesis inhibitor oxaliplatin (standard of care in PDAC) and the BH3 mimetics obatoclax. I treated the human cell line with seven concentrations of AI-10-49 and 2 specific doses of the other compounds (as described in MM). Each new compound was tested alone and in combination with AI-10-49 to then calculate via the Chou-Talalay method the combination index (CI) (Chou, 2010). All the tested compounds synergized with AI-10-49 in various concentrations (Fig. 11). Noteworthy, gemcitabine has a high synergism and effectiveness when combined with AI-10-49 (Fig. 11. B). Moreover, JQ1 showed a high combination index as previously proved (Pulikkan et al., 2018) throughout all the concentrations (Fig. 11. A). On the other hand, quisinostat (Fig. 11. C) was not so synergistically efficient as compared to the other compounds and oxaliplatin displayed synergism at high concentrations but with low cell killing (high Fa) (Fig. 11. D). Lastly, obatoclax exhibited a mild killing effect (around 50% of dead cells) and when treated with the 150 nM concentration combination the effect observed is mostly additive (Fig. 11. E). These results highlight the different opportunities available to combine novel therapies and the relevance of choosing the right concentrations.

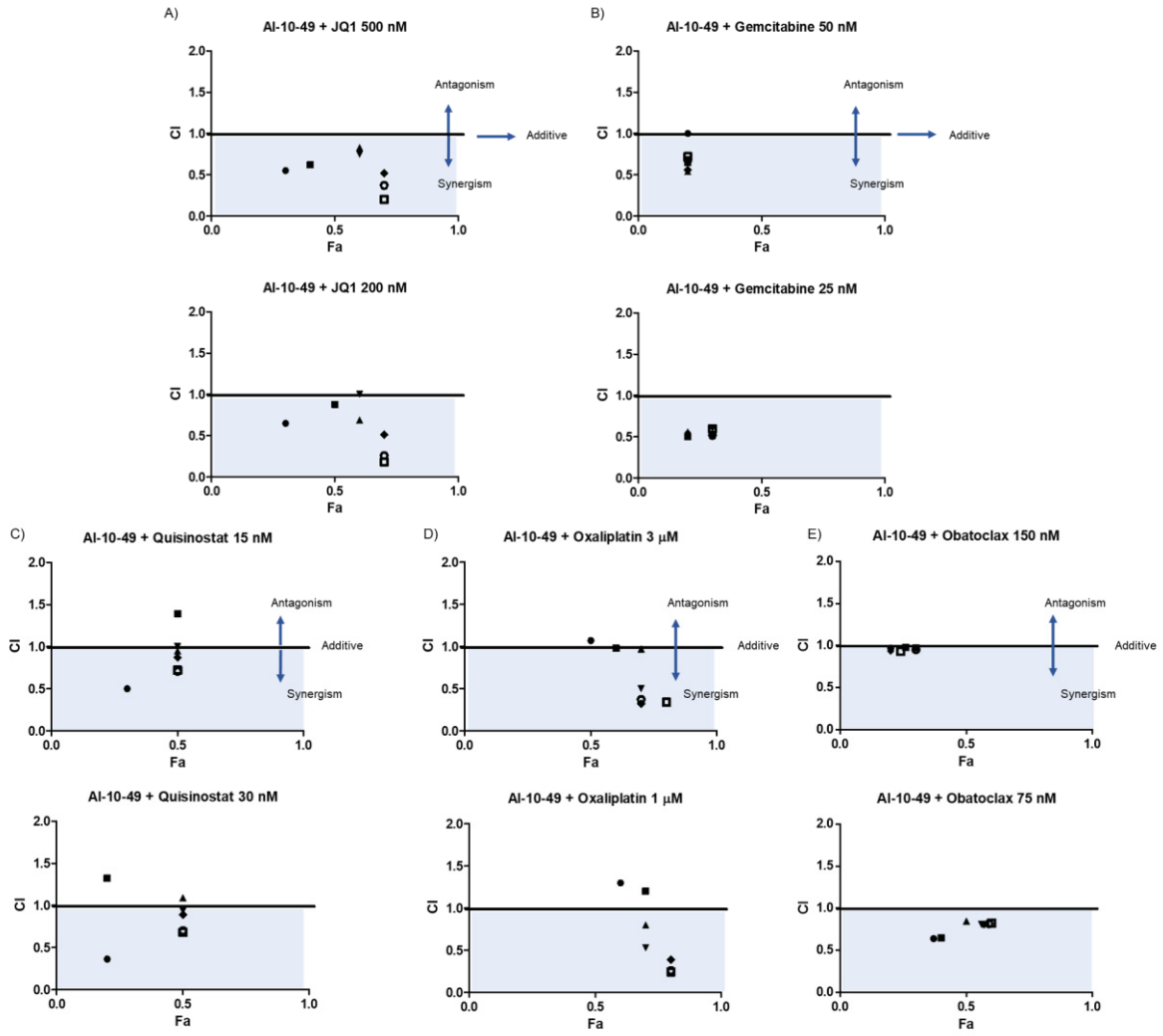

Figure 11: AI-10-49 is highly synergistic with the tested compounds. Plot showing synergism between the indicated compound at the indicated concentrations and seven doses of AI-10-49 (1200, 600, 300, 150, 75, 37.5, 18.75 nM). PSN1 and MIA-PaCa-2 cell lines were treated with AI-10-49 alone, the indicated compound alone, the combination and DMSO. The viability results (MTT assay) were used to plot an isobologram program according to the Chou-Talalay method in CompuSyn as described in section 4. 2. 1. 10. Fa, affected fraction (effect of the combination in cell viability, meaning alive after treatment); CI, combination index. When Fa<0.5, at least 50% of the cells died due to the specific combination. Each dot contains n=3 biological replicates performed as technical triplicates.

5. 2. NOXA is a key player in cell death induced by AI-10-49 treatment

5. 2. 1. NOXA expression is rapidly regulated upon AI-10-49 treatment

In the previous section it was demonstrated that AI-10-49 is a potent cell proliferation inhibitor of *NOXA* expressing cells when compared to *NOXA* deficient cells (Fig. 9. B) Pulikkan and

collaborators (Pulikkan et al., 2018) demonstrated that AI-10-49 triggers apoptosis signature within 6 h of treatment in leukemia cells which have the oncofusion CBFβ/SMMHC and a milder effect in wild type cells. Among the top regulated hits, they found a strong downregulation of *MYC* and by analysis of their RNA-seq I found *NOXA* within the most upregulated genes in the gene set Hallmark Apoptosis (data not shown). Given that pancreatic cancer cells do not harbor the mutation that leads to CBFβ/SMMHC oncofusion, I wanted to study whether AI-10-49 is an inductor of apoptosis and *NOXA* regulator in this entity. To study this, I treated pancreatic cancer cells with increasing doses of AI-10-49 for 6 h and checked *NOXA* mRNA level (Fig. 12. A). In both cell lines there is a significant *NOXA* upregulation upon AI-10-49 treatment.

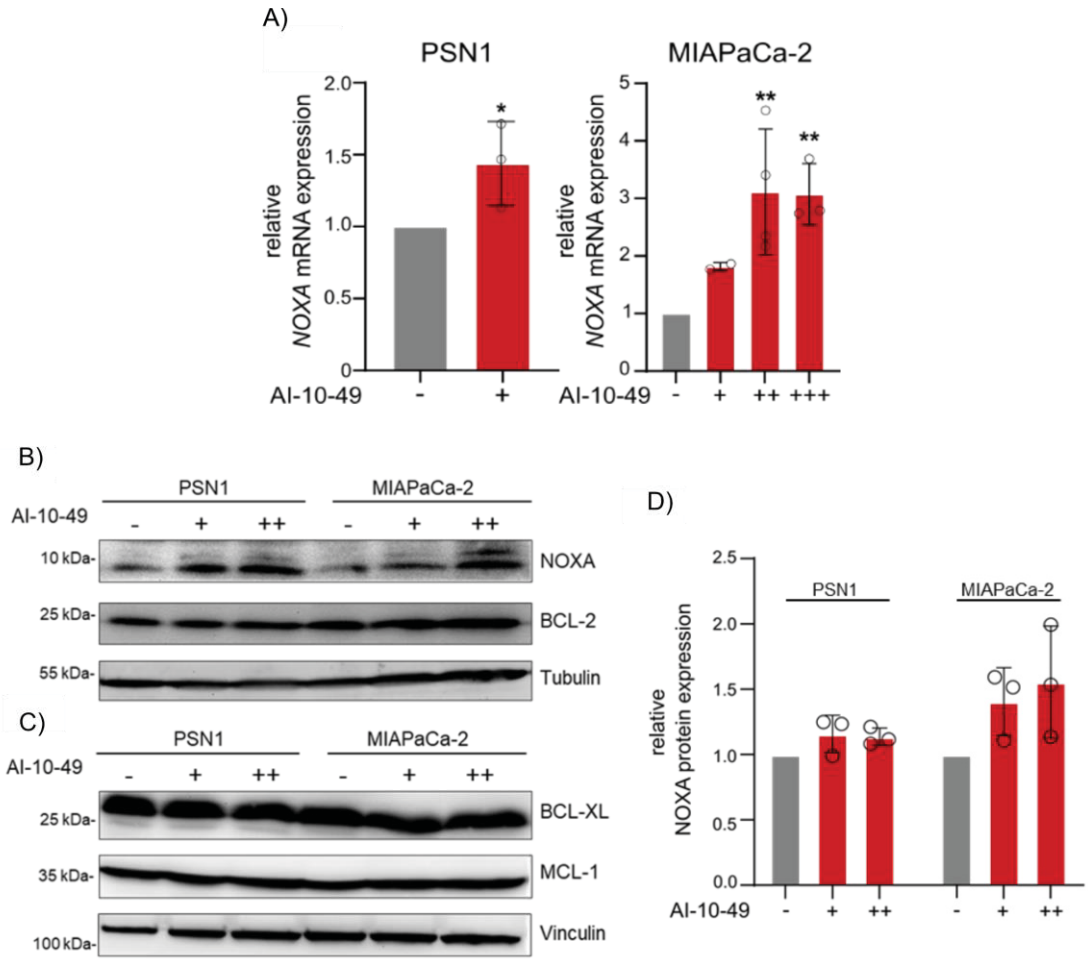

Figure 12: *NOXA* mRNA and protein expression is rapidly regulated by AI-10-49. A) Bar plot showing the qRT-PCR of *NOXA* expression in PSN1 and MIAPaCa-2 cell lines upon treatment. Cells were treated with DMSO (-) or AI-10-49 (+ 1.2 µM; ++ 3 µM, +++ 6 µM) for 6 h. *Actin* and *GAPDH* expressions were used to normalize *NOXA* mRNA expression. n=3 or n=4; all biological replicates were performed as technical triplicates. Each dot represents a biological replicate. Shown is the mean and SD. p-value of ANOVA test, Dunnet comparison,

*p<0.05, **p<0.01. **B and C)** PSN1 and MIAPaCa-2 cell lines were treated with DMSO (-) or AI-10-49 (+ 1.2 µM; ++ 3 µM) for 6 h. Two representative western blots are shown. Tubulin and Vinculin served as loading controls. n=3; all biological replicates were blotted in 2 different experiments. **D)** Quantification of NOXA protein expression relative to tubulin control. DMSO (-) protein expression was set to 1. Each dot represents a biological replicate.

To test if this *NOXA* mRNA upregulation correlated with an increase in the protein level, I did immunoblot for the PSN1 and MIAPaCa-2 cell lines after 6 h of treatment. Moreover, I analyzed whether other members of the BCL-2 protein family were regulated (Fig. 12. B, C and D). Noteworthy, there is a significant increase in NOXA protein as well as mRNA expression within a short period of AI-10-49 treatment, whereas the other proteins remain unchanged.

Interestingly, I observed that the other BCL-2 protein family members are not as tightly regulated as NOXA at short-time treatments. Therefore, I performed a long-term treatment with AI-10-49 1.2 µM to avoid complete cell death during the 72 h of the experiment (Fig. 13. A and B).

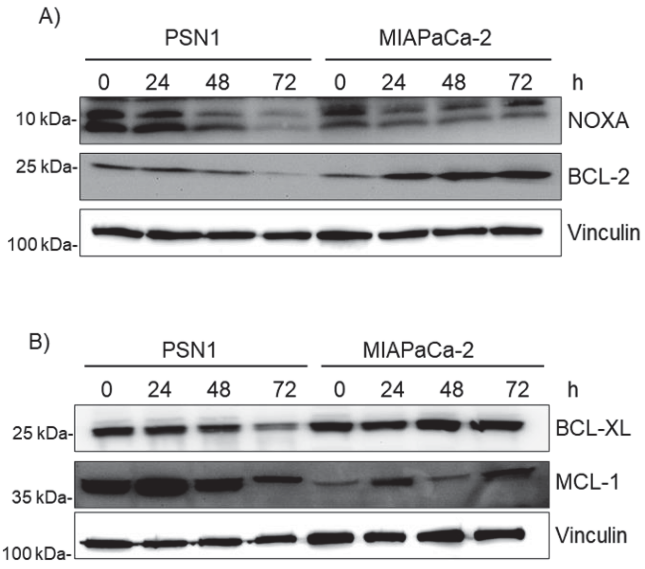

Figure 13: BCL-2 family protein regulation in AI-10-49 treated cells. A) and B) PSN1 and MIAPaCa-2 cell lines were treated with DMSO (0 h) or AI-10-49 1.2 µM for 24, 48 and 72 h. Two representative western blots are shown. Vinculin served as loading control. n=3; all biological replicates were blotted in 2 different experiments.

5. 2. 2. AI-10-49 induces G2/M arrest and apoptotic cell death

To elucidate the impact that NOXA upregulation downregulation has on pancreatic cancer cells when treated with the CBFβ/RUNX1 inhibitor (AI-10-49) I used FACS analysis to determine apoptosis and cell cycle profile.

5. 2. 2. 1. AI-10-49 treatment induces G2/M arrest

I performed cell cycle profiling on PSN1 MIAPaCa-2 cell lines after 48 h of drug treatment. When I compare the vehicle treated cells with the drug treated, it is observed a significant difference in the proportion of cells in the G2/M phase in the case of MIAPaCa-2 (Fig 14). In case of PSN1 there is a slight tendency towards this phenomenon, even though it is not statistically significant.

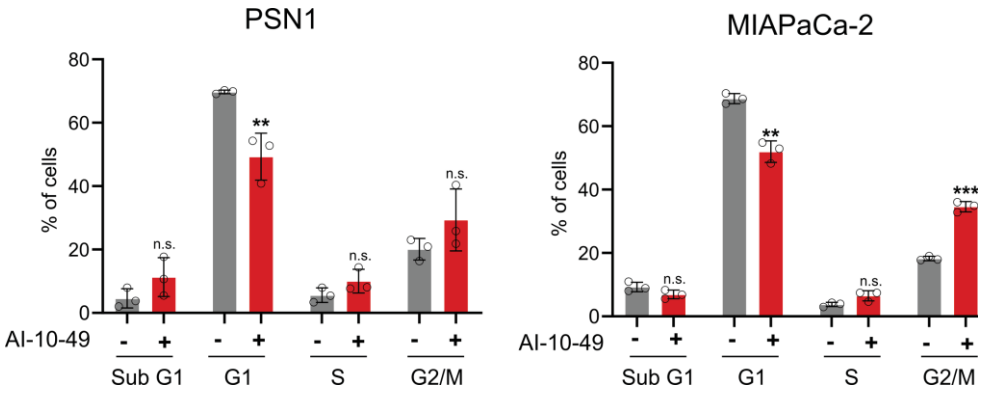

Figure 14: AI-10-49 induces G2/M arrest in pancreatic cancer cells. Cell cycle profile of MIAPaCa-2 cells after 48 h of AI-10-49 1.2 μM treatment. Each bar represents the percentage of cells in that cell phase. Shown is the mean and SD. n=3; all biological replicates were performed as technical duplicates. Each dot represents a biological replicate. P value of ANOVA test, **p<0.01, ***p<0.001, n.s.=not significant.

5. 2. 2. 2. AI-10-49 treatment drives apoptotic cell death

In line with the cell cycle profiling, I next asked whether AI-10-49 was a drug capable of triggering apoptosis. First, I performed apoptosis analysis in PSN1 and MIAPaCa-2 parental and *NOXA*^{ko} cell lines. Second, to further prove the role of NOXA in AI-10-49 mediated cell death I included a *NOXA* overexpression cell line by means of CRISPR/dCas9-VP64-MS2-HSF1 activation system (CRISPRa) (Konermann et al., 2015).

5. 2. 2. 2. 1. Establishment of a NOXA overexpression cell line (*NOXA CRISPRa*)

I designed one sgRNA targeting the promoter region of *NOXA* (Fig. 15. A) and transduced MIAPaCa-2 cells with 3 different lentiviruses carrying the overexpression system, as described in section 4. 2. 1. 4. Afterwards, I confirmed the NOXA endogenous induction system via immunoblot (Fig. 15. B).

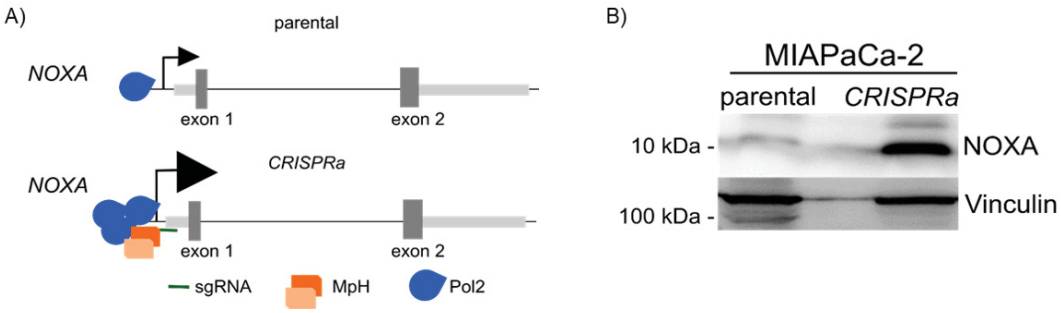

Figure 15: CRISPR/dCas9-VP64-mediated NOXA overexpression. A) Schematic representation of *dCas9-VP64-MS2-HSF1* driven *NOXA* overexpression. The different proteins are driven by one sgRNA to the endogenous *NOXA* promoter region where the transcription machinery is recruited thus inducing its expression. **B)** Representative western blot of NOXA protein in MIAPaCa-2 cells after stable transduction of the different components of *dCas9-VP64-MS2-HSF1*. Vinculin served as loading control.

5. 2. 2. 2. 2. NOXA regulates apoptotic cell death in pancreatic cancer cells

The cell line PSN1, which is characterized by a high level of *NOXA*, showed in the previous experiment a tendency towards a G2/M arrest upon AI-10-49 treatment (Fig. 14), yet not statistically significant. Therefore, I checked the apoptotic fraction in the parental line, and found that about 40% of the drug treated cells underwent apoptosis in comparison to only a 12% in the control (Fig. 16). In the case of $NOXA^{ko}$ cells, the apoptotic fraction dropped to around 23%. This experiment, together with the previous result showing that $NOXA^{ko}$ cells are more resistant to AI-10-49 treatment (Fig. 9. B), enabled me to shed light in the role NOXA plays in programmed cell death.

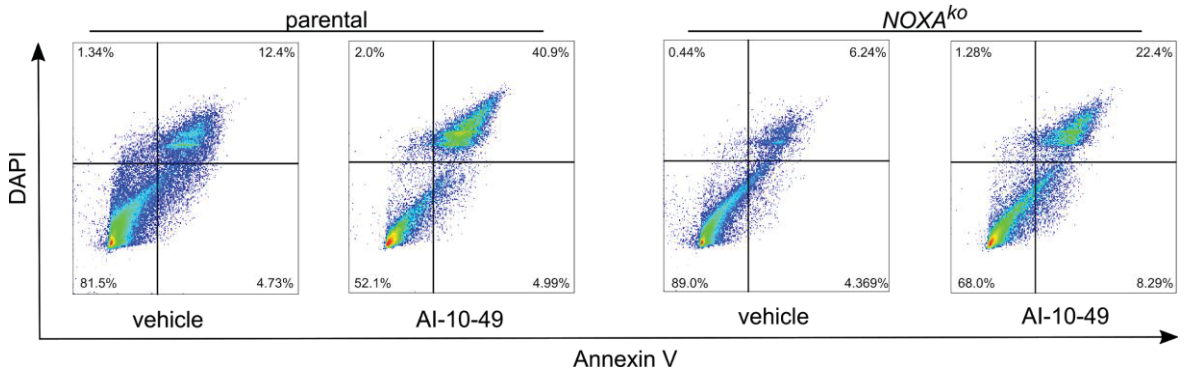

Figure 16: AI-10-49 induces apoptosis in a NOXA-dependent way. FACS analysis of Annexin V/DAPI staining of PSN1 parental and *NOXA*^{ko} cells. The cells were treated with DMSO (vehicle) or AI-10-49 1.2 µM for 48 h. A representative scatter plot of the experiment is shown. n=3; biological replicates were performed without technical replicates.

To further prove NOXA-mediated cell death triggered by AI-10-49 I included the overexpressing cell line described in the previous section (Figure 15). According to previous results, MIAPaCa-2 (parental and *NOXA*^{ko} cell lines) is more resistant to AI-10-49 induced cell death (Fig. 9) and displays a significant G2/M arrest upon treatment (Fig. 14). When *NOXA* is activated in the overexpressing line *NOXA CRISPRa*, the % of total dead cells (see 4. 2. 1. 5 for its calculation) significantly increased to a 30% in comparison to 13% of the parental control (Fig. 17). This finding reinforces the idea of the key role NOXA has in apoptotic cell death in pancreatic cancer *in vitro*.

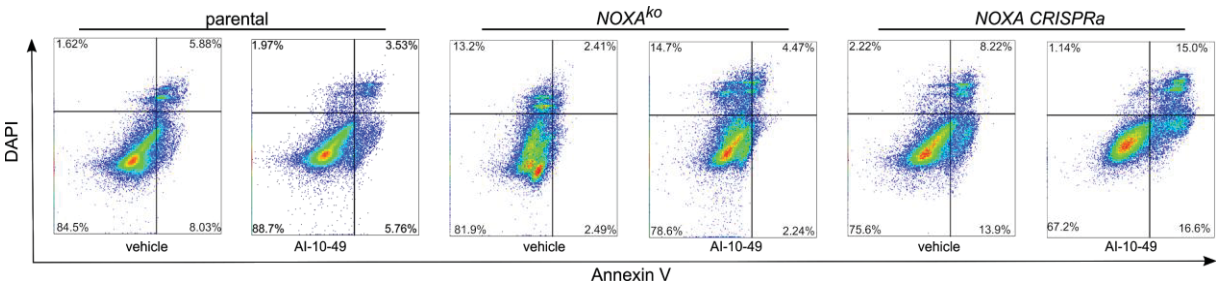

Figure 17: AI-10-49 induces apoptosis in a NOXA-dependent way. FACS analysis of Annexin V/DAPI stained MIAPaCa2 parental, *NOXA*^{ko} and *NOXA CRISPRa* cells. The cells were treated with DMSO (vehicle) or AI-10-49 1.2 µM for 48 h. A representative scatter plot of the experiment is shown. n=3; biological replicates were performed without technical replicates.

5. 2. 3. NOXA expression sensitizes pancreatic cancer cells towards AI-10-49 treatment

I showed how AI-10-49 induces apoptosis, G2/M arrest and reduces cell viability more effectively in *NOXA* expressing cells. In addition, I performed colony formation assay in *NOXA*^{ko} and overexpressing cell lines to test how the clonogenic growth could be affected by NOXA expression. In accordance to my previous results, in the *NOXA-CRISPRa* cells the clonogenic growth was drastically inhibited when treated with AI-10-49, whereas knockout cells showed a limited response towards the treatment (Fig. 18 A and B). This experiment shows evidence to support the role of NOXA in driving cell death and functioning as a strong sensitizer in PDAC.

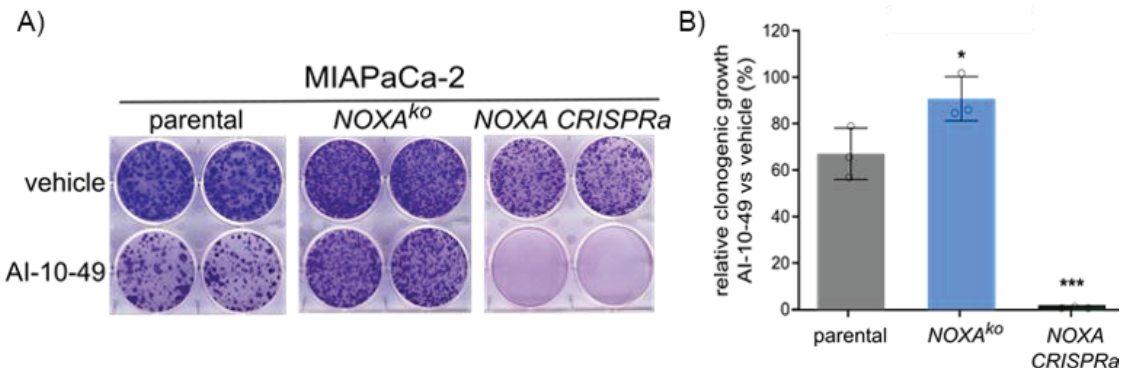

Figure. 18: NOXA expression reduces clonogenic growth. A) Representative image of clonogenic assay in MIAPaCa-2 parental, *NOXA*^{ko} and *NOXA CRISPRa*. Cells were treated for 2-3 weeks with vehicle (DMSO) or AI-10-49 400 nM. **B)** Quantification of clonogenic assay in parental, *NOXA*^{ko} and *NOXA-CRISPRa*. Each treatment was quantified and normalized against its DMSO control. Depicted is the number of colonies (%) per treatment compared to vehicle. Shown is the mean and SD. n=3; all biological replicates were performed as technical duplicates. Each dot represents a biological replicate. P value of ANOVA test, *p<0.05, ***p<0.001.

5. 2. 4. AI-10-49 treatment regulates transcriptional apoptotic pathways

To better understand the first transcriptional changes that the cells undergo when CFBβ/RUNX1 interaction is disrupted, I performed RNA-seq in several pancreatic cancer cell lines shortly treated with vehicle (DMSO) or AI-10-49. In agreement with *NOXA* upregulation after treatment (Fig. 12), gene set enrichment analysis (GSEA) of the transcriptome profiles revealed a significant enrichment in the Apoptosis signature from the Hallmark pathways

(p=0.003, q=0.025) in all AI-10-49 treated cells (Fig. 19). In vehicle treated cells I found enrichment of the gene ontology term (GO) *Chromatin remodeling* (p=0.003, q=0.146) thus indicating alterations in chromatin dynamics upon AI-10-49 treatment.

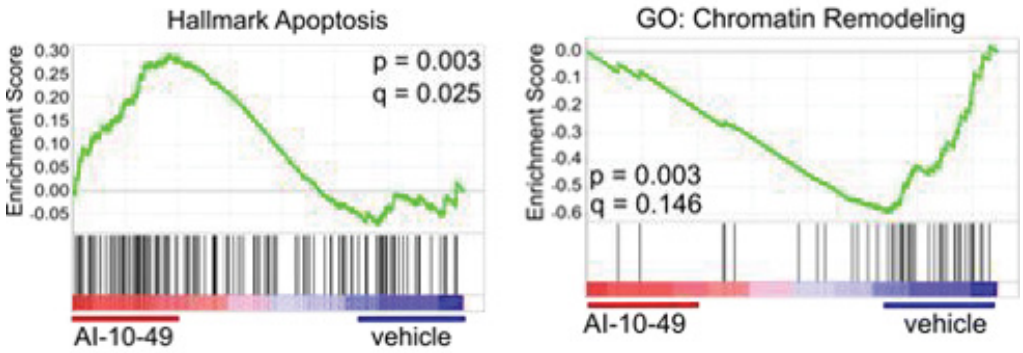

Figure 19: AI-10-49 rapidly induces apoptotic transcriptional programs. Gene set enrichment analysis of RNA-seq data of MIAPaCa-2, Panc1 and PSN1 cell lines. Cells were treated with vehicle (DMSO) or AI-10-49 3µM for 6 h and grouped according to treatment in the bioinformatics analysis. n=3 biological replicates.

5. 3. RUNX1 acts as an apoptotic regulator through NOXA protein levels and epigenetic changes

5. 3. 1. Establishment of RUNX family knockout

It was next considered how AI-10-49 induces the transcriptional activation of *NOXA*. Since AI-10-49 inhibits the interaction between CBFβ and the DNA binding proteins encoded by RUNX family (i.e., RUNX1, RUNX2 and RUNX3) as described in section 2. 5. 3. 1., I performed knockouts of the three *RUNX* genes *RUNX1*, *RUNX2* and *RUNX3* in MIAPaCa-2 cells (Fig. 20). I knocked out the same genes in PSN1 and Panc1 cell lines, yet for handling reasons I performed the following experiments with MIAPaCa-2. Those clones positive for knockout allele and negative for wild type allele were used in further experiments.

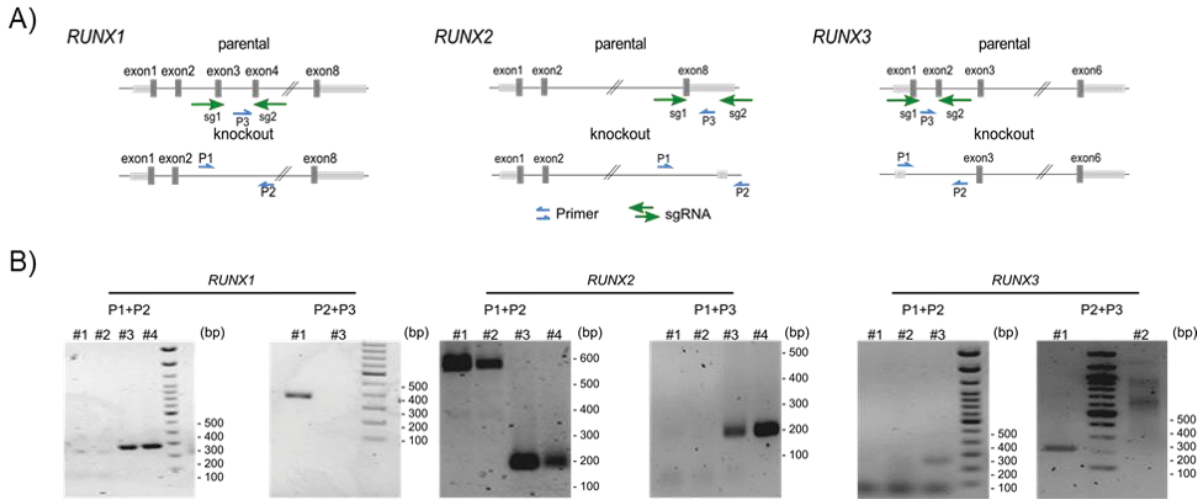

Figure 20: RUNX family knockout. A) Schematic representation of *RUNX* gene family knockout. For *RUNX1* knockout, 2 sgRNAs were designed to excise the gene region from exon 3 to exon 4. For *RUNX2* knockout, 2 sgRNAs were designed to target excision of beginning of exon 8 until stop codon. For *RUNX3* knockout, 2 sgRNAs target upstream exon 1 and end of exon 2. Each gene has its primer pair to discriminate between knockout and wild type alleles. Genotyping PCR of MIAPaCa-2 cells to screen for knockout and wild type alleles of *RUNX1*, *RUNX2* and *RUNX3* with the indicated pair of primers, according to the scheme in A). The primers are shown with their orientation (forward or reverse) and genomic position (inside or outside the knockout region). **B)** Selected clones shown in a 1.5% agarose gel of the knockout and the parental counterpart cells with the indicated primers. *RUNX1*: clones #3 and #4 are positive for the knockout band and #3 is negative for the wild type allele as shown in the P2+P3 PCR in the right. *RUNX2*: clones #1 and #2 are positive for the knockout band and negative for the wild type allele as shown in the P1+P3 PCR shown in the right. RUNX3: P1 + P2: knockout PCR, clones #3 is positive for the knockout band and negative for the wild type allele as shown in the P2+P3 PCR shown in the right. Expected PCR products are depicted in Table 31.

5. 3. 2. RUNX1 depletion leads to NOXA upregulation

It was analyzed the level of *NOXA* mRNA in MIAPaCa-2 RUNX family knockouts to check if I could reproduce the upregulation observed when the cells were treated with AI-10-49 (Fig. 12. A). I observed an induction of *NOXA* mRNA solely in *RUNX1* knockout cells (Fig. 21. A), arguing for a possible RUNX1-dependent repression of *NOXA* transcription. In addition, it was observed a significant NOXA induction in *RUNX1*^{ko} cells at the protein level (Fig. 21 B and C).

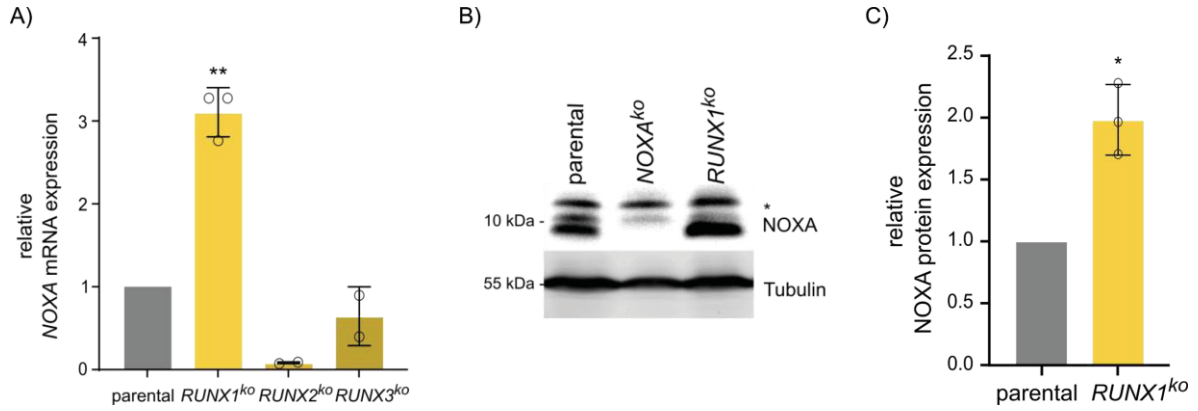

Figure 21: *RUNX1*^{ko} induces *NOXA* mRNA and protein expression. A) Bar plot showing the qPCR of *NOXA* expression in MIAPaCa-2 parental, *RUNX1-3* knockout cell lines. *NOXA* expression of the parental cell line was set to 1 and the knockouts were compared to it. Beta Actin was used to normalize *NOXA* mRNA expression. n=2 or n=3; all biological replicates were performed as technical triplicates. Shown is the mean and SD. Each dot represents a biological replicate. p-value of ANOVA test, Dunnet comparison, **p<0.01. **B)** Representative western blot analysis of NOXA protein in parental, *NOXA*^{ko} and *RUNX1*^{ko} MIAPaCa-2 cells. Tubulin served as loading control. * unspecific band. **C)** Quantification of NOXA protein expression. Parental control was set to 1. Each dot represents a biological replicate. Tubulin was used to normalize NOXA expression. n=3; shown is the mean and SD. Each dot represents a biological replicate. p-value of Student's t-test, *p<0.05.

5. 3. 3. RUNX1 deletion leads to cell growth inhibition and apoptotic cell death

Considering that AI-10-49 treatment increased *NOXA* expression thus increasing apoptosis (Fig. 16 and 17) and reducing clonogenic growth (Fig. 18), I next questioned what the cellular effects of *NOXA* upregulation due to *RUNX1* depletion are. I performed apoptosis analysis by FACS and clonogenic growth assay in a cell basal state. I observed an increase in total cell death of *RUNX1*^{ko} cells when compared to parental cells (approximately 20%) (Fig. 22. A). Accordingly, the same knockout cells showed a strong clonogenic growth inhibition (Fig. 22. B and C). These results underscore the relevance RUNX1 has as a major transcription factor in pancreatic cancer possibly playing a role in orchestrating apoptotic cell death.

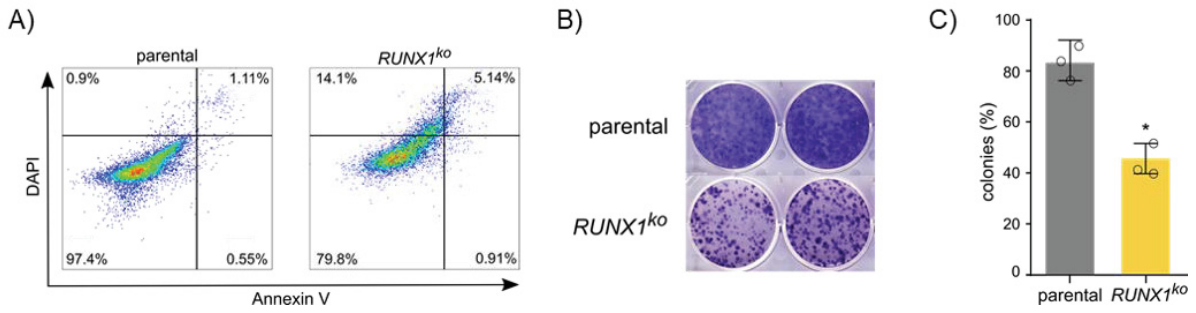

Figure 22: *RUNX1^{ko}* cells display high apoptotic fraction and impaired cell growth. A) FACS analysis of Annexin V/DAPI stained MIAPaCa2 parental and *RUNX1^{ko}*. **B)** Representative image of clonogenic assay in MIAPaCa-2 parental and *RUNX1^{ko}* cells. Cells were left to grow 2-3 weeks. **C)** Quantification of clonogenic assay in parental and *RUNX1^{ko}* shown as % of area occupied by the cells. Shown is the mean and SD. n=3; all biological replicates were performed as technical duplicates. Each dot represents a biological replicate. p-value of Student's t-test, *p<0.05.

5. 3. 4. *RUNX1^{ko}* cells activate transcriptional apoptotic pathways

I analyzed transcriptome profiles of parental and *RUNX1^{ko}* cell lines to test whether these apoptotic effects were present at the transcriptional level. *RUNX1^{ko}* cells showed a strong downregulation of the Hallmark MYC targets V1 and V2, arguing for the role RUNX1 might play in regulating major apoptotic factors in pancreatic cancer cells (Fig. 23). Even though the gene set Apoptosis from Hallmark is enriched in the *RUNX1^{ko}* cells from my RNA-seq, it is not statistically significant (Fig. 24. A). However, by analysis of the public database The Cancer Genome Atlas (TCGA) it is showed that there is a negative correlation (p=0.026) between *RUNX1* expression levels and the GO-term apoptotic pathways (Fig. 24. B). Taken together, it was corroborated that RUNX1 depletion/interference leads to activation of transcriptional apoptotic programs thus driving cell death.

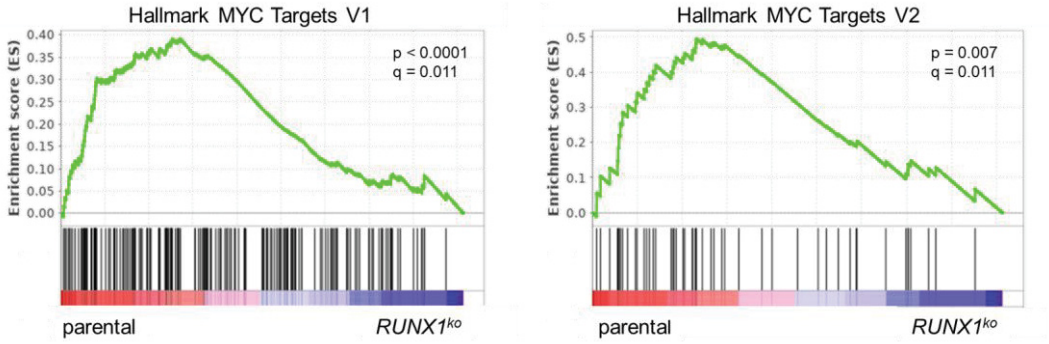

Figure 23: *RUNX1*^{ko} cells exhibit a loss in MYC activity. Gene set enrichment analysis of RNA-seq data of MIAPaCa-2 parental and *RUNX1*^{ko} cells. n=3 or n=4, biological replicates.

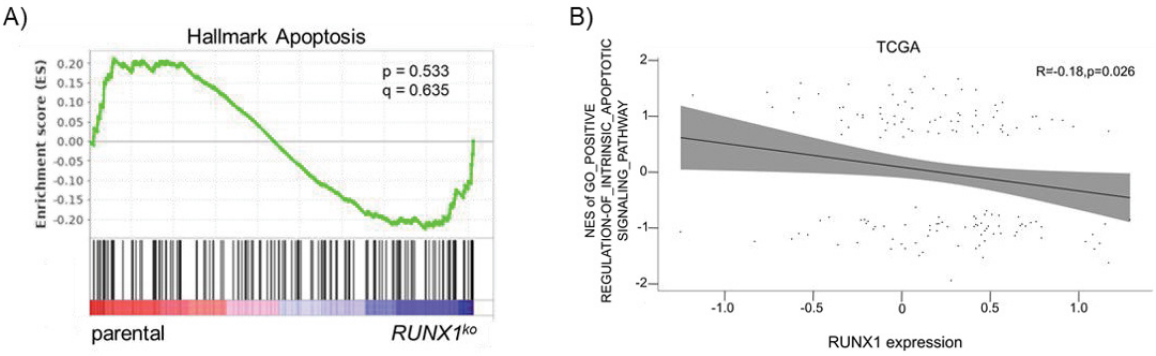

Figure 24: *RUNX1* expression correlates with transcriptional apoptotic programs. A) Gene set enrichment analysis of RNA-seq data of MIAPaCa-2 parental and *RUNX1*^{ko} cells. n=3 or n=4, biological replicates. **B)** Spearman correlation analysis of *RUNX1* mRNA expression with the normalized enrichment score of the indicated intrinsic apoptotic signaling pathway gene signature from the TCGA dataset. NES, normalized enrichment score.

5. 3. 5. RUNX1 regulates global chromatin accessibility

I then studied the epigenetic changes that might be associated with the transcriptional dysregulation observed in *RUNX1*^{ko} cells (Fig. 23 and 24). To study this, I performed assay for transposase accessible chromatin followed by high-throughput sequencing (ATAC-seq). Noteworthy, upon *RUNX1* deletion, the chromatin accessibility drastically increases (Fig. 25. A), arguing for its repressive role. Moreover, when RUNX1 is depleted, *NOXA* genome location becomes highly accessible (Fig. 25. B), supporting the idea that RUNX1 could act as a *NOXA*

repressor thus its removal triggers a significant upregulation at mRNA and protein level (Fig. 21).

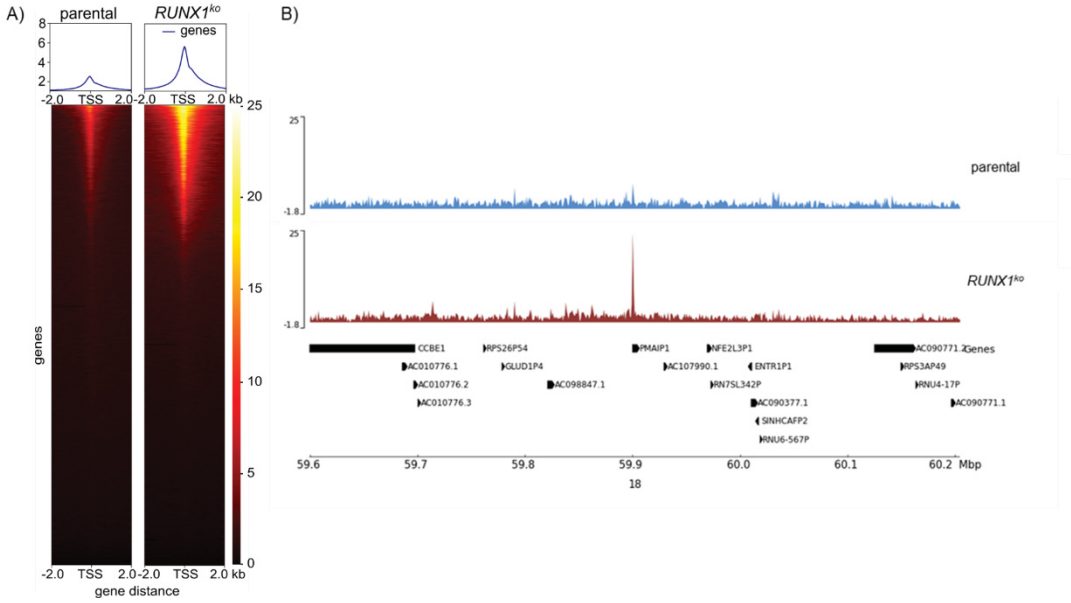

Figure 25: *RUNX1*^{ko} increases global chromatin accessibility. A) Heatmap representing the number of peaks of accessible chromatin by Omni-ATAC-seq analysis in parental and *RUNX1*^{ko} MIAPaCa-2 cells. Each line represents one gene and the plot on top is a cumulative representation of all the signal. n=2 biological replicates. TSS, transcriptional start site. **B)** Genomic visualization of *NOXA* gene (*PMAIP1*) in parental and *RUNX1*^{ko} cells (see 4. 2. 7. 3). Analysis done with the help of Stefanos Bamopoulos, Charité University Clinic.

5. 4. Pharmacological and genetic inhibition of RUNX1/CBFβ interaction induce global chromatin changes

5. 4. 1. Pharmacological inhibition of RUNX1 reduces global DNA accessibility

Given that chromatin remodeling pathways are dysregulated in AI-10-49 treated cells (Fig. 19) and *RUNX1*^{ko} cells have a strong global increase in chromatin accessibility (Fig. 25. A), I performed ATAC-seq analysis in MIAPaCa-2 cells upon CBFβ/RUNX1 inhibition. Notably, RUNX1/CBFβ interaction inhibition via AI-10-49 for only 6 h, decreased chromatin accessibility (Fig. 26. A). The intensity of the drug treated cells result is quite discrete, and the number of peaks is low, probably due to low quality of the sequencing. Nevertheless, both results show the same tendency, arguing that RUNX1 might play a major role in controlling apoptotic-related pathways in pancreatic cancer.

Moreover, when I examined in detail the genomic region of *NOXA*, I see that *RUNX1*^{ko} cells are the only ones showing a strong peak of positive accessibility (Fig. 26. B) compared to MIAPaCa-2 parental DMSO control and AI-10-49 treated cells.

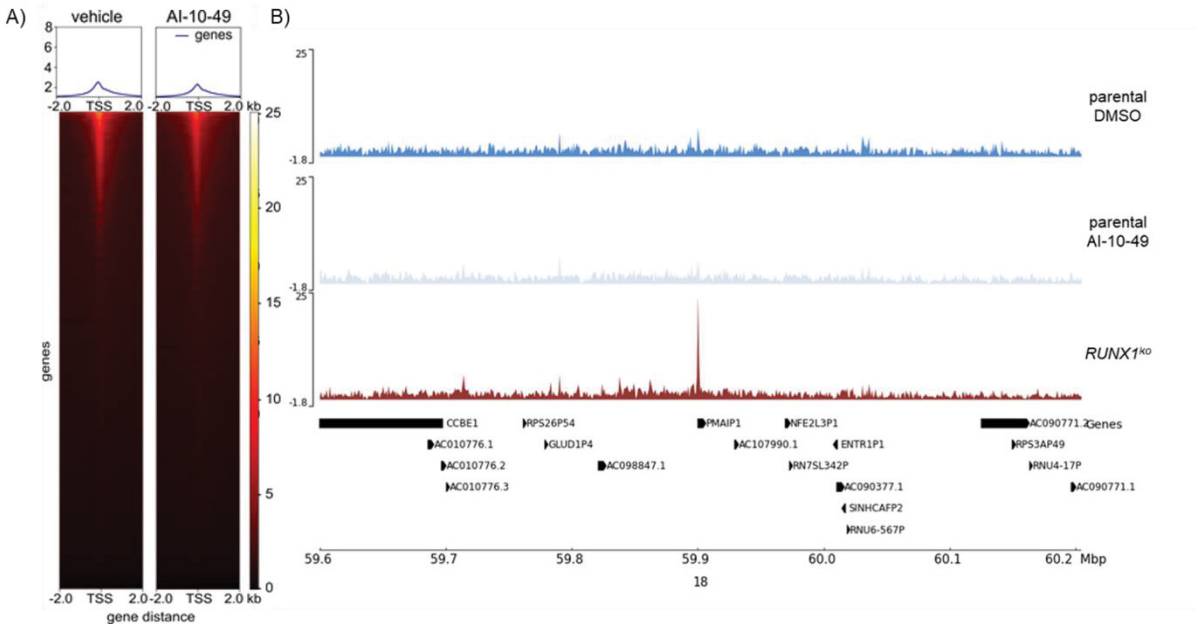

Figure 26: AI-10-49 treatment mildly reduces chromatin accessibility. **A)** Heatmap representing the number of peaks of accessible chromatin by ATAC-seq analysis in MIAPaCa-2 cells treated with DMSO (vehicle) or AI-10-49 3 µM for 6 h. Each line represents one gene and the plot on top is a cumulative representation of all the signal. n=2 biological replicates. TSS, transcriptional start site. **B)** Genomic visualization of *NOXA* gene (*PMAIP1*) in parental DMSO, parental AI-10-49 treated cells and *RUNX1*^{ko} cells (see 4. 2. 7. 3). Analysis done with the help of Stefanos Bamopoulos, Charité University Clinic.

5. 4. 2. *NOXA* promoter does not change its DNA interactions

To mechanistically understand how CBFβ/RUNX1 inhibition triggers *NOXA* expression, I performed chromosome conformation capture with high-throughput sequencing (4C-seq). This technique enabled the study of the DNA-DNA interaction of the *NOXA* promoter region (viewpoint) to the rest of the genome (Fig. 27). Comparing parental cells with RUNX1 inhibited cells, I did not observe major changes in the interaction of *NOXA* regulatory regions and the rest of the genome. Thus, the increase in *NOXA* mRNA level might be given by other factors (e.g., histone acetylation, higher accessibility) and not an increase in the interaction between the promoter of *NOXA* and its associated enhancers. Moreover, I found some regions

upstream the viewpoint with high interaction at *NOXA* promoter, pointing out their possible role as enhancer regions. However, this should be further corroborated with ChIP-seq studies for more histone marks (Calo & Wysocka, 2013).

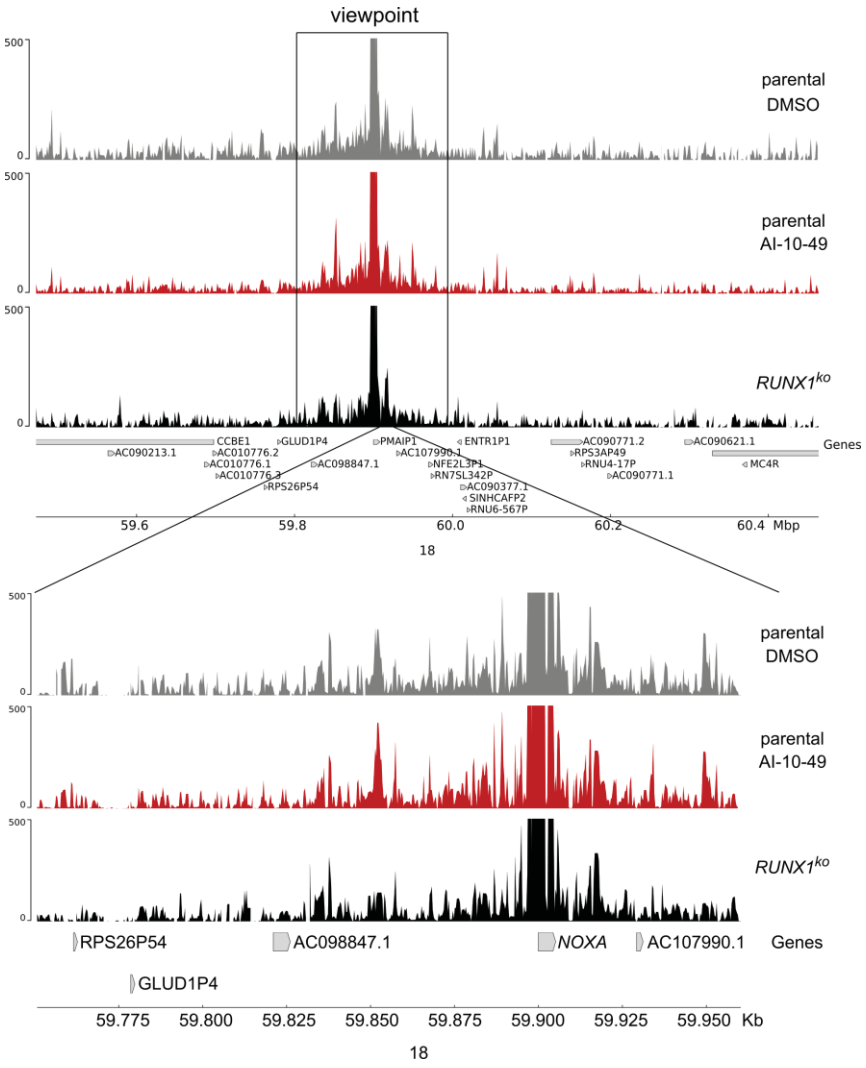

Figure 27: *NOXA* promoter does not change its DNA interacting partners or binding intensity upon RUNX1 inhibition. 4C-seq profile created in MIAPaCa-2 parental treated with DMSO or AI-10-49 3 μM for 6 h and MIAPaCa-2 *RUNX1*^{ko} cells. *NOXA* promoter region was used as a viewpoint in all 4C-seq experiments.

5. 4. 3. AI-10-49 treatment leads to global chromatin changes

I have shown that RUNX1 depletion, either by AI-10-49 treatment or RUNX1 knockout induces *NOXA* upregulation (Fig. 12. A-B and 21, respectively), *MYC* targets downregulation (Fig. 23), apoptotic signatures (Fig. 24) and global decrease in chromatin accessibility (Fig. 25 and 26).

In addition, to understand the impact of AI-10-49 mechanism to orchestrate cell death in regulating RUNX1 binding to the chromatin, I performed chromatin immunoprecipitation followed by high-throughput sequencing (ChIP-seq) in AI-10-49 MIAPaCa-2 treated cells. ChIP-seq analysis of H3K27ac peaks, which denotes transcriptionally active regions (2. 5. 1), indicated a global reduction, though mild, in this mark after 6 h of AI-10-49 treatment (Fig. 28. A and B). Notably, analysis of RUNX1 binding peaks from the ChIP-seq, showed a strong

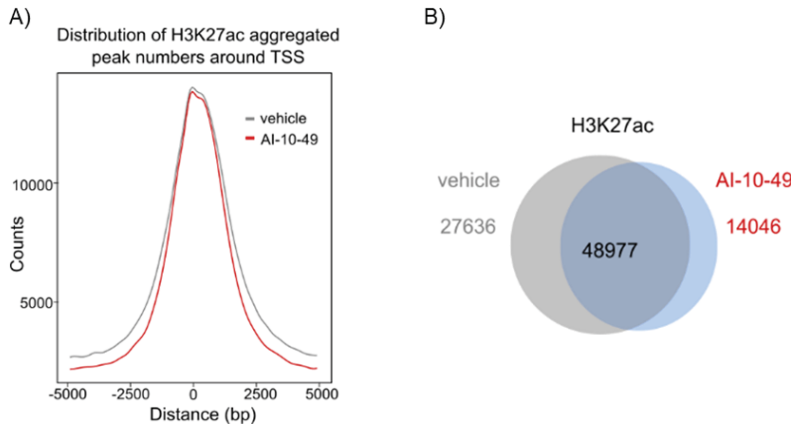

decrease in positive peaks after treatment (Fig. 29. A and B).

Figure 28: Global acetylation mildly decreases upon AI-10-49 treatment in MIAPaCa-2 cells. A and B) Aggregated peak signal from transcriptional start site (TSS) and Venn diagram

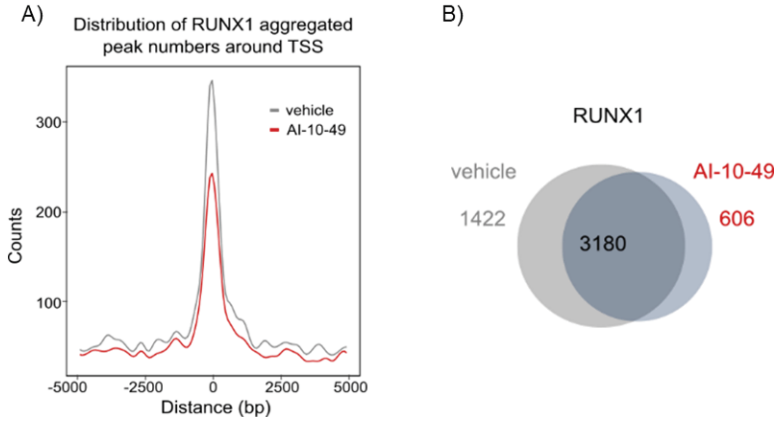

of peak distribution for H3K27ac ChIP-seq peaks in MIAPaCa-2 cells treated with vehicle (DMSO) or AI-10-49 3 μM for 6 h.

Figure 29: RUNX1 binding decreases upon AI-10-49 treatment in MIAPaCa-2 cells. A and B) Aggregated peak signal from transcriptional start site (TSS) and Venn diagram of peak distribution for RUNX1 ChIP-seq peaks in MIAPaCa-2 cells treated with vehicle (DMSO) or AI-10-49 3 μM for 6 h.

Interestingly, I found that H3K27ac is moderately increased in the region surrounding *NOXA* (Fig. 30. A) and corroborated it via ChIP-qPCR of different regulatory regions (Fig. 30. B). This result highlights the idea of RUNX1 being a *NOXA* repressor and when its activity is reduced (either via knockout or AI-10-49), as shown in the ATAC-seq results (Fig. 30. B), *NOXA* expression is highly induced. In the case of RUNX1, the pull down among experiments is quite variable, yet it shows a tendency towards a decrease in the chromatin binding after AI-10-49 treatment (Fig. 30. B).

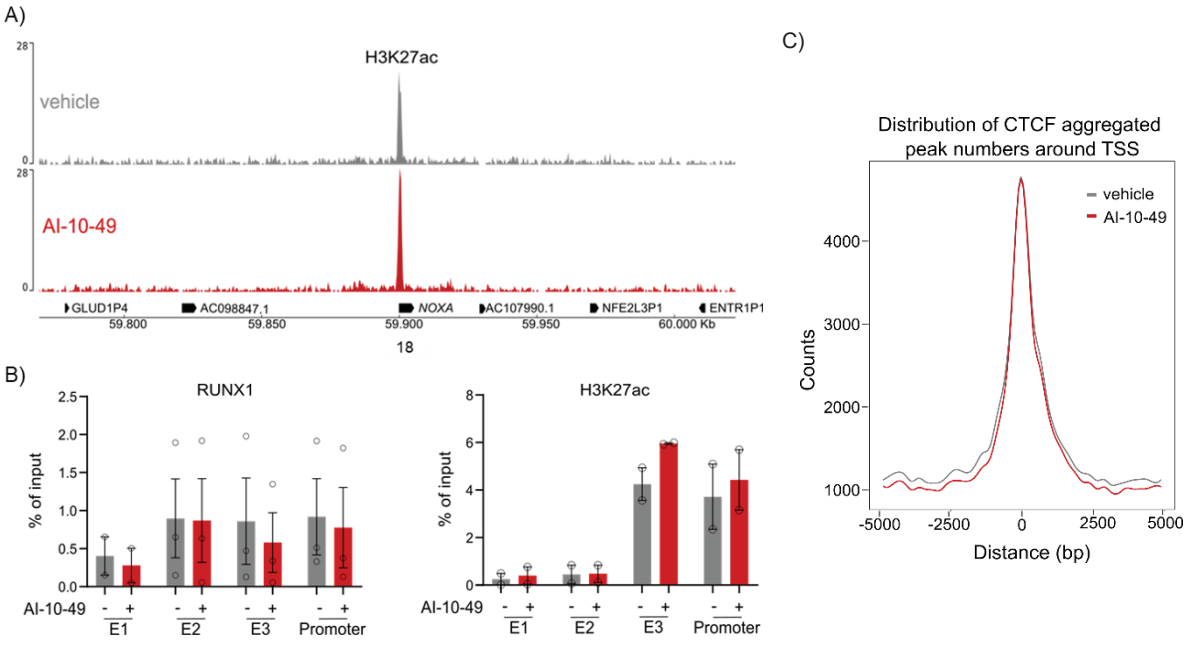

Figure 30: H3K27ac increases in *NOXA* promoter region whereas chromatin architecture remains stable. A) Genomic visualization of ChIP-seq results for H3K27ac in *NOXA* gene in MIAPaCa-2 cells treated with DMSO or AI-10-49 3 µM for 6 h. **B)** ChIP-qPCR analysis for RUNX1 (left) and H3K27ac (right) in MIAPaCa-2 cells treated with DMSO or AI-10-49 3 µM for 6 h. n=2 or n=3, each immunoprecipitation was measured as technical triplicates with qPCR (Materials and methods). Each dot represents a biological replicate. Given the differences between the experiments inherent to the pull down, the SD is high, and statistics cannot be calculated. E1, E2 and E3: putative enhancer regions according to H3K4me1 and H3K27ac ChIP-seq analysis of public database of MIAPaCa-2 and Panc1 cell lines (GEO, Query dataset GSE64557). **C)** Aggregated peak signal from transcriptional start site (TSS) of peak distribution for CTCF ChIP-seq peaks in MIAPaCa-2 cells treated with vehicle (DMSO) or AI-10-49 3 µM for 6 h.

Given the observed global changes at the chromatin level, I next analyzed the changes in its architecture. To study this, I did CTCF ChIP-seq in vehicle and AI-10-49 treated cells (Fig. 30. C). As expected, AI-10-49 does not induce architectural changes in the chromatin dynamics at short times, pointing out that the changes observed might be given by other phenomena.

5. 4. 3. 1. AI-10-49 treatment increases acetylation and RUNX1 binding only in promoter regions

To check how RUNX1 and H3K27ac marks are distributed throughout the genome, I analyzed the differential enrichment patterns (AI-10-49 compared to DMSO treatment) of these two proteins. First, I calculated the enriched regions of each treatment to then visualize how they were distributed along the different genomic features (Fig. 31). It was found a decrease in enrichment in nearly all the regions, supporting the previous result where it was shown a global decrease in ChIP-seq signal (Fig. 28 and 29). Interestingly, I found up to 2-fold enrichment in RUNX1 and H3K27ac peaks at promoter regions in AI-10-49 treated cells (Fig. 31). This result indicates that although there is a global loss of acetylation and RUNX1 binding upon treatment, both proteins are accumulated in promoter regions.

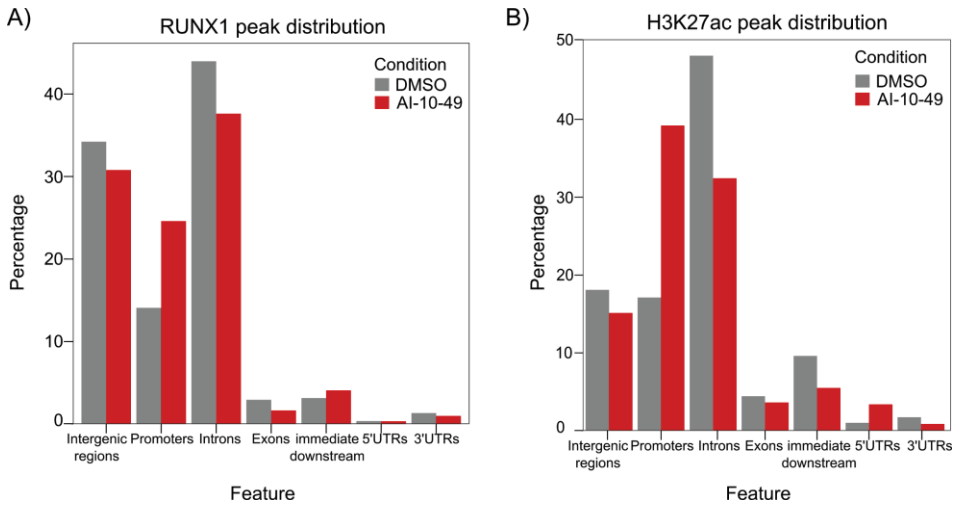

Figure 31: RUNX1 and H3K27ac are enriched in promoters upon AI-10-49 treatment. Genomic peak distribution of RUNX1 ChIP-seq (left) and H3K27ac (right) from MIAPaCa-2 cells treated with DMSO or AI-10-49 3 μM for 6 h.

In addition, I examined which gene pathways were enriched after AI-10-49 treatment. I did GO pathway analysis of these promoter sequences enriched in RUNX1 and H3K27ac after drug treatment and found a total of 205 gene sets significantly present in RUNX1 and 518 for H3K27ac. Noteworthy, I found only 29 GO terms significantly enriched that overlap between AI-10-49 ChIP-seq of RUNX1 and H3K27ac differential peaks (Fig. 32. A). Out of these 29 pathways, the most relevant were related to apoptotic pathways in response to DNA-damage stimuli and regulation of intrinsic apoptosis (Fig. 32. B). This result highlights the relevance that CBFβ/RUNX1 inhibition has in pancreatic cells and supports the knowledge that there is a redistribution of epigenetics marks after treatment towards an active pro-apoptotic pathway, coincidentally with the transcriptomic results (Fig. 19).

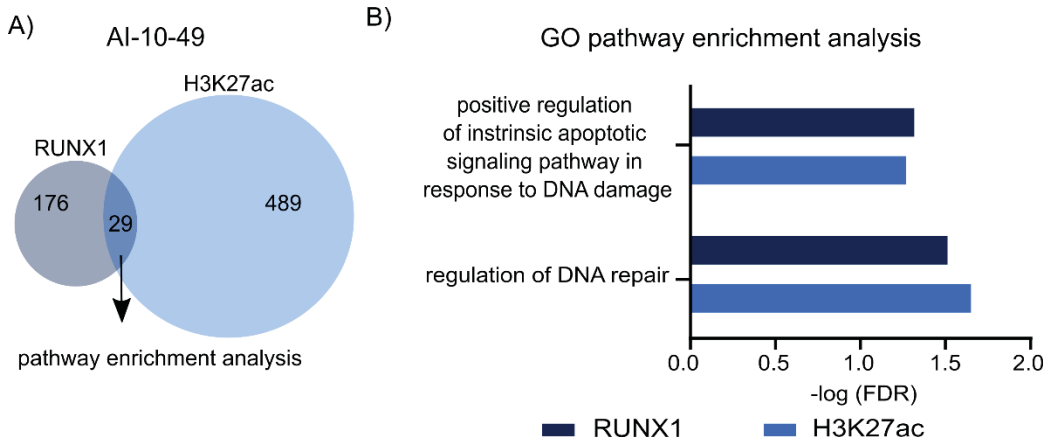

Figure 32: RUNX1 and H3K27ac in promoter regions are enriched in apoptotic pathways. A) Venn diagram of RUNX1 and H3K27ac ChIP-seq GO enrichment of differential binding in promoter regions of MIAPaCa-2 cells treated with AI-10-49 3 μM for 6 h. **B)** Representative GO terms significantly enriched in promoter regions of H3K27ac ChIP-seq and RUNX1 ChIP-seq. FDR, false discovery rate.

5. 5. AI-10-49 treatment inhibits tumor growth *in vivo*

5. 5. 1. AI-10-49 treatment impairs tumor growth in xenograft model

To validate whether CBFβ/RUNX1 inhibition driven by AI-10-49 could be effective *in vivo*, it was examined tumor growth in a PDAC xenograft model. To corroborate the results I obtained *in vitro*, in which *NOXA* expression sensitizes the cells towards the drug treatment (Fig. 18)

MIAPaCa-2 cells were transplanted in mice and followed a treatment regimen (Fig. 33. A) The cancer cells were transplanted into one flank of the mice and were left to grow until they reached 0.2 cm^3, determined as day 0 (Figure 33. A). Strikingly, the aforementioned compound almost completely inhibited tumor growth after 12 days (Fig. 33. B). In addition, the immunohistochemistry results for the proliferation marker Ki67, showed a significant decrease in AI-10-49 treated cells after 12 days (Fig. 33. C).

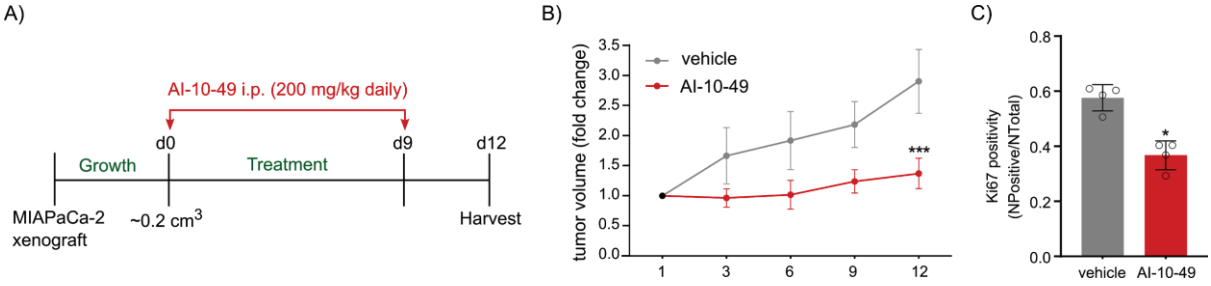

Figure 33: AI-10-49 inhibits tumor growth in MIAPaCa-2 xenograft model. A) $1x10^6$ MIAPaCa-2 cells were transplanted into recipient mice. Treatment started (d0) when tumors reached a volume of 0.2 cm^3 and it was stopped at day 9. Mice were treated with 200 mg/kg AI-10-49 intra peritoneal daily for 9 days. After 12 days the tumors were harvested and used for immunostaining. **B)** Tumor size was measured over time. AI-10-49 treated mice showed a significant tumor growth inhibition. Shown is the mean and SD. p-value of Student's t-test, ***p<0.001 (n=5 mice in each group). **C)** Quantification of Ki67 IHC staining of MIAPaCa-2 tumor xenografts treated with DMSO or AI-10-49 using the Aperio positive pixel method. Shown is the mean and SD. Each dot represents one tumor. p-value of Student's t-test, * p<0.05 (n=4 tumors per group). Data in A) and B) were provided by EPO (Experimental Pharmacology and Oncology, Berlin-Buch). Data in C was provided by Martin Schlensog and Yakup Yasar, University Clinic of Düsseldorf.

5. 5. 2. AI-10-49 inhibits more efficiently *NOXA^{high}* patient derived cells

Lastly, to validate the efficiency of AI-10-49 inhibition *ex vivo* it was used the novel culture technique of patient material known as patient derived organoids (PDOs) (Tiriac et al., 2018). 7 PDOs were isolated from PDAC patients either via fine needle aspiration (FNA) or surgery. These 7 organoids were transcriptionally profiled (RNA-seq) which enabled the clustering into "*NOXA^{high}*" and "*NOXA^{low}*" (Fig. 34. A). Pathway enrichment analyses revealed a significant enrichment of the Hallmark Apoptosis in the PDOs with a high *NOXA* expression (Fig. 34. B),

supporting the hypothesis that *NOXA*^{high} cells are prone to apoptosis. Moreover, the PDOs B250 and B203 (*NOXA*^{high}) showed the highest sensitivity towards CBFβ-RUNX1 inhibition (Fig. 34. C), supporting the xenograft results (Fig. 33. B) and the previous *in vitro* results (Fig. 12. B, 21 and 22).

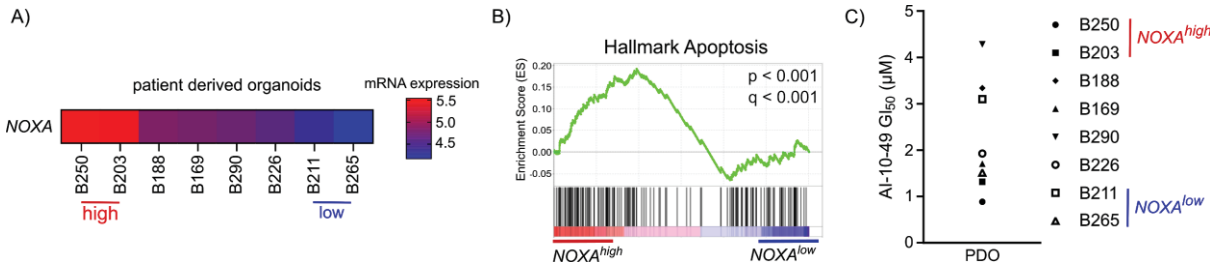

Figure 34: CBFβ/RUNX1 inhibition selectively kills *NOXA*^{high} PDOs. A) RNA-seq data of 7 PDOs were analyzed for *NOXA* expression. NOXA mRNA expression > 75% = *NOXA*^{high}; *NOXA* mRNA expression < 25% = *NOXA*^{low} **B)** GSEA of RNA-seq data of PDOs. Hallmark apoptosis signature in the *NOXA*^{high} subtype. Nominal p-value and FDR-q value is depicted. **C)** Dose-response treatment of PDOs viability measured after 72h upon AI-10-49 treatment with Cell Titer Glo®. Depicted is the GI50 value. n=2 or n=3, biological replicates were performed as technical triplicates. Data provided by Felix Orben, Technical University of Munich.

Overall, these findings bring evidence to the idea of using a new and novel axis (CBFβ-RUNX1) to be therapeutically exploited in PDAC treatment, especially for those patients characterized by a high expression of *NOXA*.

6. Discussion

Pancreatic ductal adenocarcinoma (PDAC) remains a disease with dismal prognosis and poor outcome, despite the efforts to find new therapeutic strategies. Several functional and molecular tumor profiling studies enabled the identification and validation of genes and signaling pathways that are dysregulated or mutated in PDAC (Birnbaum et al., 2016; Collisson et al., 2011). Considering the broad spectrum of signaling pathways, mutational and epigenetic landscape, it is possible to envision an era of individually adjusted therapies. It has been thoroughly studied how imbalance in anti- and pro- survival pathways can lead to apoptosis evasion and chemotherapy resistance, leading to a failure of current therapies (Mohammad et al., 2015).

Initially I performed a high-throughput drug screening, to identify novel targeted compounds to be studied for PDAC treatment. I identified a small molecule inhibitor, and I described the mechanism of action in the context of pancreatic cancer cells. The key achievements of this study are:

1. Identification of a novel compound plausible to be used in pancreatic cancer research, first developed to treat a specific subgroup of AML patients.
2. Providing evidence that NOXA protein levels, a pro-apoptotic protein usually regarded as a weak apoptotic inducer, sensitize pancreatic cancer cells towards drug treatments making them prone to programmed cell death.
3. Identification of RUNX1 as a relevant epigenetic factor in PDAC, where its pharmacological and genetic interference promotes *NOXA* expression leading to tumor cell death.
4. Supporting the efficacy of AI-10-49 treatment in xenograft (*in vivo*) and patient derived organoids (*ex vivo*) models.
5. Unravelling of an in-depth mechanistic action of RUNX1-NOXA axis which might lead to a new therapeutic window in pancreatic cancer.

6. 1. High-throughput drug screening as a powerful tool for finding new therapeutic options

In this study, by means of analyses of publicly available transcriptome profiles of PDAC patients I could discriminate between groups with high and low levels of NOXA, a pro-apoptotic protein member of the BCL-2 family. Surprisingly, high mRNA levels of this gene correlate with poorer outcomes in PDAC patients, highlighting the relevance of the balance of anti- and pro-apoptotic genes. This phenomenon could be given by a counter-upregulation of pro-survival proteins, such as MCL-1, which is the main target of NOXA anti-survival effect (Morel et al., 2009). Given that *NOXA* upregulation correlates with dismal prognosis ((Fig. 1; (Birnbaum et al., 2016)) it acquires strength as a possible marker for this aggressive subtype. Moreover, its inherent nature of pro-apoptotic protein paves the way towards a more sensible strategy, in which it might be possible to pharmacologically activate *NOXA* mRNA and protein expression thus triggering cell death. Therefore, I performed a high-throughput drug screening in human and murine cell lines with 1430 FDA approved drugs and 412 experimental compounds using *NOXA* as my focus of study (*NOXA*^{wt} and *NOXA*^{ko} cells*)*. Interestingly, I found targets similar to the CCLE public screening, proving the robustness of the method, among other compounds. By scoring and filtering the hits according to their effectiveness in *NOXA* expressing cell lines, I narrowed down the selection to one compound: AI-10-49.

The CBFβ/SMMHC inhibitor, AI-10-49, was developed to inhibit that specific oncofusion to the interaction with RUNX1 in AML (Illendula et al., 2015). However, it was proved by the developers of this compound that in absence of the oncofusion, this compound acts as the monovalent version of it and interferes with the wild type interaction of CBFβ with RUNX1 (Illendula et al., 2016). The CBFβ/RUNX1 interaction is under-studied in PDAC, possibly due to the lack of apparent importance these genes have in the mutational landscape of pancreatic cancer. With this finding, I showed how one can exploit a high-throughput drug screening to find an unexpected target in a different entity, thus broadening the possibilities of the research.

6. 2. NOXA expression sensitizes PDAC cells to AI-10-49 and regulates cell death

The functional relevance of apoptosis evasion as a mechanism of chemotherapy resistance was supported by several research studies. This phenomenon underscores the need to find new strategies to efficiently drive tumor cell death (Jullien et al., 2020; Khaw et al., 2011; Mohammad et al., 2015; Wong & Goodin, 2009). *NOXA*, long considered a weak apoptotic factor (Ploner et al., 2008; Villunger et al., 2003), was found to be strongly depleted upon use of targeted therapies creating a dependence of its counterpart pro-survival protein, MCL-1 thus leading to a therapy-resistance mechanism (Montero et al., 2019). Using genetic deletions and overexpression tools, my data shows that *NOXA* enables drug-induced cell death *in vitro* and *in vivo*, probably leading to overcoming anti-apoptotic resistance. (Fig. 16, 17 and 33). Moreover, *NOXA* overexpression induced either by AI-10-49 treatment or CRISPR/dCas9 overexpression, led to reduced clonogenic growth (Fig. 18), activation of transcriptional apoptotic pathways (Fig. 19) and cell arrest in the G2 phase (Fig. 14).

On the one hand, I hypothesize that the transcription factor *MYC*, known to regulate *NOXA* and other apoptotic genes (Nikiforov et al., 2007; Wirth et al., 2014), does not seem to play a role in *NOXA* upregulation due to its strong inhibition within hours of treatment (data not shown). On the other hand, the cell lines used are *p53* mutants, excluding the possibility of this being a p53-apoptosis mechanism in response to DNA damage (Oda et al., 2000). Therefore, I considered that other transcription factors might be required to regulate *NOXA* to in turn trigger cell death. Considering that AI-10-49 inhibits the interaction between CBFβ and RUNX1, it becomes apparent that RUNX1 could play a role in *NOXA* regulation.

6. 3. RUNX1 and not RUNX2/RUNX3 induce apoptotic cell death through *NOXA* upregulation

The function of the transcription factor family RUNX and its non-DNA-binding partner CBFβ are lineage and cell-phase specific. They can activate or repress the transcription of key regulatory genes of different cell programs, e.g., cell differentiation and growth. This context-specific ambivalence stems from the myriad of RUNX/CBFβ interactors. RUNX1, specifically,

has been thoroughly studied in hematopoietic malignancies. In a mouse model of T-cell acute lymphoblastic leukemia (T-ALL) and human T-ALL cell lines, *RUNX1* deletion led to apoptosis induction (Choi et al., 2017). Similarly, genetic knockdown of *RUNX1* inhibited cell proliferation and counter-acted the apoptotic effects induced by Leucine-rich-alpha-2-glycoprotein 1 (LRG1) in human colorectal cancer cell lines (Zhou et al., 2017). In line with these biological effects, I observed a basal apoptotic induction and cell death in *RUNX1*^{ko} pancreatic cancer cell lines (Fig. 18. A). In addition, a similar result was observed in wild type AI-10-49 treated cells (Fig. 16 and 17), a compound that interrupts its interaction with CBFβ thus destabilizing RUNX1 activity. Noteworthy, both pharmacological and genetic inhibition of *RUNX1* led to a strong upregulation of the pro-apoptotic protein NOXA (Fig. 12 A and B; Fig. 21), which was not observed in *RUNX2*^{ko} and *RUNX3*^{ko}. Moreover, genetic and pharmacological inhibition of RUNX1 exhibited MYC downregulation at the transcriptional and protein level, respectively (Fig. 23). These results bring into the scope of this study the unknown role of *RUNX1* in apoptotic pathways and how this transcription factor regulates *NOXA* expression which in turn leads to tumor cell death.

Notably, *RUNX2*^{ko} cells reduced *NOXA* mRNA level to almost a 10% when compared to the parental counterpart (Fig. 21. A). Previous work identified a super-enhancer of *RUNX2* tightly associated with *MYC* promoter in *TP53* deficient plasmacytoid dendritic cells (pDCs) producing a promotion of tumor cell survival (Kubota et al., 2019). In line with this work, it was shown the pro-oncogenic role *RUNX2* plays in *TP53* mutant pancreatic cancer cells resistant to gemcitabine treatment (Ozaki et al., 2018). Even though little is known about the role of RUNX2 in the context of pancreatic cancer, there is evidence supporting its function as a tumor progression transcription factor. Altogether, *RUNX2* rises as an attractive subject of study but given the DNA-motif binding similarity with *RUNX1* (Shen et al., 2017) and the fact that *RUNX1*^{ko} cells showed a strong *NOXA* mRNA and protein upregulation, I focused my research on the latter.

Lastly, *RUNX3* pivotal function as tumor suppressor/metastatic promoter (Whittle et al., 2015) according to *SMAD4* gene dose, demonstrated the complexity of studying the RUNX family

protein. Moreover, *RUNX3* mRNA expression in the PDAC cells was undetectable (Ct: undetermined). Given the lack of effect its knockout produced in this model, I hypothesize the involvement of *RUNX1* in the apoptotic context acquires more relevance.

6. 4. RUNX1 pharmacological and genetic inhibition leads to global changes in chromatin dynamics

Studies of RUNX1/CBFβ interaction demonstrated the applicability and value of this transcriptional complex. RUNX1 is a key regulator in driving the embryonic development of hematopoietic stem cells (HSCs). Homozygous *Runx1*-null mice with severe hemorrhaging along the central nervous system, highlighting the relevance this transcription holds in embryonic hematopoietic development (Okuda et al., 1996). In hematological malignancies, as well as in other solid tumors, *RUNX1* and *CBF*β are targets of oncogenic mutations and/or chromosomal translocations affecting their primary action (Gaidzik et al., 2016; Ghukasyan et al., 2020). In this study I experimentally demonstrated a novel epigenetic function RUNX1 displays in pancreatic cancer cells.

First, it was achieved a complete knockout of the gene *RUNX1* in pancreatic cells. After this genomic deletion, I demonstrated that in resting conditions the cells were highly apoptotic (Fig. 22. A). Analysis of the TCGA database enabled me to negatively correlate the *RUNX1* mRNA expression with transcriptional apoptotic pathways (Fig. 24. B), underscoring the possible role of RUNX1 as a major player in apoptosis. In line with the aforementioned results, ATAC-seq analyses showed a striking increase in global DNA accessibility when RUNX1 was depleted, pointing out its repressive role, whereas *NOXA* promoter region was highly accessible (Fig 25). As for the pharmacological inhibition of RUNX1, they showed similar mild decrease of accessibility, probably due to the inherent nature of the treatment (6 h) (Fig. 26). Notably, ChIP-seq analyses of RUNX1 and H3K27ac of AI-10-49 treated cells displayed an enrichment in GO apoptotic pathways (Fig. 32. B). By means of RNA-seq I found that the Apoptosis pathway from the Hallmark dataset was upregulated in AI-10-49 treated cells whereas there was a drop in enrichment of GO *Chromatin remodeling* pathway. Altogether, these results show evidence

of how *RUNX1* depletion changes the chromatin landscape of cancer cells leading to activation of programmed cell death.

In a previous study it was shown that *RUNX1* overexpression significantly correlated with poor overall survival in high-risk patients, grouped according to mRNA expression (Birnbaum et al., 2016).

In this study, I provided evidence of the role of RUNX1 in epigenetic regulation of several apoptotic programs in a MYC-NOXA dependent manner, and the molecular mechanism by which these cells overcome death resistance. Given that some changes are unclear when RUNX1 is either inhibited or knocked out, it would be necessary to prove its direct role in apoptosis. For one, overexpressing RUNX1 in knockout cells to rescue the wild type phenotype. On the other hand, blocking caspase activity and measure apoptosis in those cells would give a better understanding of why *RUNX1*^{ko} cells undergo such strong apoptotic events and cell growth impairment.

Overall, the results give further understanding of the role of RUNX1 and poses it as an attractive target to be further investigated as a potential treatment in pancreatic cancer.

6. 5. AI-10-49 treatment efficiently kills pancreatic cancer cells *in vivo*

Apoptosis resistance is one of the 6 hallmarks of cancer and one of the reasons for drug resistance (Hanahan & Weinberg, 2011). Understanding the regulation of genes associated with apoptotic pathways allows a better comprehension of tumor biology. In PDAC, many attempts have been made to describe novel prognostic markers and develop new therapeutic strategies (Arlt et al., 2013; Birnbaum et al., 2016; Muth et al., 2020). Here, I found proof of the relevance RUNX1 has in this context, enhancing tumor cell death in a *NOXA*-dependent fashion. It was demonstrated that AI-10-49, a novel compound originally developed for a specific subgroup of AML patients, regulates *NOXA* mRNA and protein levels to induce efficient cell killing *in vitro* (Fig. 18). In addition, the RUNX1/CBFβ inhibitor dramatically reduced tumor volume in the xenograft model (Fig. 33) and did not show toxicity in mice (Pulikkan et

al., 2018). Notably, this compound selectively killed tumor cells with high *NOXA* expression in PDOs, supporting the *in vitro* and *in vivo* results (Fig. 34).

Given the existent gap between the lab results to success in clinical trials, I support the idea of rationally designing drug combinations that could potentially benefit patients (Hamacher et al., 2008). On the one hand, it has been previously proposed a proper patient stratification to tackle difficulties in the clinic, e.g., drug resistance (Biederstädt et al., 2020; Lankes et al., 2020). On the other hand, it is logical to draw a plan in which several drugs are used to treat different patients. It was shown how the combination of a novel small molecule, AI-10-49, positively interacts with a well-established set of standard of care drugs (Fig. 11). I believe that this should be further investigated *in vivo*, though preferably in PDOs.

It is worth mentioning that the understanding of PDAC biology and the unravelling of the pathways that reign the main obstacles in its treatment is a thorough job that needs to be addressed. It was demonstrated for the first time the key role of RUNX1-NOXA in driving apoptosis in PDAC. Therefore, I believe this study represents an important step to establish novel options to target a $NOXA^{high}$ subgroup of patients characterized by a dismal prognosis.

7. References

Adams, J. M., & Cory, S. (2007). *Bcl-2-regulated apoptosis : mechanism and therapeutic potential*. https://doi.org/10.1016/j.coi.2007.05.004

Adams, J. M., & Cory, S. (2018). The BCL-2 arbiters of apoptosis and their growing role as cancer targets. *Cell Death and Differentiation*, *25*(1), 27–36. https://doi.org/10.1038/cdd.2017.161

Arlt, A., Müerköster, S. S., & Schäfer, H. (2013). Targeting apoptosis pathways in pancreatic cancer. *Cancer Letters*, *332*(2), 346–358. https://doi.org/10.1016/j.canlet.2010.10.015

Bailey, P., Chang, D. K., Nones, K., Johns, A. L., Patch, A. M., Gingras, M. C., Miller, D. K., Christ, A. N., Bruxner, T. J. C., Quinn, M. C., Nourse, C., Murtaugh, L. C., Harliwong, I., Idrisoglu, S., Manning, S., Nourbakhsh, E., Wani, S., Fink, L., Holmes, O., … Grimmond, S. M. (2016). Genomic analyses identify molecular subtypes of pancreatic cancer. *Nature*, *531*(7592), 47–52. https://doi.org/10.1038/nature16965

Batut, B., Hiltemann, S., Bagnacani, A., Baker, D., Bhardwaj, V., Blank, C., Bretaudeau, A., Brillet-Guéguen, L., Čech, M., Chilton, J., Clements, D., Doppelt-Azeroual, O., Erxleben, A., Freeberg, M. A., Gladman, S., Hoogstrate, Y., Hotz, H. R., Houwaart, T., Jagtap, P., … Grüning, B. (2018). Community-Driven Data Analysis Training for Biology. *Cell Systems*, *6*(6), 752-758.e1. https://doi.org/10.1016/j.cels.2018.05.012

Beger, H. G., Rau, B., Gansauge, F., Poch, B., & Link, K. H. (2003). Treatment of pancreatic cancer: Challenge of the facts. *World Journal of Surgery*, *27*(10), 1075–1084. https://doi.org/10.1007/s00268-003-7165-7

Biederstädt, A., Hassan, Z., Schneeweis, C., Schick, M., Schneider, L., Muckenhuber, A., Hong, Y., Siegers, G., Nilsson, L., Wirth, M., Dantes, Z., Steiger, K., Schunck, K., Langston, S., Lenhof, H. P., Coluccio, A., Orben, F., Slawska, J., Scherger, A., … Keller, U. (2020). SUMO pathway inhibition targets an aggressive pancreatic cancer subtype. *Gut*, 1–11. https://doi.org/10.1136/gutjnl-2018-317856

Birnbaum, D. J., Bertucci, F., Finetti, P., Adélaïde, J., Giovannini, M., Turrini, O., Delpero, J. R., Raoul, J. L., Chaffanet, M., Moutardier, V., Birnbaum, D., & Mamessier, E. (2016).

Expression of genes with copy number alterations and survival of patients with pancreatic Adenocarcinoma. *Cancer Genomics and Proteomics*, *13*(3), 191–200.

Blackford, A., Serrano, O. K., Wolfgang, C. L., Parmigiani, G., Jones, S., Zhang, X., Parsons, D. W., Lin, J. C. H., Leary, R. J., Eshleman, J. R., Goggins, M., Jaffee, E. M., Iacobuzio-Donahue, C. A., Maitra, A., Cameron, J. L., Olino, K., Schulick, R., Winter, J., Herman, J. M., … Hruban, R. H. (2009). SMAD4 gene mutations are associated with poor prognosis in pancreatic cancer. *Clinical Cancer Research*, *15*(14), 4674–4679. https://doi.org/10.1158/1078-0432.CCR-09-0227

Bolger, A. M., Lohse, M., & Usadel, B. (2014). Trimmomatic: A flexible trimmer for Illumina sequence data. *Bioinformatics*, *30*(15), 2114–2120. https://doi.org/10.1093/bioinformatics/btu170

Boxer, L. M., & Dang, C. V. (2001). Translocations involving c-myc and c-myc function. *Oncogene*, *20*(40 REV. ISS. 4), 5595–5610. https://doi.org/10.1038/sj.onc.1204595

Calo, E., & Wysocka, J. (2013). Modification of Enhancer Chromatin: What, How, and Why? *Molecular Cell*, *49*(5), 825–837. https://doi.org/10.1016/j.molcel.2013.01.038

Cannon, A., Thompson, C., Hall, B. R., Jain, M., Kumar, S., & Batra, S. K. (2018). Desmoplasia in pancreatic ductal adenocarcinoma: Insight into pathological function and therapeutic potential. *Genes and Cancer*, *9*(3–4), 78–86. https://doi.org/10.18632/genesandcancer.171

Carbonare, L. D., Innamorati, G., & Valenti, M. T. (2012). Transcription Factor Runx2 and its Application to Bone Tissue Engineering. *Stem Cell Reviews and Reports*, *8*(3), 891–897. https://doi.org/10.1007/s12015-011-9337-4

Chen, L., Willis, S. N., Wei, A., Smith, B. J., Fletcher, J. I., Hinds, M. G., Colman, P. M., Day, C. L., Adams, J. M., Huang, D. C. S., Parade, R., & Victoria, P. (2005). *Differential Targeting of Prosurvival Bcl-2 Proteins by Their BH3-Only Ligands Allows Complementary Apoptotic Function*. *17*, 393–403. https://doi.org/10.1016/j.molcel.2004.12.030

Cheng, Y., Yang, H., Sun, Y., Zhang, H., Yu, S., Lu, Z., & Chen, J. (2017). RUNX1 promote

invasiveness in pancreatic ductal adenocarcinoma through regulating miR-93. *Oncotarget*, *8*(59), 99567–99579. https://doi.org/10.18632/oncotarget.20433

Choi, Ah., Illendula, A., Pulikkan, J. A., Roderick, J. E., Tesell, J., Yu, J., Hermance, N., Zhu, L. J., Castilla, L. H., Bushweller, J. H., & Kelliher, M. A. (2017). RUNX1 is required for oncogenic Myb and Myc enhancer activity in T-cell acute lymphoblastic leukemia. *Blood*, *130*(15), 1722–1733. https://doi.org/10.1182/blood-2017-03-775536

Chou, T. C. (2006). Theoretical basis, experimental design, and computerized simulation of synergism and antagonism in drug combination studies. *Pharmacological Reviews*, *58*(3), 621–681. https://doi.org/10.1124/pr.58.3.10

Chou, T. C. (2010). Drug combination studies and their synergy quantification using the chou-talalay method. *Cancer Research*, *70*(2), 440–446. https://doi.org/10.1158/0008-5472.CAN-09-1947

Christensen, C. L., Kwiatkowski, N., Abraham, B. J., Carretero, J., Al-Shahrour, F., Zhang, T., Chipumuro, E., Herter-Sprie, G. S., Akbay, E. A., Altabef, A., Zhang, J., Shimamura, T., Capelletti, M., Reibel, J. B., Cavanaugh, J. D., Gao, P., Liu, Y., Michaelsen, S. R., Poulsen, H. S., … Wong, K. K. (2014). Targeting Transcriptional Addictions in Small Cell Lung Cancer with a Covalent CDK7 Inhibitor. *Cancer Cell*, *26*(6), 909–922. https://doi.org/10.1016/j.ccell.2014.10.019

Chuang, L. S. H., Ito, K., & Ito, Y. (2013). RUNX family: Regulation and diversification of roles through interacting proteins. *International Journal of Cancer*, *132*(6), 1260–1271. https://doi.org/10.1002/ijc.27964

Cicenas, J., Kvederaviciute, K., Meskinyte, I., Meskinyte-Kausiliene, E., & Skeberdyte, A. (2017). KRAS, TP53, CDKN2A, SMAD4, BRCA1, and BRCA2 mutations in pancreatic cancer. *Cancers*, *9*(5). https://doi.org/10.3390/cancers9050042

Collisson, E. A., Bailey, P., Chang, D. K., & Biankin, A. V. (2019). Molecular subtypes of pancreatic cancer. *Nature Reviews Gastroenterology and Hepatology*, *16*(4), 207–220. https://doi.org/10.1038/s41575-019-0109-y

Collisson, E. A., Sadanandam, A., Olson, P., Gibb, W. J., Truitt, M., Gu, S., Cooc, J.,

Weinkle, J., Kim, G. E., Jakkula, L., Feiler, H. S., Ko, A. H., Olshen, A. B., Danenberg, K. L., Tempero, M. A., Spellman, P. T., Hanahan, D., & Gray, J. W. (2011). Subtypes of pancreatic ductal adenocarcinoma and their differing responses to therapy. *Nature Medicine*, *17*(4), 500–504. https://doi.org/10.1038/nm.2344

Daniell, H. (2012). MYC on the path to cancer. *Cell*, *76*(October 2009), 211–220. https://doi.org/10.1016/j.cell.2012.03.003.MYC

Del Chiaro, M., Verbeke, C., Salvia, R., Klöppel, G., Werner, J., McKay, C., Friess, H., Manfredi, R., Van Cutsem, E., Löhr, M., Segersvärd, R., Abakken, L., Adham, M., Albin, N., Arnelo, U., Bruno, M., Cahen, D., Cappelli, C., Costamagna, G., … Zamboni, G. (2013). European experts consensus statement on cystic tumours of the pancreas. *Digestive and Liver Disease*, *45*(9), 703–711. https://doi.org/10.1016/j.dld.2013.01.010

Delbridge, A. R. D., & Strasser, A. (2015). The BCL-2 protein family , BH3-mimetics and cancer therapy. *Cell Death and Differentiation*, 1–10. https://doi.org/10.1038/cdd.2015.50

Distler, M., Kersting, S., Niedergethmann, M., Aust, D. E., Franz, M., Rückert, F., Ehehalt, F., Pilarsky, C., Post, S., Saeger, H. D., & Grützmann, R. (2013). Pathohistological subtype predicts survival in patients with intraductal papillary mucinous neoplasm (IPMN) of the pancreas. *Annals of Surgery*, *258*(2), 324–330. https://doi.org/10.1097/SLA.0b013e318287ab73

Doench, J. G., Fusi, N., Sullender, M., Hegde, M., Vaimberg, E. W., Donovan, K. F., Smith, I., Tothova, Z., Wilen, C., Orchard, R., Virgin, H. W., Listgarten, J., & Root, D. E. (2016). Optimized sgRNA design to maximize activity and minimize off-target effects of CRISPR-Cas9. *Nature Biotechnology*, *34*(2), 184–191. https://doi.org/10.1038/nbt.3437

Eilers, M., & Eisenman, R. N. (2008). Myc's broad reach. *Genes and Development*, *22*(20), 2755–2766. https://doi.org/10.1101/gad.1712408

Escot, C., Theillet, C., Lidereau, R., Spyratos, F., Champeme, M. H., Gest, J., & Callahan, R. (1986). Genetic alteration of the c-myc protooncogene (MYC) in human primary breast carcinomas. *Proceedings of the National Academy of Sciences of the United States of*

America, *83*(13), 4834–4838. https://doi.org/10.1073/pnas.83.13.4834

Fasanella, K. E., & McGrath, K. (2009). Cystic lesions and intraductal neoplasms of the pancreas. *Best Practice and Research: Clinical Gastroenterology*, *23*(1), 35–48. https://doi.org/10.1016/j.bpg.2008.11.011

Feng, J., Liu, T., Qin, B., Zhang, Y., & Liu, X. S. (2012). Identifying ChIP-seq enrichment using MACS. *Nature Protocols*, *7*(9), 1728–1740. https://doi.org/10.1038/nprot.2012.101

Ferrari, N., Mcdonald, L., Morris, J. S., Cameron, E. R., & Blyth, K. (2013). RUNX2 in mammary gland development and breast cancer. *Journal of Cellular Physiology*, *228*(6), 1137–1142. https://doi.org/10.1002/jcp.24285

Forrester, K., Almoguera, C., Han, K., Grizzle, W. E., & Perucho, M. (1987). Detection of high incidence of KRAS oncogenes during human colon tumorigenesis. *Nature*, *327*, 298–303.

Friedlander, S. Y. G., Chu, G. C., Snyder, E. L., Girnius, N., Dibelius, G., Crowley, D., Vasile, E., Depinho, R. A., & Jacks, T. (2009). Article Context-Dependent Transformation of Adult Pancreatic Cells by Oncogenic K-Ras. *Cancer Cell*, *16*(5), 379–389. https://doi.org/10.1016/j.ccr.2009.09.027

Fritsche, P., Seidler, B., Schüler, S., Schnieke, A., Göttlicher, M., Schmid, R. M., Saur, D., & Schneider, G. (2009). HDAC2 mediates therapeutic resistance of pancreatic cancer cells via the BH3-only protein NOXA. *Gut*, *58*(10), 1399–1409. https://doi.org/10.1136/gut.2009.180711

Fu, Y., Sander, J. D., Reyon, D., Cascio, V. M., & Joung, J. K. (2014). Improving CRISPR-Cas nuclease specificity using truncated guide RNAs. *Nature Biotechnology*, *32*(3), 279–284. https://doi.org/10.1038/nbt.2808

Fukamachi, H., & Ito, K. (2004). Growth regulation of gastric epithelial cells by Runx3. *Oncogene*, *23*(24), 4330–4335. https://doi.org/10.1038/sj.onc.1207121

Gaidzik, V. I., Teleanu, V., Papaemmanuil, E., Weber, D., Paschka, P., Hahn, J., Wallrabenstein, T., Kolbinger, B., Köhne, C. H., Horst, H. A., Brossart, P., Held, G., Kündgen, A., Ringhoffer, M., Götze, K., Rummel, M., Gerstung, M., Campbell, P.,

Kraus, J. M., … Döhner, H. (2016). RUNX1 mutations in acute myeloid leukemia are associated with distinct clinico-pathologic and genetic features. In *Leukemia* (Vol. 30, Issue 11). https://doi.org/10.1038/leu.2016.126

Gamberi, G., Benassi, M. S., Bohling, T., Ragazzini, P., Molendini, L., Sollazzo, M. R., Pompetti, F., Merli, M., Magagnoli, G., Balladelli, A., & Picci, P. (1998). C-myc and c-fos in human osteosarcoma: Prognostic value of mRNA and protein expression. *Oncology*, *55*(6), 556–563. https://doi.org/10.1159/000011912

Ghukasyan, L. G., Krasnov, G. S., Muravenko, O. V., Ikonnikova, A. Y., Yurasov, R. A., Baidun, L. V., Ibragimova, S. Z., & Nasedkina, T. V. (2020). Driver Mutations in Acute Myeloid Leukemia with Inversion of Chromosome 16. *Molecular Biology*, *54*(3), 341–348. https://doi.org/10.1134/S0026893320030073

Goldstein, D., El-Maraghi, R. H., Hammel, P., Heinemann, V., Kunzmann, V., Sastre, J., Scheithauer, W., Siena, S., Tabernero, J., Teixeira, L., Tortora, G., Van Laethem, J. L., Young, R., Penenberg, D. N., Lu, B., Romano, A., & Von Hoff, D. D. (2015). Nab-paclitaxel plus gemcitabine for metastatic pancreatic cancer: Long-term survival from a phase III trial. *Journal of the National Cancer Institute*, *107*(2), 1–10. https://doi.org/10.1093/jnci/dju413

Grasso, C., Jansen, G., & Giovannetti, E. (2017). Drug resistance in pancreatic cancer : impact of altered energy metabolism. *Critical Reviews in Oncology / Hematology*. https://doi.org/10.1016/j.critrevonc.2017.03.026

Green, D. R., Kroemer, G., Green, D. R., & Kroemer, G. (2014). *The Pathophysiology of Mitochondrial Cell Death*. *626*(2004). https://doi.org/10.1126/science.1099320

Hamacher, R., Schmid, R. M., Saur, D., & Schneider, G. (2008). Apoptotic pathways in pancreatic ductal adenocarcinoma. *Molecular Cancer*, *7*, 1–10. https://doi.org/10.1186/1476-4598-7-64

Hammill, A. K., Uhr, J. W., & Scheuermann, R. H. (1999). Annexin V staining due to loss of membrane asymmetry can be reversible and precede commitment to apoptotic death. *Experimental Cell Research*, *251*(1), 16–21. https://doi.org/10.1006/excr.1999.4581

Hanahan, D., & Weinberg, R. A. (2011). Hallmarks of cancer: The next generation. *Cell*, *144*(5), 646–674. https://doi.org/10.1016/j.cell.2011.02.013

Happo, L., & Strasser, A. (2012). *BH3-only proteins in apoptosis at a glance*. https://doi.org/10.1242/jcs.090514

Hershko, T., & Ginsberg, D. (2004). Up-regulation of Bcl-2 Homology 3 (BH3)-only Proteins by E2F1 Mediates Apoptosis. *Journal of Biological Chemistry*, *279*(10), 8627–8634. https://doi.org/10.1074/jbc.M312866200

Hruban, R. H., Adsay, N. V., Albores-Saavedra, J., Compton, C., Garrett, E. S., Goodman, S. N., Kern, S. E., Klimstra, D. S., Klöppel, G., Longnecker, D. S., Lüttges, J., & Offerhaus, G. J. A. (2001). Pancreatic intraepithelial neoplasia: A new nomenclature and classification system for pancreatic duct lesions. *American Journal of Surgical Pathology*, *25*(5), 579–586. https://doi.org/10.1097/00000478-200105000-00003

Hu, Z. I., Shia, J., Stadler, Z. K., Varghese, A. M., Capanu, M., Salo-Mullen, E., Lowery, M. A., Diaz, L. A., Mandelker, D., Yu, K. H., Zervoudakis, A., Kelsen, D. P., Iacobuzio-Donahue, C. A., Klimstra, D. S., Saltz, L. B., Sahin, I. H., & O'Reilly, E. M. (2018). Evaluating mismatch repair deficiency in pancreatic adenocarcinoma: Challenges and recommendations. *Clinical Cancer Research*, *24*(6), 1326–1336. https://doi.org/10.1158/1078-0432.CCR-17-3099

Hulsen, T., de Vlieg, J., & Alkema, W. (2008). BioVenn - A web application for the comparison and visualization of biological lists using area-proportional Venn diagrams. *BMC Genomics*, *9*, 1–6. https://doi.org/10.1186/1471-2164-9-488

Iacobuzio-Donahue, C. A., Klimstra, D. S., Adsay, N. V., Wilentz, R. E., Argani, P., Sohn, T. A., Yeo, C. J., Cameron, J. L., Kern, S. E., & Hruban, R. H. (2000). Dpc-4 protein is expressed in virtually all human intraductal papillary mucinous neoplasms of the pancreas: Comparison with conventional ductal adenocarcinomas. *American Journal of Pathology*, *157*(3), 755–761. https://doi.org/10.1016/S0002-9440(10)64589-0

Illendula, A., Gilmour, J., Grembecka, J., Tirumala, V. S. S., Boulton, A., Kuntimaddi, A., Schmidt, C., Wang, L., Pulikkan, J. A., Zong, H., Parlak, M., Kuscu, C., Pickin, A., Zhou,

Y., Gao, Y., Mishra, L., Adli, M., Castilla, L. H., Rajewski, R. A., … Bushweller, J. H. (2016). Small Molecule Inhibitor of CBFβ-RUNX Binding for RUNX Transcription Factor Driven Cancers. *EBioMedicine*, *8*, 117–131. https://doi.org/10.1016/j.ebiom.2016.04.032

Illendula, A., Pulikkan, J. A., Zong, H., Grembecka, J., Xue, L., Sen, S., Zhou, Y., Boulton, A., Kuntimaddi, A., Gao, Y., Rajewski, R. A., Guzman, M. L., Castilla, L. H., & Bushweller, J. H. (2015). A small-molecule inhibitor of the aberrant transcription factor CBFβ-SMMHC delays leukemia in mice. *Science*, *347*(6223), 779–784. https://doi.org/10.1126/science.aaa0314

Inoue, K. ichi, Ozaki, S., Shiga, T., Ito, K., Masuda, T., Okado, N., Iseda, T., Kawaguchi, S., Ogawa, M., Bae, S. C., Yamashita, N., Itohara, S., Kudo, N., & Ito, Y. (2002). Runx3 controls the axonal projection of proprioceptive dorsal root ganglion neurons. *Nature Neuroscience*, *5*(10), 946–954. https://doi.org/10.1038/nn925

Jalili, V., Afgan, E., Gu, Q., Clements, D., Blankenberg, D., Goecks, J., Taylor, J., & Nekrutenko, A. (2020). Corrigendum: The Galaxy platform for accessible, reproducible and collaborative biomedical analyses: 2020 update. *Nucleic Acids Research*, *48*(14), 8205–8207. https://doi.org/10.1093/nar/gkaa554

Jones, S., Zhang, X., Parsons, D. W., Lin, J. C. H., Leary, R. J., Angenendt, P., Mankoo, P., Carter, H., Kamiyama, H., Jimeno, A., Hong, S. M., Fu, B., Lin, M. T., Calhoun, E. S., Kamiyama, M., Walter, K., Nikolskaya, T., Nikolsky, Y., Hartigan, J., … Kinzler, K. W. (2008). Core signaling pathways in human pancreatic cancers revealed by global genomic analyses. *Science*, *321*(5897), 1801–1806. https://doi.org/10.1126/science.1164368

Jost, P. J., Grabow, S., Gray, D., Mckenzie, M. D., Nachbur, U., Huang, D. C. S., Bouillet, P., Thomas, H. E., Borner, C., & Silke, J. (2010). XIAP acts as a switch between type I and type II FAS-induced apoptosis signalling. *Nature*, *460*(7258), 1035–1039. https://doi.org/10.1038/nature08229.XIAP

Joung, J., Konermann, S., Gootenberg, J. S., Abudayyeh, O. O., Platt, R. J., Brigham, M. D., Sanjana, N. E., & Zhang, F. (2017). Genome-scale CRISPR-Cas9 knockout and

transcriptional activation screening. *Nature Protocols*, *12*(4), 828–863. https://doi.org/10.1038/nprot.2017.016

Jullien, M., Gomez-Bougie, P., Chiron, D., & Touzeau, C. (2020). Restoring Apoptosis with BH3 Mimetics in Mature B-Cell Malignancies. *Cells*, *9*(3), 717. https://doi.org/10.3390/cells9030717

Kaniwa, F., Kuthadi, V. M., Dinakenyane, O., & Schroeder, H. (2017). Space-efficient k-mer algorithm for generalised suffix tree. *ArXiv*, *7*(1), 1–10. https://doi.org/10.5121/ijitcs.2017.7101

Kawate, S., Fukusato, T., Ohwada, S., Watanuki, A., & Morishita, Y. (1999). Amplification of c-myc in hepatocellular carcinoma: Correlation with clinicopathologic features, proliferative activity and p53 overexpression. *Oncology*, *57*(2), 157–163. https://doi.org/10.1159/000012024

Kelly, P. N., & Strasser, A. (2011). The role of Bcl-2 and its pro-survival relatives in tumourigenesis and cancer therapy. *Cell Death and Differentiation*, *1*, 1–11. https://doi.org/10.1038/cdd.2011.17

Kerr, J. F. R., Wyllie, A. H., & Currie, A. R. (1972). Apoptosis: a Basic Biological Phenomenon With Wide-Ranging Implications in Tissue Kinetics. *Br. J. Cancer*, *26*, 239–257.

Khaw, S. L., Huang, D. C. S., & Roberts, A. W. (2011). Overcoming blocks in apoptosis with BH3-mimetic therapy in haematological malignancies. *Pathology*, *43*(6), 525–535. https://doi.org/10.1097/PAT.0b013e32834b1b34

Kim, D., Langmead, B., & Salzberg, S. L. (2015). HISAT: A fast spliced aligner with low memory requirements. *Nature Methods*, *12*(4), 357–360. https://doi.org/10.1038/nmeth.3317

Kim, J. Y., Ahn, H. J., Ryu, J. H., Suk, K., & Park, J. H. (2004). BH3-only Protein Noxa Is a Mediator of Hypoxic Cell Death Induced by Hypoxia-inducible Factor 1α. *Journal of Experimental Medicine*, *199*(1), 113–123. https://doi.org/10.1084/jem.20030613

Kim, K. H., & Sederstrom, J. M. (2015). Assaying cell cycle status using flow cytometry.

Current Protocols in Molecular Biology, *2015*(July), 28.6.1-28.6.11. https://doi.org/10.1002/0471142727.mb2806s111

Konermann, S., Brigham, M. D., Trevino, A. E., Joung, J., Abudayyeh, O. O., Barcena, C., Hsu, P. D., Habib, N., Gootenberg, J. S., Nishimasu, H., Nureki, O., & Zhang, F. (2014). Genome-scale transcriptional activation by an engineered CRISPR-Cas9 complex. *Nature*, *517*(7536), 583–588. https://doi.org/10.1038/nature14136

Konermann, S., Brigham, M. D., Trevino, A. E., Joung, J., Abudayyeh, O. O., Barcena, C., Hsu, P. D., Habib, N., Gootenberg, J. S., Nishimasu, H., Nureki, O., & Zhang, F. (2015). Genome-scale transcriptional activation by an engineered CRISPR-Cas9 complex. *Nature*, *517*(7536), 583–588. https://doi.org/10.1038/nature14136

Kortlever, R. M., Sodir, N. M., Wilson, C. H., Littlewood, T. D., Evan, G. I., Kortlever, R. M., Sodir, N. M., Wilson, C. H., Burkhart, D. L., Pellegrinet, L., Swigart, L. B., Littlewood, T. D., & Evan, G. I. (2017). *Myc Cooperates with Ras by Programming Inflammation and Immune Suppression Article Myc Cooperates with Ras by Programming Inflammation and Immune Suppression*. 1301–1315. https://doi.org/10.1016/j.cell.2017.11.013

Kouzarides, T. (2007). Chromatin Modifications and Their Function. *Cell*, *128*(4), 693–705. https://doi.org/10.1016/j.cell.2007.02.005

Kubota, S., Tokunaga, K., Umezu, T., Yokomizo-Nakano, T., Sun, Y., Oshima, M., Tan, K. T., Yang, H., Kanai, A., Iwanaga, E., Asou, N., Maeda, T., Nakagata, N., Iwama, A., Ohyashiki, K., Osato, M., & Sashida, G. (2019). Lineage-specific RUNX2 super-enhancer activates MYC and promotes the development of blastic plasmacytoid dendritic cell neoplasm. *Nature Communications*, *10*(1), 1–16. https://doi.org/10.1038/s41467-019-09710-z

Kuwana, T., Bouchier-hayes, L., Chipuk, J. E., Bonzon, C., Sullivan, B. A., Green, D. R., Newmeyer, D. D., & Diego, S. (2005). *BH3 Domains of BH3-Only Proteins Differentially Regulate Bax-Mediated Mitochondrial Membrane Permeabilization Both Directly and Indirectly*. *17*, 525–535. https://doi.org/10.1016/j.molcel.2005.02.003

Kvansakul, M., & Hinds, M. G. (2014). *The Bcl-2 family : structures , interactions and targets*

for drug discovery. https://doi.org/10.1007/s10495-014-1051-7

Labi, V., Grespi, F., Baumgartner, F., & Villunger, A. (2008). Targeting the Bcl-2-regulated apoptosis pathway by BH3 mimetics: A breakthrough in anticancer therapy? *Cell Death and Differentiation*, *15*(6), 977–987. https://doi.org/10.1038/cdd.2008.37

Ladanyi, M., Kum Park, C., Lewis, R., Jhanwar, S. C., Healey, J. H., & Huvos, A. G. (1993). Sporadic amplification of the myc gene in human osteosarcomas. In *Diagnostic Molecular Pathology* (Vol. 2, Issue 1, pp. 163–167). https://doi.org/10.1097/00019606-199309000-00004

Lankes, K., Hassan, Z., Doffo, M. J., Schneeweis, C., Rad, R., Keller, U., Saur, D., Reichert, M., Wirth, M., Immunology, T., Franklin, B., Genomics, F., & Therapy, E. C. (2020). Targeting the ubiquitin-proteasome system in a pancreatic cancer subtype with hyperactive MYC. *Molecular Oncolgy*. https://doi.org/10.1002/1878-0261.12835

Lau, C. C., Harris, C. P., Lu, X. Y., Perlaky, L., Gogineni, S., Chintagumpala, M., Hicks, J., Johnson, M. E., Davino, N. A., Huvos, A. G., Meyers, P. A., Healy, J. H., Gorlick, R., & Rao, P. H. (2004). Frequent Amplification and Rearrangement of Chromosomal Bands 6p12-p21 and 17p11.2 in Osteosarcoma. *Genes Chromosomes and Cancer*, *39*(1), 11–21. https://doi.org/10.1002/gcc.10291

Levanon, D., Bettoun, D., Harris-Cerruti, C., Woolf, E., Negreanu, V., Eilam, R., Bernstein, Y., Goldenberg, D., Xiao, C., Fliegauf, M., Kremer, E., Otto, F., Brenner, O., Lev-Tov, A., & Groner, Y. (2002). The Runx3 transcription factor regulates development and survival of TrkC dorsal root ganglia neurons. *EMBO Journal*, *21*(13), 3454–3463. https://doi.org/10.1093/emboj/cdf370

Li, J., Kleeff, J., Guweidhi, A., Esposito, I., Berberat, P. O., Giese, T., Büchler, M. W., & Friess, H. (2004). RUNX3 expression in primary and metastatic pancreatic cancer. *Journal of Clinical Pathology*, *57*(3), 294–299. https://doi.org/10.1136/jcp.2003.013011

Li, Q. L., Ito, K., Sakakura, C., Fukamachi, H., Inoue, K. ichi, Chi, X. Z., Lee, K. Y., Nomura, S., Lee, C. W., Han, S. B., Kim, H. M., Kim, W. J., Yamamoto, H., Yamashita, N., Yano, T., Ikeda, T., Itohara, S., Inazawa, J., Abe, T., … Ito, Y. (2002). Causal relationship

between the loss of RUNX3 expression and gastric cancer. *Cell*, *109*(1), 113–124. https://doi.org/10.1016/S0092-8674(02)00690-6

Livak, K. J., & Schmittgen, T. D. (2001). Analysis of relative gene expression data using real-time quantitative PCR and the 2-ΔΔCT method. *Methods*, *25*(4), 402–408. https://doi.org/10.1006/meth.2001.1262

Lou, Y., Javed, A., Hussain, S., Colby, J., Frederick, D., Pratap, J., Xie, R., Gaur, T., van Wijnen, A. J., Jones, S. N., Stein, G. S., Lian, J. B., & Stein, J. L. (2009). A Runx2 threshold for the cleidocranial dysplasia phenotype. *Human Molecular Genetics*, *18*(3), 556–568. https://doi.org/10.1093/hmg/ddn383

Lucille, D., Maria, D., & Heyl, F. (2020). ATAC-Seq data analysis (Galaxy Training Materials). In *ATAC-Seq data analysis (Galaxy Training Materials).* /training-material/topics/epigenetics/tutorials/atac-seq/tutorial.html

Lüttges, J., Neumann, S., Jesnowski, R., Borries, V., & Löhr, M. (2003). *Lack of Apoptosis in PanIN-1 and PanIN-2 Lesions Associated with Pancreatic Ductal Adenocarcinoma Is Not Dependent on K- ras Status*. *27*(3), 57–62.

Macarulla, T., Carrato, A., Díaz, R., García, A., Laquente, B., Sastre, J., Álvarez, R., Muñoz, A., & Hidalgo, M. (2018). Management and supportive treatment of frail patients with metastatic pancreatic cancer. *Journal of Geriatric Oncology*. https://doi.org/10.1016/j.jgo.2018.06.005

Mann, K. M., Ying, H., Juan, J., Jenkins, N. A., & Copeland, N. G. (2016). KRAS-related proteins in pancreatic cancer. *Pharmacology and Therapeutics*, *168*, 29–42. https://doi.org/10.1016/j.pharmthera.2016.09.003

Matthaei, H., Dal Molin, M., & Maitra, A. (2013). Identification and analysis of precursors to invasive pancreatic cancer. *Methods in Molecular Biology*, *980*, 1–12. https://doi.org/10.1007/978-1-62703-287-2_1

McDonald, L., Ferrari, N., Terry, A., Bell, M., Mohammed, Z. M., Orange, C., Jenkins, A., Muller, W. J., Gusterson, B. A., Neil, J. C., Edwards, J., Morris, J. S., Cameron, E. R., & Blyth, K. (2014). RUNX2 correlates with subtype-specific breast cancer in a human

tissue microarray, and ectopic expression of Runx2 perturbs differentiation in the mouse mammary gland. *DMM Disease Models and Mechanisms*, *7*(5), 525–534. https://doi.org/10.1242/dmm.015040

McGuigan, A., Kelly, P., Turkington, R. C., Jones, C., Coleman, H. G., & McCain, R. S. (2018). Pancreatic cancer: A review of clinical diagnosis, epidemiology, treatment and outcomes. *World Journal of Gastroenterology*, *24*(43), 4846–4861. https://doi.org/10.3748/wjg.v24.i43.4846

Mevel, R., Draper, J. E., Lie-A-Ling, M., Kouskoff, V., & Lacaud, G. (2019). RUNX transcription factors: Orchestrators of development. *Development (Cambridge)*, *146*, 1–19. https://doi.org/10.1242/dev.148296

Mizrahi, J. D., Surana, R., Valle, J. W., & Shroff, R. T. (2020). Pancreatic cancer. *The Lancet*, *395*(10242), 2008–2020. https://doi.org/10.1016/S0140-6736(20)30974-0

Moffitt, R. A., Marayati, R., Flate, E. L., Volmar, K. E., Loeza, S. G. H., Hoadley, K. A., Rashid, N. U., Williams, L. A., Eaton, S. C., Chung, A. H., Smyla, J. K., Anderson, J. M., Kim, H. J., Bentrem, D. J., Talamonti, M. S., Iacobuzio-Donahue, C. A., Hollingsworth, M. A., & Yeh, J. J. (2015). Virtual microdissection identifies distinct tumor- and stroma-specific subtypes of pancreatic ductal adenocarcinoma. *Nature Genetics*, *47*(10), 1168–1178. https://doi.org/10.1038/ng.3398

Mohammad, R. M., Muqbil, I., Lowe, L., Yedjou, C., Hsu, H. Y., Lin, L. T., Siegelin, M. D., Fimognari, C., Kumar, N. B., Dou, Q. P., Yang, H., Samadi, A. K., Russo, G. L., Spagnuolo, C., Ray, S. K., Chakrabarti, M., Morre, J. D., Coley, H. M., Honoki, K., … Azmi, A. S. (2015). Broad targeting of resistance to apoptosis in cancer. *Seminars in Cancer Biology*, *35*, S78–S103. https://doi.org/10.1016/j.semcancer.2015.03.001

Montero, J., Gstalder, C., Kim, D. J., Sadowicz, D., Miles, W., Manos, M., Cidado, J. R., Secrist, J. P., Tron, A. E., Flaherty, K., Hodi, F. S., Yoon, C. H., Letai, A., Fisher, D. E., & Haq, R. (2019). Destabilization of NOXA mRNA as a common resistance mechanism to targeted therapies. *Nature Communications*. https://doi.org/10.1038/s41467-019-12477-y

Mootha, V. K., Lindgren, C. M., Eriksson, K. F., Subramanian, A., Sihag, S., Lehar, J., Puigserver, P., Carlsson, E., Ridderstråle, M., Laurila, E., Houstis, N., Daly, M. J., Patterson, N., Mesirov, J. P., Golub, T. R., Tamayo, P., Spiegelman, B., Lander, E. S., Hirschhorn, J. N., … Groop, L. C. (2003). PGC-1α-responsive genes involved in oxidative phosphorylation are coordinately downregulated in human diabetes. *Nature Genetics*, *34*(3), 267–273. https://doi.org/10.1038/ng1180

Morel, C., Carlson, S. M., White, F. M., & Davis, R. J. (2009). Mcl-1 Integrates the Opposing Actions of Signaling Pathways That Mediate Survival and Apoptosis. *Molecular and Cellular Biology*, *29*(14), 3845–3852. https://doi.org/10.1128/mcb.00279-09

Moujalled, D. M., Pomilio, G., Ghiurau, C., Ivey, A., Salmon, J., Rijal, S., Macraild, S., Zhang, L., Teh, T. C., Tiong, I. S., Lan, P., Chanrion, M., Claperon, A., Rocchetti, F., Zichi, A., Kraus-Berthier, L., Wang, Y., Halilovic, E., Morris, E., … Wei, A. H. (2019). Combining BH3-mimetics to target both BCL-2 and MCL1 has potent activity in pre-clinical models of acute myeloid leukemia. *Leukemia*, *33*(4), 905–917. https://doi.org/10.1038/s41375-018-0261-3

Muckenhuber, A., Berger, A. K., Schlitter, A. M., Steiger, K., Konukiewitz, B., Trumpp, A., Eils, R., Werner, J., Friess, H., Esposito, I., Klöppel, G., Ceyhan, G. O., Jesinghaus, M., Denkert, C., Bahra, M., Stenzinger, A., Sprick, M. R., Jäger, D., Springfeld, C., & Weichert, W. (2018). Pancreatic ductal adenocarcinoma subtyping using the biomarkers hepatocyte nuclear factor-1A and cytokeratin-81 correlates with outcome and treatment response. *Clinical Cancer Research*, *24*(2), 351–359. https://doi.org/10.1158/1078-0432.CCR-17-2180

Murray, A. W. (2004). Recycling the Cell Cycle: Cyclins Revisited. *Cell*, *116*(2), 221–234. https://doi.org/10.1016/S0092-8674(03)01080-8

Muth, S. T., Saung, M. T., Blair, A. B., Henderson, M. G., Thomas, D. L., & Zheng, L. (2020). CD137 agonist-based combination immunotherapy enhances activated, effector memory T cells and prolongs survival in pancreatic adenocarcinoma. *Cancer Letters*. https://doi.org/10.1016/j.canlet.2020.11.041

Naik, E., Michalak, E. M., Villunger, A., Adams, J. M., & Strasser, A. (2007). Ultraviolet radiation triggers apoptosis of fibroblasts and skin keratinocytes mainly via the BH3-only protein Noxa. *Journal of Cell Biology*, *176*(4), 415–424. https://doi.org/10.1083/jcb.200608070

Nikiforov, M. A., Riblett, M., Tang, W.-H., Gratchouck, V., Zhuang, D., Fernandez, Y., Verhaegen, M., Varambally, S., Chinnaiyan, A. M., Jakubowiak, A. J., & Soengas, M. S. (2007). Tumor cell-selective regulation of NOXA by c-MYC in response to proteasome inhibition. *Proceedings of the National Academy of Sciences*, *104*(49), 19488–19493. https://doi.org/10.1073/pnas.0708380104

Notta, F., Chan-Seng-Yue, M., Lemire, M., Li, Y., Wilson, G. W., Connor, A. A., Denroche, R. E., Liang, S. Ben, Brown, A. M. K., Kim, J. C., Wang, T., Simpson, J. T., Beck, T., Borgida, A., Buchner, N., Chadwick, D., Hafezi-Bakhtiari, S., Dick, J. E., Heisler, L., … Gallinger, S. (2016). A renewed model of pancreatic cancer evolution based on genomic rearrangement patterns. *Nature*, *538*(7625), 378–382. https://doi.org/10.1038/nature19823

Oda, E., Ohki, R., Murasawa, H., Nemoto, J., Shibue, T., Yamashita, T., Tokino, T., Taniguchi, T., & Tanaka, N. (2000). Noxa, a BH3-only member of the Bcl-2 family and candidate mediator of p53-induced apoptosis. *Science*, *288*(5468), 1053–1058. https://doi.org/10.1126/science.288.5468.1053

Okuda, T., Van Deursen, J., Hiebert, S. W., Grosveld, G., & Downing, J. R. (1996). AML1, the target of multiple chromosomal translocations in human leukemia, is essential for normal fetal liver hematopoiesis. *Cell*, *84*(2), 321–330. https://doi.org/10.1016/S0092-8674(00)80986-1

Ormerod, M. G. (2002). Investigating the relationship between the cell cycle and apoptosis using flow cytometry. *Journal of Immunological Methods*, *265*(1–2), 73–80. https://doi.org/10.1016/S0022-1759(02)00071-6

Orth, M., Metzger, P., Gerum, S., Mayerle, J., Schneider, G., Belka, C., Schnurr, M., & Lauber, K. (2019). Pancreatic ductal adenocarcinoma: Biological hallmarks, current

status, and future perspectives of combined modality treatment approaches. *Radiation Oncology*, *14*(1), 1–20. https://doi.org/10.1186/s13014-019-1345-6

Otálora-Otálora, B. A., Henríquez, B., López-Kleine, L., & Rojas, A. (2019). RUNX family: Oncogenes or tumor suppressors (Review). *Oncology Reports*, *42*(1), 3–19. https://doi.org/10.3892/or.2019.7149

Ouyang, L., Shi, Z., Zhao, S., Wang, F. T., Zhou, T. T., Liu, B., & Bao, J. K. (2012). Programmed cell death pathways in cancer: A review of apoptosis, autophagy and programmed necrosis. *Cell Proliferation*, *45*(6), 487–498. https://doi.org/10.1111/j.1365-2184.2012.00845.x

Owens, T. W., Rogers, R. L., Best, S. A., Ledger, A., Mooney, A. M., Ferguson, A., Shore, P., Swarbrick, A., Ormandy, C. J., Simpson, P. T., Carroll, J. S., Visvader, J. E., & Naylor, M. J. (2014). Runx2 is a novel regulator of mammary epithelial cell fate in development and breast cancer. *Cancer Research*, *74*(18), 5277–5286. https://doi.org/10.1158/0008-5472.CAN-14-0053

Ozaki, T., Yu, M., Yin, D., Sun, D., Zhu, Y., Bu, Y., & Sang, M. (2018). Impact of RUNX2 on drug-resistant human pancreatic cancer cells with p53 mutations. *BMC Cancer*, *18*(1), 1–15. https://doi.org/10.1186/s12885-018-4217-9

Pan, S.-T., Li, Z.-L., He, Z.-X., Qiu, J.-X., & Zhou, S.-F. (2016). Molecular mechanisms for tumor resistance to chemotherapy. *Clinical and Experimental Pharmacoly and Physiology*, *43*(8), 723–737. https://doi.org/10.1111/1440-1681.12581

Pekowska, A., Benoukraf, T., Zacarias-Cabeza, J., Belhocine, M., Koch, F., Holota, H., Imbert, J., Andrau, J. C., Ferrier, P., & Spicuglia, S. (2011). H3K4 tri-methylation provides an epigenetic signature of active enhancers. *EMBO Journal*, *30*(20), 4198–4210. https://doi.org/10.1038/emboj.2011.295

Ploner, C., Kofler, R., & Villunger, A. (2008). Noxa: At the tip of the balance between life and death. *Oncogene*, *27*, S84–S92. https://doi.org/10.1038/onc.2009.46

Portt, L., Norman, G., Clapp, C., Greenwood, M., & Greenwood, M. T. (2011). Anti-apoptosis and cell survival: A review. *Biochimica et Biophysica Acta - Molecular Cell Research*,

1813(1), 238–259. https://doi.org/10.1016/j.bbamcr.2010.10.010

Provenzano, P. P., Cuevas, C., Chang, A. E., Goel, V. K., Von Hoff, D. D., & Hingorani, S. R. (2012). Enzymatic Targeting of the Stroma Ablates Physical Barriers to Treatment of Pancreatic Ductal Adenocarcinoma. *Cancer Cell*, *21*(3), 418–429. https://doi.org/10.1016/j.ccr.2012.01.007

Pulikkan, J. A., Hegde, M., Ahmad, H. M., Belaghzal, H., Illendula, A., Yu, J., O'Hagan, K., Ou, J., Muller-Tidow, C., Wolfe, S. A., Zhu, L. J., Dekker, J., Bushweller, J. H., & Castilla, L. H. (2018). CBFβ-SMMHC Inhibition Triggers Apoptosis by Disrupting MYC Chromatin Dynamics in Acute Myeloid Leukemia. *Cell*, *174*(1), 172-186.e21. https://doi.org/10.1016/j.cell.2018.05.048

Puthalakath, H., & Strasser, A. (2002). *Keeping killers on a tight leash : transcriptional and post- translational control of the pro-apoptotic activity of BH3- only proteins*. 505–512. https://doi.org/10.1038/sj/cdd/4400998

Quante, A. S., Ming, C., Rottmann, M., Engel, J., Boeck, S., Heinemann, V., Westphalen, C. B., & Strauch, K. (2016). Projections of cancer incidence and cancer-related deaths in Germany by 2020 and 2030. *Cancer Medicine*, *5*(9), 2649–2656. https://doi.org/10.1002/cam4.767

Rahib, L., Smith, B. D., Aizenberg, R., Rosenzweig, A. B., Fleshman, J. M., & Matrisian, L. M. (2014). Projecting cancer incidence and deaths to 2030: The unexpected burden of thyroid, liver, and pancreas cancers in the united states. *Cancer Research*, *74*(11), 2913–2921. https://doi.org/10.1158/0008-5472.CAN-14-0155

Ren, B., Liu, X., & Suriawinata, A. A. (2019). Pancreatic Ductal Adenocarcinoma and Its Precursor Lesions: Histopathology, Cytopathology, and Molecular Pathology. *American Journal of Pathology*, *189*(1), 9–21. https://doi.org/10.1016/j.ajpath.2018.10.004

Ritchie, M. E., Phipson, B., Wu, D., Hu, Y., Law, C. W., Shi, W., & Smyth, G. K. (2015). Limma powers differential expression analyses for RNA-sequencing and microarray studies. *Nucleic Acids Research*, *43*(7), e47. https://doi.org/10.1093/nar/gkv007

Sawai, Y., Yamao, K., Bhatia, V., Chiba, T., Mizuno, N., Sawaki, A., Takahashi, K., Tajika,

M., Shimizu, Y., Yatabe, Y., & Yanagisawa, A. (2011). Erratum: Development of pancreatic cancers during long-term follow-up of side-branch intraductal papillary mucinous neoplasms (Endoscopy (2010) 42 (1077-1084)). *Endoscopy*, *43*(1), 43. https://doi.org/10.1055/s-0030-1256071

Schafer, K. A. (1998). *The cell cycle, a review*. Vet Pathol 35:461-478.

Scheitz, C. J. F., Lee, T. S., McDermitt, D. J., & Tumbar, T. (2012). Defining a tissue stem cell-driven Runx1/Stat3 signalling axis in epithelial cancer. *EMBO Journal*, *31*(21), 4124–4139. https://doi.org/10.1038/emboj.2012.270

Scheitz, C. J. F., & Tumbar, T. (2013). New insights into the role of Runx1 in epithelial stem cell biology and pathology. *Journal of Cellular Biochemistry*, *114*(5), 985–993. https://doi.org/10.1002/jcb.24453

Schober, M., Jesenofsky, R., Faissner, R., Weidenauer, C., Hagmann, W., Michl, P., Heuchel, R. L., Haas, S. L., & Lö, J. (2014). *Desmoplasia and Chemoresistance in Pancreatic Cancer*. 2137–2154. https://doi.org/10.3390/cancers6042137

Shen, N., Zhao, J., Schipper, J., Zhang, Y., Bepler, T., Leehr, D., Bradley, J., Horton, J., Lapp, H., & Gordan, R. (2017). Intrinsic specificity differences between transcription factor paralogs partly explain their differential in vivo binding. *BioRxiv*, 27–33. https://doi.org/10.1101/208561

Shin, M. H., He, Y., Marrogi, E., Piperdi, S., Ren, L., Khanna, C., Gorlick, R., Liu, C., & Huang, J. (2016). A RUNX2-Mediated Epigenetic Regulation of the Survival of p53 Defective Cancer Cells. *PLoS Genetics*, *12*(2), 1–25. https://doi.org/10.1371/journal.pgen.1005884

Siegel, R. L., Miller, K. D., & Jemal, A. (2020). Cancer statistics, 2020. *CA: A Cancer Journal for Clinicians*, *70*(1), 7–30. https://doi.org/10.3322/caac.21590

Sodir, N. M., Kortlever, R. M., Barthet, V. J. A., Campos, T., Pellegrinet, L., Kupczak, S., Anastasiou, P., Brown Swigart, L., Soucek, L., Arends, M. J., Littlewood, T. D., & Evan, G. I. (2020). Myc instructs and maintains pancreatic adenocarcinoma phenotype. *Cancer Discovery*, CD-19-0435. https://doi.org/10.1158/2159-8290.cd-19-0435

Sood, R., Kamikubo, Y., & Liu, P. (2017). Role of RUNX1 in hematological malignancies. *Blood*, *129*(15), 2070–2082. https://doi.org/10.1182/blood-2016-10-687830

Spicuglia, S., & Vanhille, L. (2012). Chromatin signatures of active enhancers. *Nucleus*, *3*(2), 126–131. https://doi.org/10.4161/nucl.19232

Stadhouders, R., Kolovos, P., Brouwer, R., Zuin, J., Van Den Heuvel, A., Kockx, C., Palstra, R. J., Wendt, K. S., Grosveld, F., Van Ijcken, W., & Soler, E. (2013). Multiplexed chromosome conformation capture sequencing for rapid genome-scale high-resolution detection of long-range chromatin interactions. *Nature Protocols*, *8*(3), 509–524. https://doi.org/10.1038/nprot.2013.018

Strasser, A., Cory, S., & Adams, J. M. (2011). Deciphering the rules of programmed cell death to improve therapy of cancer and other diseases. *EMBO Journal*, *30*(18), 3667–3683. https://doi.org/10.1038/emboj.2011.307

Tanaka, S. (2018). *Molecular Analysis for Therapeutic Targets of Pancreatic Cancer*. 127–144. https://doi.org/10.1007/978-981-10-6469-2_8

Tiriac, H., Belleau, P., Engle, D. D., Plenker, D., Deschênes, A., Somerville, T. D. D., Froeling, F. E. M., Burkhart, R. A., Denroche, R. E., Jang, G. H., Miyabayashi, K., Young, C. M., Patel, H., Ma, M., Lacomb, J. F., Palmaira, R. L. D., Javed, A. A., Huynh, J. C., Johnson, M., … Tuveson, D. A. (2018). Organoid profiling identifies common responders to chemotherapy in pancreatic cancer. *Cancer Discovery*, *8*(9), 1112–1129. https://doi.org/10.1158/2159-8290.CD-18-0349

Torres, C., & Grippo, P. J. (2018). Pancreatic cancer subtypes: a roadmap for precision medicine. *Annals of Medicine*, *50*(4), 277–287. https://doi.org/10.1080/07853890.2018.1453168

Vaccaro, V., Sperduti, I., & Milella, M. (2011). FOLFIRINOX versus Gemcitabine for Metastatic Pancreatic Cancer. *The New England Journal of Medicine*, 768–769.

Vermeulen, K., Van Bockstaele, D. R., & Berneman, Z. N. (2003). The cell cycle: A review of regulation, deregulation and therapeutic targets in cancer. *Cell Proliferation*, *36*(3), 131–149. https://doi.org/10.1046/j.1365-2184.2003.00266.x

Villunger, A., Michalak, E. M., Coultas, L., Ausserlechner, M. J., Adams, J. M., & Strasser, A. (2003). *p53- and Drug-Induced Apoptotic Responses Mediated by BH3-Only Proteins Puma and Noxa*. *302*(November), 1036–1038.

Vimalraj, S., Arumugam, B., Miranda, P. J., & Selvamurugan, N. (2015). Runx2: Structure, function, and phosphorylation in osteoblast differentiation. *International Journal of Biological Macromolecules*, *78*, 202–208. https://doi.org/10.1016/j.ijbiomac.2015.04.008

Von Hoff, D. D., Ervin, T., Arena, F. P., Chiorean, E. G., Infante, J., Moore, M., Seay, T., Tjulandin, S. A., Ma, W. W., Saleh, M. N., Harris, M., Reni, M., Dowden, S., Laheru, D., Bahary, N., Ramanathan, R. K., Tabernero, J., Hidalgo, M., Goldstein, D., … Renschler, M. F. (2013). Increased Survival in Pancreatic Cancer with nab-Paclitaxel plus Gemcitabine. *New England Journal of Medicine*, *369*(18), 1691–1703. https://doi.org/10.1056/nejmoa1304369

Waddell, N., Pajic, M., Patch, A., Chang, D. K., Kassahn, K. S., Bailey, P., Johns, A. L., Miller, D., Nones, K., Quek, K., Quinn, M. C. J., Robertson, A. J., Fadlullah, M. Z. H., Bruxner, T. J. C., Christ, A. N., Harliwong, I., Idrisoglu, S., Manning, S., Nourse, C., … Grimmond, S. M. (2015). *Whole genomes redefine the mutational landscape of pancreatic cancer*. https://doi.org/10.1038/nature14169

Whittle, M. C., Izeradjene, K., Geetha Rani, P., Feng, L., Carlson, M. A., DelGiorno, K. E., Wood, L. D., Goggins, M., Hruban, R. H., Chang, A. E., Calses, P., Thorsen, S. M., & Hingorani, S. R. (2015). RUNX3 controls a metastatic switch in pancreatic ductal adenocarcinoma. *Cell*, *161*(6), 1345–1360. https://doi.org/10.1016/j.cell.2015.04.048

Wirth, M., Stojanovic, N., Christian, J., Paul, M. C., Stauber, R. H., Schmid, R. M., Häcker, G., Krämer, O. H., Saur, D., & Schneider, G. (2014). MYC and EGR1 synergize to trigger tumor cell death by controlling NOXA and BIM transcription upon treatment with the proteasome inhibitor bortezomib. *Nucleic Acids Research*, *42*(16), 10433–10447. https://doi.org/10.1093/nar/gku763

Witkiewicz, A. K., McMillan, E. A., Balaji, U., Baek, G. H., Lin, W. C., Mansour, J., Mollaee, M., Wagner, K. U., Koduru, P., Yopp, A., Choti, M. A., Yeo, C. J., McCue, P., White, M.

A., & Knudsen, E. S. (2015). Whole-exome sequencing of pancreatic cancer defines genetic diversity and therapeutic targets. *Nature Communications*, *6*, 1–11. https://doi.org/10.1038/ncomms7744

Wong, S. T., & Goodin, S. (2009). Overcoming drug resistance in patients with metastatic breast cancer. *Pharmacotherapy*, *29*(8), 954–965. https://doi.org/10.1592/phco.29.8.954

Yokota, A., Huo, L., Lan, F., Wu, J., & Huang, G. (2020). The Clinical, Molecular, and Mechanistic Basis of RUNX1 Mutations Identified in Hematological Malignancies. *Molecules and Cells*, *43*(2), 145–152. https://doi.org/10.14348/molcells.2019.0252

Yoshida, C. A., Yamamoto, H., Fujita, T., Furuichi, T., Ito, K., Inoue, K. I., Yamana, K., Zanma, A., Takada, K., Ito, Y., & Komori, T. (2004). Runx2 and Runx3 are essential for chondrocyte maturation, and Runx2 regulates limb growth through induction of Indian hedgehog. *Genes and Development*, *18*(8), 952–963. https://doi.org/10.1101/gad.1174704

Youle, R. J., & Strasser, A. (2008). *The BCL-2 protein family : opposing activities that mediate cell death*. *9*(january), 47–59. https://doi.org/10.1038/nrm2308

Zamboni, G., Hirabayashi, K., Castelli, P., & Lennon, A. M. (2013). Precancerous lesions of the pancreas. *Best Practice and Research: Clinical Gastroenterology*, *27*(2), 299–322. https://doi.org/10.1016/j.bpg.2013.04.001

Zhang, Y., Liu, T., Meyer, C. A., Eeckhoute, J., Johnson, D. S., Bernstein, B. E., Nussbaum, C., Myers, R. M., Brown, M., Li, W., & Shirley, X. S. (2008). Model-based analysis of ChIP-Seq (MACS). *Genome Biology*, *9*(9). https://doi.org/10.1186/gb-2008-9-9-r137

Zhao, X., Ren, Y., Lawlor, M., Shah, B. D., Park, P. M. C., Lwin, T., Wang, X., Liu, K., Wang, M., Gao, J., Li, T., Xu, M., Silva, A. S., Lee, K., Zhang, T., Koomen, J. M., Jiang, H., Sudalagunta, P. R., Meads, M. B., … Tao, J. (2019). BCL2 Amplicon Loss and Transcriptional Remodeling Drives ABT-199 Resistance in B Cell Lymphoma Models. *Cancer Cell*, *35*(5), 752-766.e9. https://doi.org/10.1016/j.ccell.2019.04.005

Zhou, Y., Zhang, X., Zhang, J., Fang, J., Ge, Z., & Li, X. (2017). LRG1 promotes proliferation and inhibits apoptosis in colorectal cancer cells via RUNX1 activation. *PLoS ONE*,

12(4), 1–14. https://doi.org/10.1371/journal.pone.0175122

Zhu, L. J., Gazin, C., Lawson, N. D., Pagès, H., Lin, S. M., Lapointe, D. S., & Green, M. R. (2010). ChIPpeakAnno: A Bioconductor package to annotate ChIP-seq and ChIP-chip data. *BMC Bioinformatics*, *11*. https://doi.org/10.1186/1471-2105-11-237

Figure Index

Table index

List of abbreviations

%	percentage
<	minor
>	higher
Δ	delta
°C	grad Celsius
4C	circular chromatin conformation capture
4C-seq	circular chromatin conformation capture sequencing
5'	five prime end of a DNA sequence
3'	three prime end of a DNA sequence
+	positive/plus
5-FU	5-Fluorouracil
µg	microgram
µM	micromolar
ADM	acinar-to-ductal metaplasia
AML	Acute Myeloid Leukemia
ANOVA	analysis of variance
APAF-1	apoptotic protease activating factor 1
APS	ammonium persulfate
ATP	adenosine triphosphate
BAD	BCL-2 associated agonist of cell death
BAK	BcCL2 Homologous Antagonist/Killer
BAX	BCL-2 associated X protein
BCL-2	B-cell lymphoma 2
BCL-W (BCL2L2)	BCL-2-Like Protein 2
BCL-XL	BCL-2-Like Protein 1
BET	bromodomain and extra terminal domain
BH domain	BCL-2 homology (BH) domain
BID	BH3 interacting domain death agonist
BIK	BCL-2 interacting killer
BIM (BCL2L11)	BCL-2 interacting mediator of cell death
blast	blasticidin
BMF	BCL-2 modifying factor
bp	base pair
BRCA 1/2	*breast cancer early onset genes*
BRD4	bromodomain-containing protein 4
BRG1	*SMARCA4* gene
BSA	bovine serum albumin
$CaCl_2$	calcium chloride
Cas9	CRISPR-associated protein 9
CCLE	Cancer Cell Line Encyclopedia
CDK	cyclin-dependent kinase
CDKN2A CIP/KIP	*cyclin-dependent kinase Inhibitor 2A*
cDNA	complementary DANN
ChIP	chromatin immunoprecipitation
ChIP-seq	chromatin immunoprecipitation sequencing
chr	chromosome
CO_2	carbon dioxide

CRISPR	Clustered Regularly Interspaced Short Palindromic Repeats
CRISPRa	CRISPR activation system
Ct	threshold cycle
CTCF	CCCTC-binding factor, zinc finger protein
cyt c	cytochrome c
dCas9	defective Cas9
ddH_2O	bi-distilled water
DISC	death inducing signaling complex
DMEM	Dulbecco's Modified Eagle Medium
DMSO	Dimethyl sulfoxide
DNA	desoxyribonucleic acid
DNMT	DNA-methyltransferase
DTT	Dithiothreitol
E. coli	*Escherichia coli*
e. g.	exempli gratia
EDTA	ethylenediaminetetraacetic acid
EGR1	early growth response protein 1
Enh	Enhancer
FACS	fluorescence activated cell sorting/scanning
FAIRE	Formaldehyde-Assisted Isolation of Regulatory Elements
FBS	fetal bovine serum
FDA	Food and Drug Administration
FDR	false discovery rate
FOLFIRINOX	folinic acid, 5-FU, irinotecan, oxaliplatin
FWD	forward
g	Earth's gravitational force, relative centrifuge force
g	gram
GAPDH	*glyceraldehyde 3-phosphate dehydrogenase*
GEO	Gene Expression Omnibus
GI_{50}	growth inhibitory concentration 50
GO	Gene Ontology
h	hour
H3K27ac	histone three lysine twenty-seven acetylation
H3K4me1	histone three lysine four mono-methylation
H3K4me2	histone three lysine four di-methylation
H3K4me3	histone three lysine four tri-methylation
HCl	Hydrogen chloride
HRK	Harakiri, BCL2 interacting protein
HRP	horseradish peroxidase
HSF1	Heat Shock Transcription Factor 1
hygro	hygromycin
i.e.	id est
i.p.	intraperitoneal injection
IAPs	inhibitors of apoptosis proteins
IgG	immunoglobulin G
IP	immunoprecipitation
IPMN	intraductal papillary mucinous neoplasm
kb	kilobase
KCl	calcium chloride

kDa	kilodalton
ko	knockout
KRAS	*Kirsten rat sarcoma viral oncogene homolog*
lenti	lentivirus
log	logarithm
M	molar
MCL-1	Myeloid Cell Leukemia Sequence 1
$MgCl_2$	magnesium chloride
min	minute
miR-93	*microRNA-93*
ml	mililiter
mM	milimolar
MOM	mitochondrial outer membrane
MYC	myelocytomatosis oncogene
n	number
NaCl	sodium chloride
NES	normalized enrichment score
nM	nanomolar
NOXA	*PMAIP1* gene (*Phorbol-12-Myristate-13-Acetate-Induced Protein 1*)
Omni-ATAC-seq	Omni-Assay for Transposase-Accessible Chromatin with sequencing
OS	overall survival
p300	E1A-binding protein, 300kDa
PALB2	*partner and localizer of BRCA2*
PAM	Protospacer adjacent motif
PanIN	intraepithelial neoplasia
PBS	phosphate buffered saline
PCR	polymerase chain reaction
PDAC	pancreatic ductal adenocarcinoma
PEG	polyethylene glycol
PEI	polyethylenimine
Pen/Strep	penicillin/streptomycin
pH	pondus Hydrogeni
PI	propidium iodide
PI3K	phosphoinositide 3-kinase
PMSF	phenylmethylsulphonyl fluoride
Pol II	RNA polymerase II
PRC1	Polycomb Repressive Complex 1
prom	promoter
PUMA (BBC3)	*P53 up-regulated modulator of apoptosis*
puro	puromycin
PVDF	polyvinylidene fluoride
qRT-PCR	quantitative real time/reverse transcriptase PCR
R26	Rosa26 locus
REV	reverse
RNA	ribonucleic acid
RNA-seq	RNA sequencing
rpm	rounds per minute
RPMI	Roswell Park Memorial Institute
RT	room temperature/reverse transcription

RUNX1-3	*Runt-Related Transcription Factor 1-3*
SAM	Synergistic Activation Mediator
SD	standard deviation
SDS	sodiumvdodecylvsulfate
SDS-PAGE	sodium dodecyl sulfate polyacrylamide gel electrophoresis
sec	second
seq	sequencing
sgRNA	single guide RNA
SMAC	Second Mitochondria-Derived Activator of Caspase
SMAD4	*mothers against decapentaplegic homolog 4*
STRING	Search Tool for the Retrieval of Interacting Genes/Proteins
SUMO	small ubiquitin-like modifier
T4 PNK	T4 polynucleotide kinase
T75/T75	75 cm^2, 175 cm^2 flasks
tBID	truncated BID
TBS	Tris-buffered saline
TCGA	The Cancer Genome Atlas
TEMED	N,N,N',N'-Tetramethylendiamine
TGF-β	Transforming Growth Factor Beta 1
TNF	tumor necrosis factor
TP53	*tumor protein p53*
Tween	polyoxethylene-sorbitan-monolaureate
U	unit
UTR	untranslated region
UV	ultra violet
V	voltage
wt	wild type
XIAP	X-chromosome linked inhibitor of apoptosis protein
TSS	transcriptional start site
x	times